Assessment of Groundwater Potential Zones in the Lower Jordan Valley Using Remote Sensing Approaches

A thesis for the degree of Doctor of Engineering Approved by the Faculty of Civil Engineering, Geosciences and Environmental Sciences of the Karlsruhe Institute of Technology (KIT)

By

M.Sc. Eng. Nawras Shatnawi

From

JORDAN

Karlsruhe, February 2014

Supervisors:

1. Prof Dr. S. Hinz

Karlsruhe Institute of Technology, Germany

2. Prof Dr. H. Hötzl

Karlsruhe Institute of Technology, Germany

3. Prof. Dr. A. Al-Zoubi

Al-Balqa Applied University, Jordan

Date of thesis defense: 13th of February, 2014

I hereby declare that all information in this document has been obtained and presented in accordance with academic rules and ethical conduct. I also declare that, as required by these rules and conduct, I have fully cited and referenced all material and results that are not original to this work.

Name, Last name: Nawras Shatnawi

Signature:

الخلاصة

يقع الاردن في منطقة جافة الى شبه جافة ويعتبر أحد أفقر دول العالم من حيث توافر مصار المياه . يعتبر وادي الاردن من أهم المناطق الزراعية في الاردن الا أنه ايضا يعاني من شح في المياه ، ولذا جاء مشروع سمارت (SMART) وهو واحد من أهم المشاريع الرائدة في المنطقة ـ والممول من وزارة التعليم والبحث الالمانيةـ من أجل تطوير الادارة المتكاملة لمشاريع المياه في منطقة وادي الاردن. تساهم هذه الدراسة كجزء من مشروع سمارت في البحث عن مصادر للمياه الجوفية وادارتها في الجانب الاردني لوادي الاردن، حيث أن الهدف الرئيس من هذه الدراسة هو دعم عملية استكشاف مناطق تواجد المياه الجوفية من خلال استخدام تقنيات الاستشعار عن بعد.

تم تقسيم منطقة الدراسة الي عدة مناطق بناء على أهمية ودور كل منطقة في تشكيل المياه الجوفية وتخزينها بالاعتماد على العديد من العوامل والمتغيرات والتي تؤثر على عملية الجريان السطحي وترشيح مياه الأمطار للاسفل. وللقيام بذلك تم دراسة تسعة عوامل مهمة في تشكيل المياه الجوفية باستخدام طريقة التسلسل الهرمي التحليلي Analytical AHP-Hierarchy Principle وطريقة المنطق المشوش Fuzzy Logic وهذه العوامل هي: طوبوغرافية المنطقة من خلال عمل نموذج رقمي للارتفاعات باستخدام صور أقمار صناعية عالية الوضوح(CARTOSAT) ، العوامل الجيومورفولوجية ، الميول الموجودة في المنطقة ، شبكة الاودية و تصريف المياه ، الغطاء النباتي ،وكثافة الشقوق (السمات) والتي تم استخلاصها جميعا من صور الأقمار الصناعية المختلفة باستخدام تقنيات الاستشعار عن بعد، كم تم استخدام خرائط مختلفة من عدة مصادر تمثل جيولوجية المنطقة وغطاء التربة بالاضافة الى توزيع مياه الأمطار فيها.

من أجل استخلاص خريطة الغطاء النباتي للمنطقة تم استخدام صور القمرالصناعي (LANDSAT) لموسمين متتاليين: شتاء 2010 وصيف 2011 حيث أظهرت النتائج دقة عالية تصل الى 90.33 % ومعامل كابا K= 0.948 مما جعل تصنيف وتقسيم الغطاء النباتي أكثر موضوعية. تم في هذه الدراسة استخلاص خريطة للشقوق (السمات) الموجودة في المنطقة باستخدام طريقتين هما : الطريقة اليدوية التقليدية والطريقة شبه الاتوماتيكية حيث أظهرت الطريقة الاولى أن الطول الكلي لهذه الشقوق يساوي 173.4 كم ،بينما أظهرت الطريقة الثانية أن الطول الكلي يساوي 145 كم وهذا يعتبر مقبولا بالمقارنة مع خريطة التراكيب الجيولوجية المتوفرة للمنطقة.

تركز هذه الدراسة على امكانية استخدام صور الأقمار الصناعية في استخراج نماذج الارتفاعات الرقمية عالية الدقة والوضوح وكذلك استخراج المعاملات المورفومترية بالاضافة الى شبكات تصريف المياه والجريان السطحي. تم عرض طريقة العمل والتحقق وتقييم النتائج لنماذج الارتفاعات الرقمية والتي تم استخلاصها من صور القمر الصناعي ذات الوضوح المكاني 2.5 متر ، ومن ثم تم استخدام نموذجين للتحقق من النتائج حسب عدد نقاط التحكم والربط الارضية ، حيث اظهر النموذج الأول متوسط فروقات بين الارتفاعات بحدود 3.27 متر وبانحراف معياري 4.68 ومربع متوسط الخطأ بمقدار 4.37 مترا فيما أظهر النموذج الثاني أن متوسط الفروقات يساوي 2.23 مترا وبانحراف معياري 2.4 فيما كان مربع متوسط الخطأ 2.37 مترا مما يشير الى مدى فاعلية ودقة هذه الصور خصوصا في محاكات الارتفاعات في المناطق الجبلية شديدة الانحدار.

أظهرت النتائج أن منطقة الدراسة يمكن تقسيمها الى عدة مناطق من حيث احتمالية تواجد المياه الجوفية فيها باستخدام طريقة التسلسل الهرمي التحليلي والمنطق المشوش وهذه المناطق هي:

- منطقة ذات احتمالية عالية لتواجد المياه الجوفية: و تقع في المنطقة الشرقية الوسطى من منطقة الدراسة والتي تقع في منطقة الجرف الصخري الذي يحتوي على تراكيب مجموعة عجلون الجيولوجية (تراكيب الفحيص – حمر- شعيب) والتي تحتوي على صخور جيرية متصلبة ضمن منطقة شقوق عالية الكثافة مما يتيح امكانية تسرب وترشيح المياه السطحية الى الاسفل بكل سهولة، و تشكل هذه المنطقة حوالي 12.6% من اجمالي مساحة منطقة الدراسة.

- المنطقة ذات الاحتمالية المتوسطة لتواجد المياه الجوفية : وتقع في الجزء الشمالي من منطقة الدراسة وخاصة الجزء الشمالي من الجرف، حيث تحتوي على تراكيب الكرنب الجيولوجية والتي تتكون من الطمي والصخور الرملية ، وتقع ضمن منطقة شقوق متوسطة الكثافة نسبيا، كما يمكن أن نجد هذه المنطقة ذات الخصائص المتوسطة نسبيا في المنطقة الغربية من وادي الاردن خصوصا في الأودية العميقة .

- المنطقة ذات الاحتمالية الضعيفة والضعيفة جدا لوجود المياه الجوفية فيها : وتقع بشكل عام في المنطقة الغربية من منطقة الدراسة والتي تحتوي على تراكيب اللسان الجيولوجية ذات النفاذية القليلة للمياه، كما يمكن تواجد هذه المنطقة ذات الخصائص الضعيفة في منطقة الزور العميقة في وادي الاردن والتي تعرف بقلة معدلات الهطول فيها بالاضافة الي تواجد تراكيب اللسان والطمي قليلة النفاذية.

تم استخدام البيانات المتوفرة في وزارة المياه والري الاردنية بخصوص الابار الجوفية التي تقع في منطقة الدراسة من أجل التحقق من نتائج ودقة الخرائط المستخلصة ، وعلى الرغم من وجود توافق في المناطق عالية الاحتمالية ونتائج الابار الجوفية الا أنه لا يوجد نسق واضح يربط بينها ، لذا تم الاستفادة من نتائج دراسات جيوفيزيائية تم عملها في المنطقة من أجل التحقق من دقة النتائج ، حيث اظهرت نتائج الدراسات الجيوفيزيائية للمنطقة وجود ترابط واضح بينها وبين نتائج هذه الدراسة وخصوصا النتائج المستخلصة باستخدام طريقة المنطق المشوش Fuzzy logic في استخلاص خرائط احتمالية تواجد المياه الجوفية.

تم عمل دراسة تحليل الحساسية حيث أظهرت النتائج حساسية جميع العوامل والمتغيرات المستخدمة في هذه الدراسة مع وجود حساسية أكبر للعوامل الجيولوجية والجيومورفولوجية وكذلك لكثافة تواجد الشقوق. وأوصت الدراسة باستخدام هذا النوع من الخرائط في البحث عن المياه الجوفية وخصوصا في المناطق ذات الاحتمالية العالية والتي لم يتم البحث فيها بعد.

Kurzfassung

Jordanien liegt in einer ariden bis semi-ariden Region und ist eines an Wasserressourcen ärmsten Ländern der Welt. Das Jordantal ist ein wichtiges Gebiet für die landwirtschaftliche Nutzung, leidet aber an der zunehmenden Wasserknappheit. Deshalb wurde vom Bundesministerium für Bildung und Forschung (BMBF) das SMART-Projekt initiiert, um einen integrierten Ansatz zum Wasserressourcenmanagement im unteren Jordantal zu entwickeln. Diese Studie trägt sowohl zum SMART-Projekt als auch der Region bei, indem Grundwassererkundung und -management im jordanischen Teil des unteren Jordantals unterstützt werden. Hauptziel ist eine verbesserte Entdeckung potentieller Grundwasservorkommen durch die Kombination von Fernerkundungs- und analytischen Methoden.

In dieser Studie wird die Landschaft entsprechend ihrem Grundwasserpotential, welches als Potential zur Grundwasserneubildung definiert ist, in verschiedene Klassen unterteilt. Dies geschieht auf Basis unterschiedlicher Kontrollparameter, die durch die Oberflächenbeschaffenheit und die Versickerung von Niederschlagswasser in den tieferen Untergrund beeinflusst werden. Zur Evaluierung und Gewichtung der relevanten Parameter wurden zwei Methoden angewandt: Der Analytische Hierarchieprozess (AHP) und Fuzzylogik. Zur Erzeugung einer Karte der Grundwasserpotentialzonen (GWPZ) für das Untersuchungsgebiet wurden in dieser Forschungsstudie neun Parameter ausgewählt. Die integrierten Parameter sind: topographische Höhe (erzeugt als hochaufgelöstes digitales Höhenmodell), morphologische Klassifizierung, Neigung, Entwässerungsnetze, Landnutzung/-bedeckung und Lineamentdichte. Diese wurden unter Verwendung von Fernerkundungsdaten und –methoden erzeugt. Zusätzlich standen Daten über Geologie/Lithologie, Erdreich und jährlichen Niederschlag aus verschiedenen Quellen zur Verfügung.

Zur Erzeugung einer thematischen Karte über die Landnutzung/-bedeckung wurden LANDSAT-5 und 7 Bilder der Winter- und Sommersaison von 2010 und 2011 kombiniert. Die Gesamtgenauigkeit beträgt 90,33 % und der Kappa Koeffizient 0,948. Diese hohe Genauigkeit vereinfacht die Unterscheidung der Klassen. Außerdem wurden in dieser Arbeit Lineamentkarten durch digitale Verarbeitung von CARTOSAT-1 Bildern erzeugt. Die Erfassung der Lineaments erfolgte mit manuellen und semi-automatischen Methoden, wobei die Gesamtlänge bei der manuelle Extraktion 173,4 km und bei der semi-automatische Extraktion 145 km beträgt. Diese Werte erscheinen im Vergleich zu einer existierenden strukturellen Lineamentkarte sinnvoller.

Die vorgestellte Arbeit zeigt die Vorteile der Verwendung von hochaufgelösten Satellitenbildern zur Erfassung digitaler Geländemodelle (DGM), morphologischer Parameter und der Ableitung von Entwässerungsnetzen. Es werden Methodik, Referenzdatenvalidierung und die Beurteilung von CARTOSAT-1 Daten mit 2,5 m Auflösung zur DGM Generierung vorgestellt. Zur Beurteilung der Genauigkeit der generierten DGM in Abhängigkeit der Anzahl der verwendeten GCPs wurden zwei Modelle genutzt. Das erste Modell liefert eine mittlere Höhendifferenz von 3,27 m mit 4,68 m Standardabweichung und einem mittleren

quadratischen Fehler (RMSE) von 4,37m, was 1,89 Pixel entspricht. Das zweite Modell hat eine mittlere Differenz von 2,23 m mit 2,4 m Standardabweichung und einem RMSE von 2,37 m, was 0,94 Pixel entspricht. Diese Ergebnisse sind sehr hoch, vor allem in steilen bergigen Geländen.

Die verwendeten Methoden zur Erzeugung der GPWZ Karten – AHP und Fuzzylogik – zeigten relativ gleiche Ergebnisse. Diesen entsprechend wurde das Untersuchungsgebiet in 5 Zonen aufgeteilt:

- Zone mit sehr hohem und hohem Grundwasserpotential: hauptsächlich im mittleren östlichen Teil der Karte gelegen. Der östliche Teil repräsentiert den Steilhang mit hartem Sedimentgestein. Die mittlere Teil ist dominiert von der Ajlun Gruppe mit der Fuhays-Hummar-Shua'ab Formation. Deren Kalkfelsen sind stark verkarstet. Zudem zeigt diese Zone eine hohe Dichte an Lineamenten, was eine hohe Grundwasserneubildung begünstigt. Zonen mit hohem Potential bedecken 12,6 % des Untersuchungsgebietes.
- Zone mit moderatem Grundwasserpotential: hauptsächlich im nördlichen und südlichen Teil des östlichen Steilhanggebietes gelegen. Diese Gebiete werden durch die dominierenden Ausläufe der Cornub Gruppe geprägt. Sie bestehen aus Sand- und Schluffstein, mit einer generell niedrigeren Lineamentdichte. Teils moderate GWPZ sind auch im westlichen Teil des Jordantals zu finden, vor allem in Gegenden in denen tiefe Wadis den wasserundurchlässigen Lisan-Mergel zerteilen.
- Zone mit geringem und sehr geringem Grundwasserpotential: hauptsächlich im westlichen Teil der Karte mit der Lisan Ebene und der tieferen Zor Terassenebene des neuen Jordankanals gelegen. Neben der geringen Niederschlagmenge sind sowohl der gering durchlässige Lisan-Mergel als auch die Ton- und Schluffsteinsedimente im Zortal für die geringe Grundwasserneubildung verantwortlich.

Unterlagen des Ministeriums für Wasser und Bewässerung (WAI) von bestehenden Brunnen in der oberen Grundwasserschicht wurden zur Verifikation der Ergebnisse verwendet. Obwohl die ergiebigsten Brunnen in Zonen mit sehr hohem und hohem Grundwasserpotential lokalisiert wurden, zeigten die verwendeten Daten keinen offensichtlichen Zusammenhang zwischen Ergiebigkeit der Brunnen und den GWPZ. Zur zusätzlichen Kontrolle, vor allem des westlichen Kartenteils, wurden die Ergebnisse mit Daten aus geophysikalischen Studien verglichen. Die Verifikation mit Messungen von Bodenradar, kernmagnetischer Resonanz und vertikalem Echolot zeigten, dass die GPWZ Karte, welche mit dem Fuzzylogik Ansatz erzeugt wurde, eine höhere Signifikanz hat als die Karte, welche aus dem AHP Ansatz resultiert.

Eine Sensitivitätsanalyse zeigte, dass die generierte GPWZ Karte empfindlich gegenüber allen Parametern mit höherer Signifikanz für Geologie und Lithologie, Morphologie und Lineamentdichte ist. Die Arbeit empfiehlt die Verwendung der generierten GWPZ Karten als Referenz für zukünftige Untersuchungen, vor allem in den vielversprechenden Zonen mit hohem Grundwasserpotential.

ABSTRACT

Jordan is located in an arid to semi-arid region, and considered as one of the poorest countries in the world in water resources. Jordan valley is an important area for agricultural uses, but suffers under the increasing water scarcity, Therefore SMART project, which is one of the pioneer projects in the area funded by the German Federal Ministry of Education and Research (BMBF), was launched to develop an integrated water resources management approach in the Lower Jordan valley. This study contributes to SMART project as well as to the area by supporting the Groundwater exploration and management in the Jordanian side of the Lower Jordan Valley. The main goal is to improve the discovery of potential groundwater occurrences by a new combination of remote and analytical techniques.

In this study the landscape is classified into different classes according to their groundwater potential, which is defined in this study as the potential of groundwater recharge on the basis of the different controlling parameters, which influence the infiltration of rain and surface flow into the deep underground and generating thereby the groundwater. For the evaluating and weighting of the relevant parameters two methods were applied: Analytical Hierarchy Principle (AHP) and Fuzzy logic. 9 parameters were selected and integrated in this research study to generate a Groundwater Potential Zone (GWPZ) Map for the study area. The integrated parameters are: topographic elevation (created as a high resolution digital elevation model), morphologic classification, slope decline, drainage network, land use/land cover and lineament density, which all were prepared and extracted in this research using remote sensing data and techniques, in addition to that geology/lithology, soil and yearly rainfall was used , which were provided from different sources.

In order to generate land cover/land use thematic map of the area we have combined LANDSAT-5 and 7 temporal images acquired in winter and summer seasons of the years 2010 and 2011. The overall accuracy is 90.33 %, and the Kappa statistics value is 0.948, this high accuracy makes distinction between the classes easier. In this study we also generate lineaments map through digital processing of remotely sensed data of CARTOSAT-1 images, we use for Manual and Semi-Automatic methods extracting lineaments, total length of manually extracted lineaments is 173.4 km, where it is 145 km in case of Semi-Automatically extracted lineaments, and that is more reasonable compared with an existing structural lineament map.

The presented work focuses on the benefit of using high resolution satellite images for extracting digital terrain model (DTM), morphometric parameters and derivation of drainage networks. We present methodology, ground truth validation and assessment for DTM generation by CARTOSAT-1 data of 2.5m spatial resolution. Two models were used to assess the accuracy of the generated DTM depending on the number of used GCP's; the first model showed mean difference in elevation of 3.27 m with 4.68 standard deviation and Root Mean Square Error (RMSE) of 4.73 which equals (1.89) pixels, where the second model showed mean difference in elevation of 2.23 m with 2.4 standard deviation and Root Mean Square Error (RMSE) of 2.37 which equals (0.94) pixels, these results considered quite high especially in steeply mountainous area.

The used methods for generating GWPZ maps -AHP and Fuzzy logic -showed relatively similar results; according to that the study area is divided into several zones:

- Very high and high groundwater potential zone: mainly located in the Middle Eastern part of the map. The Eastern part represents the escarpment with the sedimentary hard rocks, the middle part is dominated by the Ajlun group with Fuhays-Hummar-Shua'ab formation, their limestone rocks are intensively karstified in addition this zone shows high lineament density and therefore favors high recharge rates into the underground. The high potential area covers 12.6 %.

- Moderate groundwater potential zone: located mainly in the northern and southern part of the Eastern escarpment area. These areas are characterized by the dominating outcrop of the Kurnub group, which consists of sand- and siltstones, with a general lower lineament density. Partly the moderate GWPZ is also found in the Western part with the Jordan valley floor, especially in areas where the deep cut wadis dissect the impervious Lisan marls.

- Poor and very poor groundwater potential zone: located mainly in the Western part of the map with the Lisan terrace plain and the deeper Zor terrace level of the recent Jordan River channel. Beside the low precipitation data in this area, the less permeable Lisan marls as well as the clayey and silti flood sediments in the Zor are responsible for the low groundwater recharge in this area.

Data collected from records of Ministry of Water and Irrigation (WAI) of existing wells in the upper aquifers were used to verify the results, although the wells with the highest yield were located in high and very high groundwater potential zones. The used data showed no

obvious trend controlling the relation between wells yield and GWPZ. In order to get an additional control especially for the Western part of the map the results were compared with data obtained from geophysical studies (ground truth) and used to verify the results, Ground Penetrating Radar (GPR), Nuclear Magnetic Resonance (NMR) and Vertical Electrical Sounding (CVES) results revealed that the GWPZ map generated by the Fuzzy logic approach shows higher significant than the map generated by AHP model.

Sensitivity analysis indicated that the generated GWPZ map is sensitive to all the parameters with higher significance to geology and lithology, morphology and lineament density. The study recommends using the generated groundwater potential map as a reference for future exploration especially in the promising high Groundwater potential zones.

ACKNOWLEDGEMENTS

offering support and love. My kids Omar and Raya the source of my inspiration. The nights while I was away from them were truly difficult.

I would like to thank my parents who raised me with a love of science and supported me in all my pursuits; their prayer for me was what sustained me thus far as always. My brothers and sisters are also thanked for giving me their unequivocal support throughout.

 I could not have completed my research without the support of all these wonderful people!

This dissertation is dedicated to my home country -Jordan, to my family and friends.

CONTENTS

List of Figures

List of Tables

1. Introduction

1.1 General Background

Jordan is considered among the poorest countries in water resources in the world, nowadays Jordan is facing life-threatening situation due to sharply increase in population, which leads to high demand on the limited water resources. Therefore many projects were introduced to the area to manage the water issues of Jordan. One of the introduced projects is SMART project (Sustainable Management of Available Water Resources with Innovative Technologies) which is a research project sponsored by the German Federal Ministry of Education and Research (BMBF). The goal of this project is to develop a transferable approach for Integrated Water Resources Management (IWRM) in the water shortage region of the Lower Jordan Valley. The necessity of exploring new groundwater resources in this arid to semi-arid area as part of SMART project motivated the researcher to search for new options and alternatives for the exploration and finding new water resources, thus a new mapping concept for groundwater potential zones of the lower Jordan valley was developed in this thesis study by using advanced remote sensing tools in order to support planners and decision makers in their reconnaissance of additional groundwater resources.

The main purpose of this study is to addressing a new method to Integrated Water Resources Management in Jordan by generating and assessing groundwater potential zones. To achieve this goal, the study included an in-depth analysis and comparison of different parameters used in the past for generating such maps. The resulting map is specifically aimed to improve the understanding of groundwater distribution in the lower Jordan valley. This will form the basis for exploring new groundwater locations that have high groundwater potential.

To carry out this research the Lower Jordan Valley has to be classified into areas of different groundwater potentials, and that needs the adduction and integration of many different parameters as: geology & lithology, rainfall intensity, soil, geomorphology drainage density or geo-lineaments. For each relevant parameter it was necessary to produce weighted maps of the study area, in which the distribution of the parameter intensity for groundwater recharge was documented. In addition available land cover/use map, digital elevation model, morphological maps as well as specific land-use thematic map were adapted, however they were not satisfying the high resolution requirements of this research study, therefore all of these maps were prepared and extracted in this thesis research using remote sensing data and

techniques. The final resulting Groundwater-Potential-Zone (GWPZ) maps were achieved by integrating all parameter maps in a mathematical overlaying procedure. Full detailed methodology of this work is introduced in the next chapters.

This thesis contributes to the field of water resources and remote sensing by assessing and mapping the groundwater potential zones in the study area by two methods; Analytical-hierarchy-principle and Fuzzy logic, and also to use hydrogeologic data of existing wells and geophysical studies for verifying the results of the two methods.

1.2 Objectives of this Research

- The main objective of this work implies the development and compilation of the Groundwater-Potential-Zones map of the study area – starting from the conceptual idea and planning over the implementation of the different operation steps to the final composition of the map. In this connection the groundwater potential refers and are mainly defined by parameters, which enable to assess the infiltration of precipitation into the underground or in other word to assess the yearly recharge rate for the groundwater. In order to reach this main objective the following steps have to be achieved:

1. To ascertain, calibrate and standardize factors and properties which are important for the occurrence of groundwater and which can be identified with remote techniques.

2. Integration of Geophysical data to determine characteristics that are key components in hydrological processes.

3. To create an integrated GIS and Remote sensing database for the lower Jordan Valley area.

4. To develop and implement Fuzzy logic , AHP spatial model for prediction of groundwater potential zones.

5. Development and application of a model that simulates the whole contributing factors for exploration of potential groundwater resources.

6. To utilize the generated map for the improvement of the management of groundwater resources in the Jordan valley.

- Minor objectives of the study are:

1- Analysis of remote sensing data sets to have a clear idea about land use (vegetation, water bodies...), settlements, and geological features.

2- To generate land use / land cover map through digital processing of remotely sensed data of LANDSAT images.

3- To generate High resolution DTM of the lower Jordan Valley.

4- To generate lineaments map through digital processing of remotely sensed data of CARTOSAT-1 images

1.3 Description of study area

For the investigation of this thesis work a study area was selected which is located in the lower Jordan Valley in Jordan and extends approximately from the Dead Sea 50 km to the north and 15 km to the east of the Dead Sea covering most of the southern parts of the lower Jordan valley as shown in Figure 1.1.a and 1.1.b, the coordinates of the study area are: (31°45′43″-32°12 ′44″ Latitude and 35°30′55″-35°41′04″ Longitude), and between (3516803.23 -3567120.33 N) and (738227.6 – 753014.63 E) referenced on the Universal Transverse Mercator coordinate system UTM.

The Jordan Valley follows a main geosutur, which is caused by a leftlateral transform fault, which extends from the Red Sea up to the Taurus mountain chain in Turkey and along which the Arabian Plate has been shifted 107 km to the north compared with the Levantine and African Plate in the west since the Upper-Miocene (Niocal and Rayan, 1999; Kesten, 2004).

The floor of the Lower Jordan Valley slopes from Lake Tiberias (Sea of Galilee) gradually from 210m below MSL to about 414m below MSL (the current level of the Dead Sea), extending from the North to the Dead Sea, with a length of 105 km ,width a width varies from 10 km on the north, to 4–5 km in Wadi Malih area and to 25 km in the area of the northern shore of the Dead Sea; it is surrounded in the east and west by high mountains (Belitzky, 2002).
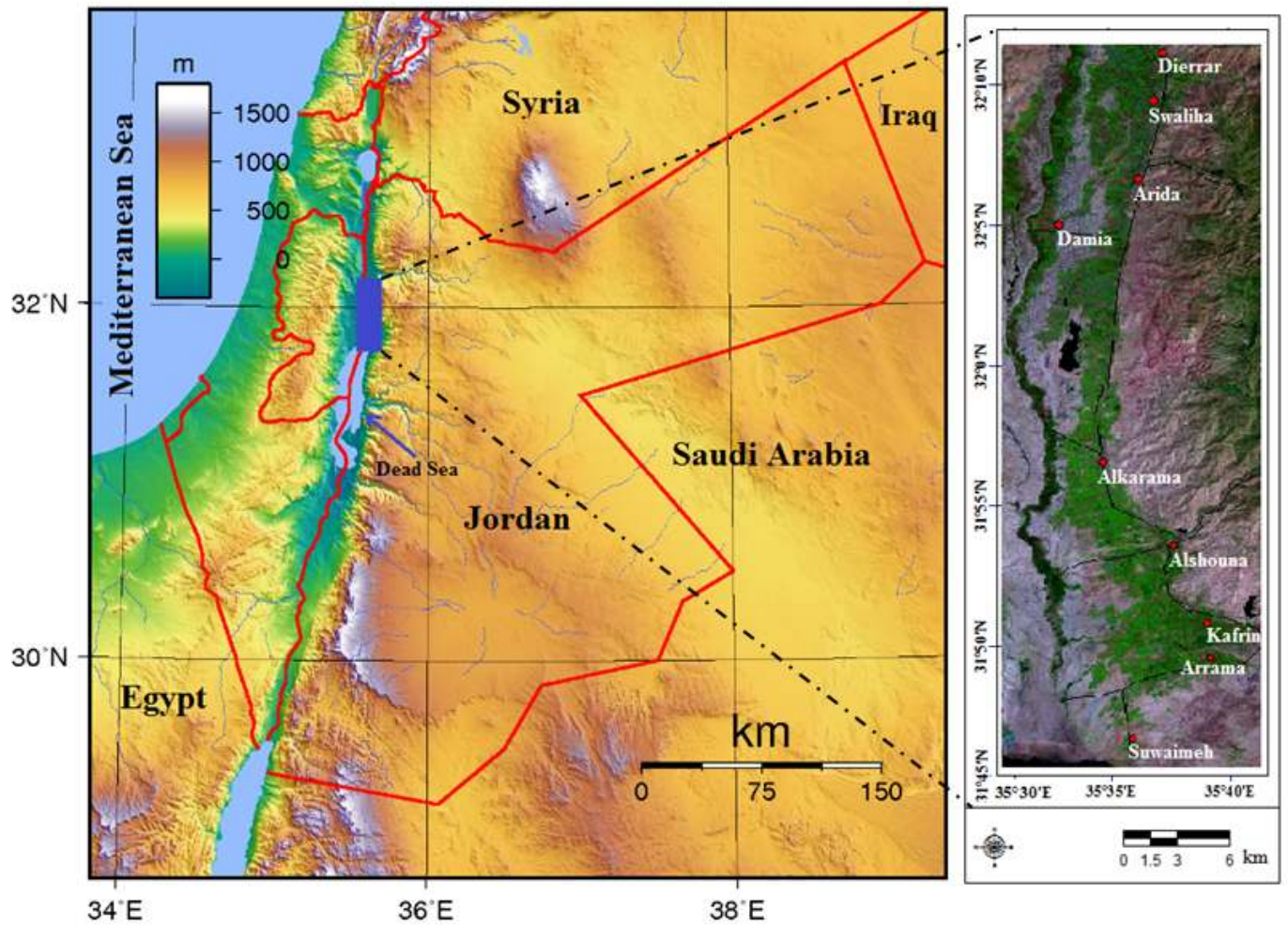
Figure 1.1.a: Location of the study area in the Jordan valley north of the Dead Sea.

Image to the left: Topographic map of Jordan, available online on:

(http://www.worldofmaps.net/uploads/pics/topography-jordan.png); Right: Landsat image of the study

area with the larger villages of the area
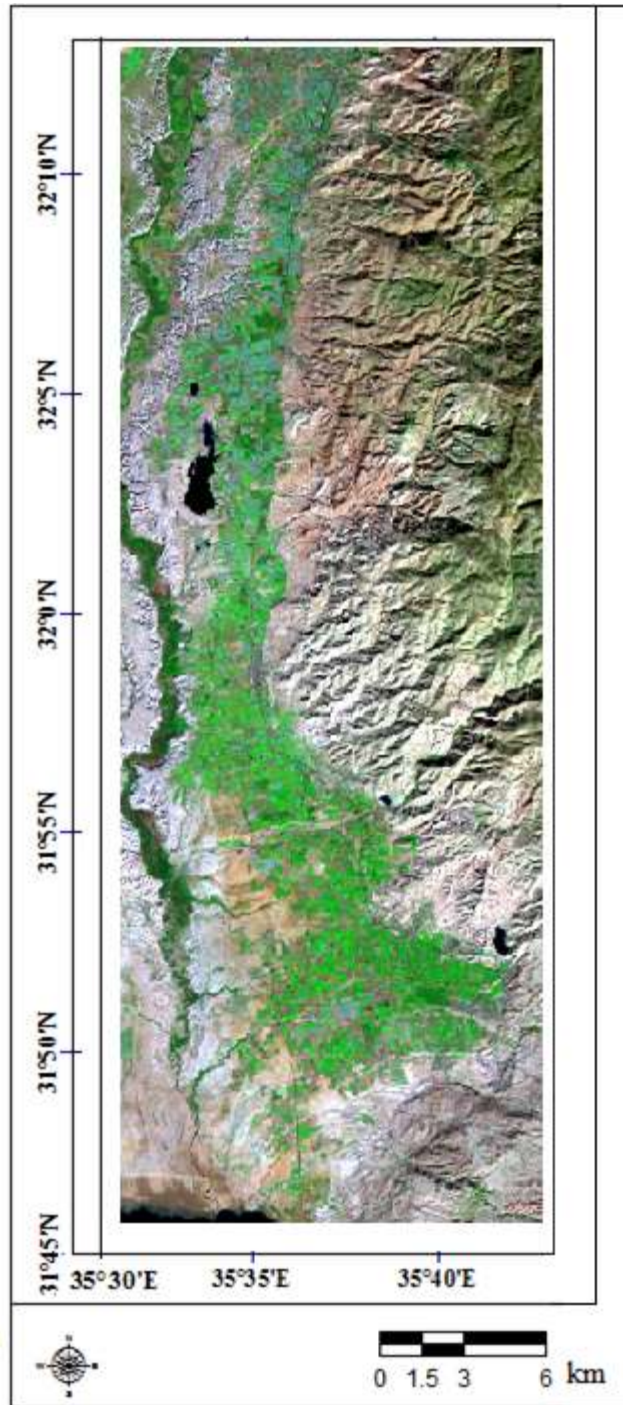
Figure 1.1.b: The study area shown in a satellite image from LANDSAT-7 from 2011.

This map with the longitude -latitude coordinates is used as the basic map for further displays in this thesis.

Geologically the JV floor is partly composed of undifferentiated Neogene formations, wide areas are covered by the Young Pleistocene Lake Lisan formation and by young talus deposits, fan deposits and terrace deposits mainly of Holocene age (Salameh & Bandel, 2013). These sediments have together a thickness of 30-50 m. They are underlain by marine

and continental sediments of several hundred meters. Geophysical studies revealed that the underground of the Jordan Valley is structured in several separate small basins like the Jericho-Shuna basin and Damia basin which are located in the study area as shown in Figure 1.2, another two sub basins are located in the north of the lower Jordan valley which are Bet-Shean and Bakura (Al-Zoubi *et al.*, 2012). Probably they are generated by the transform movement causing kind of small pull-apart-basins, like this is realized in a larger version in the Dead Sea.
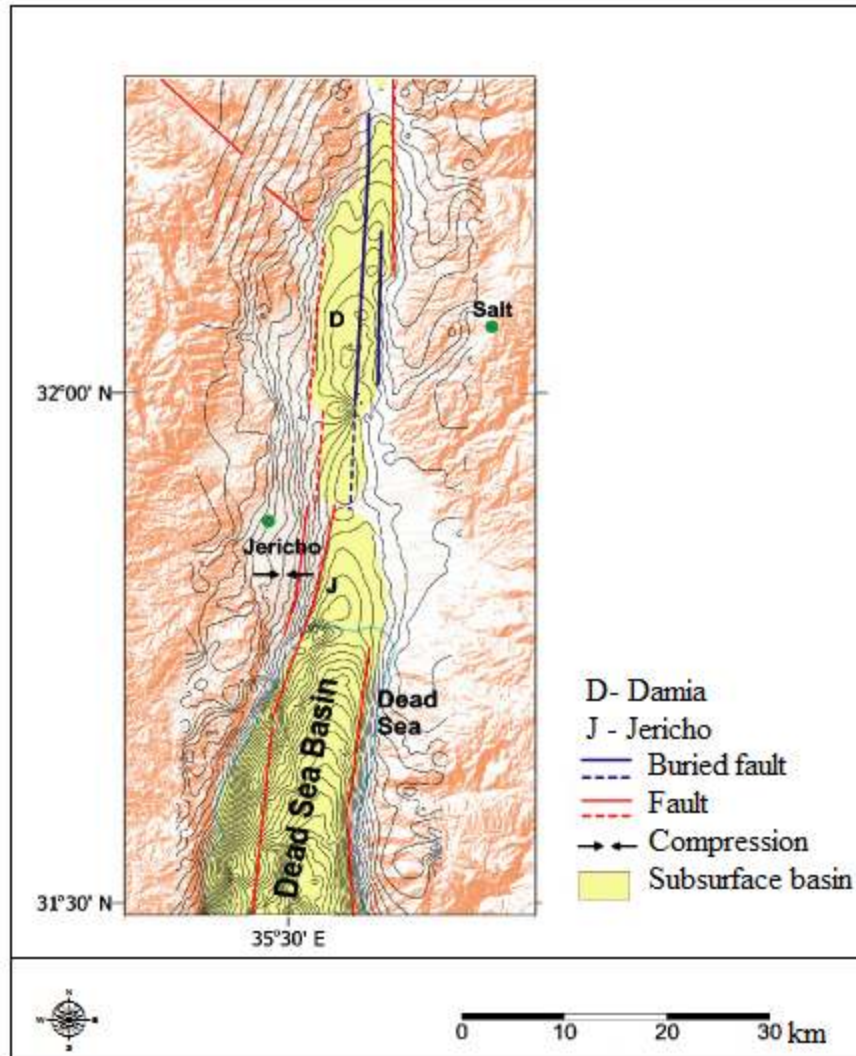
Figure 1.2: Subsurface basins along the Dead Sea transform

(Stirling *et al.*, 1996; Wesnousky, 1988)

On the surface the valley floor shows a characteristic morphological differentiation with the Al Zhor zone in the middle, it is the young Holocene erosional channel of the Jordan cutting into the Lisan Lake sediments which form now a wide terrace plain, the so-called Al-Ghor. The transition from the lower Al-Zhor to the Al-Ghor is called Al-Katar. A schematic

topographic cross section of the Jordan Valley and the neighboring escarpment is shown in Figure 1.3.a and 1.3.b. The escarpment consists of the sedimentary bedrocks which are formed by Paleozoic to Lower Cretaceous sandstones, shales, partly some evaporates and the Upper Cretaceous carbonate sequence.
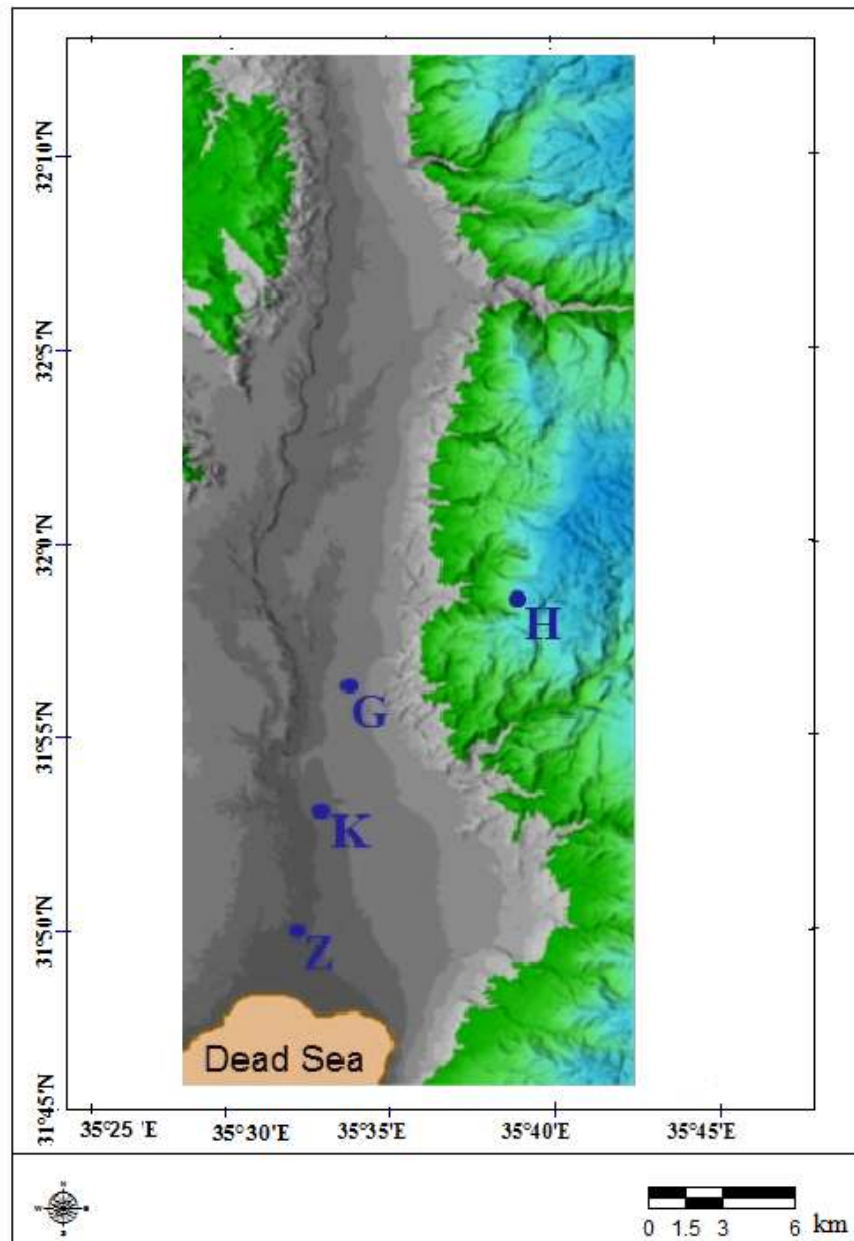
Figure 1.3.a: Digital Terrain Model showing morphological features of the Jordan River Basin (Extracted from CARTOSAT-1 image 2011). (Z:Al- Zhor, K:Al- Katar G:AL-Ghor, H: Highlands).
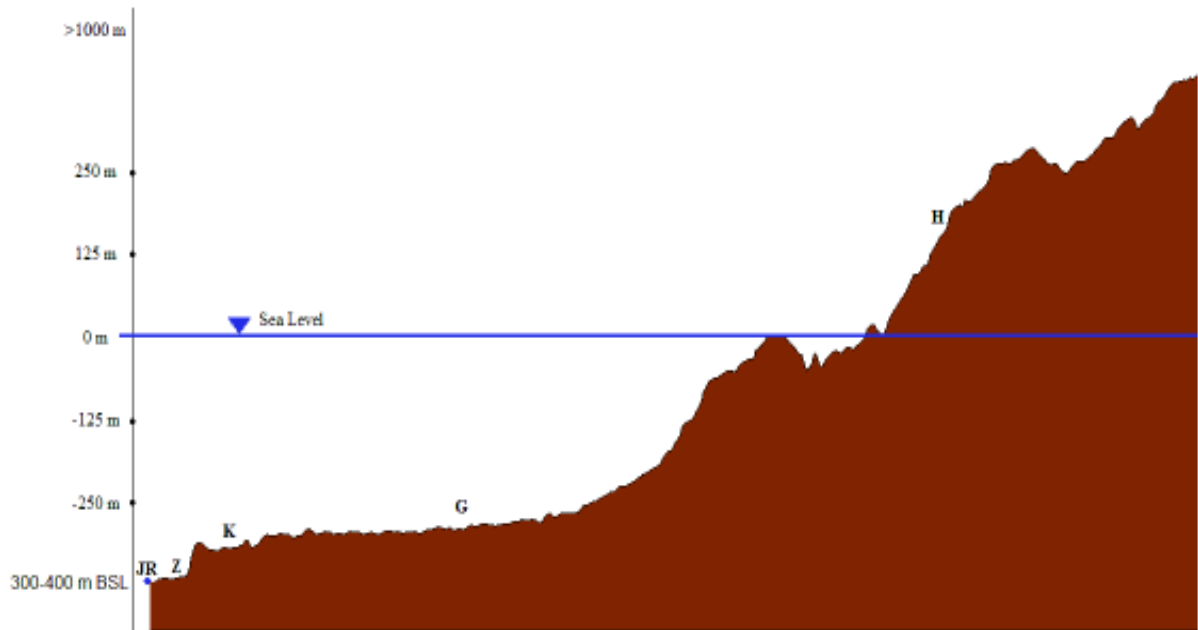
Figure1.3.b: Topographic cross section of the Jordan River Basin in Jordan.

(JR: Jordan River, Z: Al- Zhor, K: Al- Katar G: AL-Ghor, H: Highlands)

1.4 Related work

In general many different methods are used to prepare groundwater potential zones such as: ground surveys and geophysical methods, these conventional methods need a lot of work, consumes time, money and efforts. With the use of remote sensing and geographic information system (GIS) technologies, the mapping of groundwater potential zones can be achieved in shorter time. Remotely sensed data are usually cost-effective compared to the conventional methods of hydrological surveys and particularly are of great significance for remote as well as data-scarce regions (Machiwal *et al.*, 2011). Several studies were carried out in the past for identifying the groundwater potential zones by GIS based spatial modeling, for the evaluation of groundwater resources, vulnerability of groundwater and to facilitate the artificial recharge.

Waters *et al.* (1990), Engman and Gurney (1991), Chopra and Sharma (1993), Saraf *et al.* (1994), Krishnamurthy and Srinivas (1995), Bonham-Carter (1996), and Dubey *et al.* (1999) carried out studies to identify the groundwater potential zones in different areas considering parameters such as: morphological features, drainage factor and soil. Shahid *et al.* (2000) generated groundwater potential zones for Midnapur District, West Bengal, India in a soft

rock area using different parameters like: lithology, geomorphology, drainage density, slope, net recharge soil, and surface water bodies.

Rao and Jugran (2003), proved that remote sensing and GIS are useful tools for groundwater studies they have carried out studies using these tools to handle large and complex spatial data for natural resources management. Sener *et al*. (2005), Sreedevi *et al*. (2005), Ghayoumian *et al*. (2007) compared and evaluated various factors that govern the groundwater potential zones after analyzing different landforms and geomorphologic features.

Rao (2006) computed a groundwater potential index for Guntur district, Andhra Pradesh, wherein the relative evaluation of groundwater potential zones was done by integrating all the related factors of the occurrence and the movement of the groundwater resources.

Rather and Andrabi (2012) developed a spatial model using remote sensing and fuzzy techniques under GIS environment to predict groundwater potential zones, the applied fuzzy logic technique used in this analysis is found to be suitable to predict the ground water potential zones in the region under GIS environment. They recommended fuzzy modeling to be applied in other regions for the generation and prediction of the ground water potential zones.

(Al Mohammad, 2009) Integrated GIS and remote sensing for mapping Groundwater potential zones, in this study 8 different parameters were used: geomorphology, soil texture, lithology, elevation, slope, annual rainfall, drainage density, and lineament density. Sensitivity analysis testing these parameters indicated that all parameters are significant but the most effective parameters: lineaments density, geomorphology, drainage density and annual rainfall.

In Jordan several studies were carried out to identify GWPZ during in the last few years, El-Naqa *et al*. (2009) investigated the hydrogeological and groundwater resources in Wadi Araba Basin by integrating GIS, Remote sensing data, field investigations and geological knowledge of the study area. The extracted groundwater potential zones were verified using collected data from existing wells.

Hammouri *et al*. (2012) carried out a study by integrating remote sensing and GIS for locating promising areas for groundwater exploration in central parts of Jordan, this study evaluated different parameters influence the natural occurrence of groundwater such as;

lineament length an density, drainage length and density ,slope steepness, elevation, geological formation. The results were verified by water level measurements in the production wells that spread over the study area, by results of hydrogeological model of the area and by yield of production wells existed in the area.

1.5 Thesis Organization

In chapter one a background is introduced in addition to description of the related work for last 25 years , the motivation of this research is introduced in this chapter , in addition to that the main and minor objectives of this study is also presented.

Chapter two reviews the basics of groundwater potential zones as well as Analytical Hierarchy Principle and fuzzy logic. Extraction of land cover/land use thematic map from remote sensing data is discussed here; in addition to that extraction of lineaments from remote sensing data is also presented in this chapter. A complete description of the generation of digital Terrain models from high resolution satellite images is also presented.

In chapter 3, a comprehensive presentation of the methodology is outlined and explained. This chapter has two parts: in the first part, the generation of groundwater potential zones using Analytical Hierarchy Principle (AHP) is described on details, the second section of this chapter deals with the application of fuzzy logic approach in the generation of groundwater potential zones. The extraction of lineaments map, generation land cover/use map and the processes of generating digital Terrain model are presented in details.

In chapter 4, the results of the two approaches (AHP and fuzzy logic) are introduced and compared to each other, the results of the two approaches are evaluated and tested using information collected from existing wells in the area, ground truth data (results from geophysical study) is used to verify the results of the two approaches.

Finally, chapter 5 presents summary and concluding remarks on the used methods in generating groundwater potential zones. This chapter also discusses the outcome of the study and the different generated maps and results. Lastly, the importance of this study with its two approaches is presented and discussed.

The references of this research are presented in chapter 6.

2. BASIC METHODS

2.1 Creation of different thematic maps

The main aim of this study is to develop a Groundwater potential zones map for the lower Jordan valley by fuzzy logic and AHP spatial model to be used for the exploration of groundwater. Unfortunately most of the available maps don't meet the requirements of this research study, therefore it was necessary to generate all of these maps.

In this chapter general descriptions of the used methods is given in details, all the terms and the definitions used in this research are introduced and discussed. The used data consists of several thematic maps representing parameters which are essential in the occurrence and formation of groundwater, it also consists of LANDSAT images and CARTOSAT images from the years 2010 and 2011; the summary of the used data is shown in Table 2.1 below.

TABLE 2.1: USED GIS AND REMOTE SENSING DATA

No	Data	Source	Date	Resultant Map	Scale/GSD
1	Geology and Lithology	Natural Resources Authority	1989	Geology Map	1:50,000
2	Structural Geology	Natural Resources Authority	1989	Structural Map	1:50,000
3	Soil	Ministry of Agriculture	1995	Soil Map	1:50,000
4	Well Locations	Ministry of Water and Irrigation	2009	Well Locations Map	/
5	Rainfall	Ministry of Water and Irrigation	2009	Rainfall Map	/
6	ASTER30 SRTM90	NASA,METI/ERSDAC Cgiar /csi	Oct 2011	DEM , 3D Model Geomorphological parameters Lineaments map	30m, 90m

	LANDSAT 5	USGS	Dec 2010	Land cover /use	30m
	LANDSAT 7	USGS	Jun 2011	Land cover /use	30m
7	CARTOSAT1	Euro Map	Oct2011	DTM Lineaments map Geomorphological parameters	2.5m

2.2 Description of Parameters and weighting criteria

Selection of the parameters is a key factor in defining GWPZ, we can notice from previous studies that not all of the used parameters give satisfactory results; this depends on the nature of each study area. Al Saud M. (2010) summarized different studies used remote sensing for groundwater exploration from the literature for the year 1963 till the year 2008 and classified the relation between the used parameters and the results as shown in Table 2.2.

In this study 9 parameters were used to identify the GWPZ map of the study area, these parameters are: geology& lithology, geomorphology, lineament density, slope, soil type, rainfall, elevation, drainage density and land use. Weighting criteria used in this research mainly based on literature review as well as on the assessment of experts in the related fields. In further steps sensitivity analysis was carried out to determine the importance of each parameter in the generated map.

Table 2.2: Selection of studies that have used remote sensing for groundwater exploration

Authors	Year	Parameters	Results
Meisler	1963	Lineaments	Unsatisfactory
Rauch & LaRiccia	1978	Lineaments	Unsatisfactory
Taylor	1980	Lineaments ,Fracture Traces	Unsatisfactory
El-Shazly et al	1983	Geomorphic Features, Land cover, Vegetation , Geologic Units	Assumption
Seelan	1983	Lithology , Morphology , Soil , Land Use	Unsatisfactory
Salman	1983	Drainage Characteristics	Assumption
Ahmad et al.	1984	Lineaments , Drainage Intensity	Assumption
El-Baz	1992	Topography , Lineaments , Drainage	Satisfactory
Gustafsson	1994	Lineaments , Vegetation	Satisfactory
Teeuw	1995	Lineaments	Satisfactory
Sander et al.	1996	Vegetation, Drainage, Lithology , Lineaments	Satisfactory
Savane et al.	1996	Lithology , Lineaments	Satisfactory
Edet et al-	1998	Lineaments , Drainage	Satisfactory
Robinson et al.	1999	Drainage , Lineaments	Assumption
Das	2000	Geology, Geomorphology, Soils , Land Cover ,Land Use , Lineaments	Assumption
Bilal and Ammar	2002	Lineaments, Drainage , Lithology	Satisfactory
Sener et al.	2005	Geology , Lineaments, land use	Satisfactory
Kumar et al.	2007	Geomorphology, Geology, Fractures, Slope	Satisfactory
Ganapuram et al.	2008	Morphology, Geologic Structures, Drainage, Slope, Land Cover, Land Use	Assumption

From these literatures 9 parameters were selected for this study, which proofed helpful especially under the arid conditions of Jordan. They are summarized here below:

2.2.1 Drainage density (km/km^2):

Drainage density is defined as the total length of the stream in a given area (Horton 1932, 1945),it varies with a number of factors including: rock type, permeability of the surface, infiltration capacity, soil type, vegetation, relief, rainfall intensity duration and amount, antecedent rainfall conditions and human activities in time (Nagle, 2000) .

Regions with high drainage densities will have limited infiltration, promote considerable runoff, and have at least moderately erodible surface materials (Peterse *et al.*, 2011) .Thus when comparing two terrain types, the one that contains the greatest drainage density is usually less permeable, which means less groundwater recharge rate (Edet *et al.*, 1998).

A drainage network was generated Using CARTOSAT-1 data of 2.5m spatial resolution from the year 2011, which is shown in Figure 2.1.
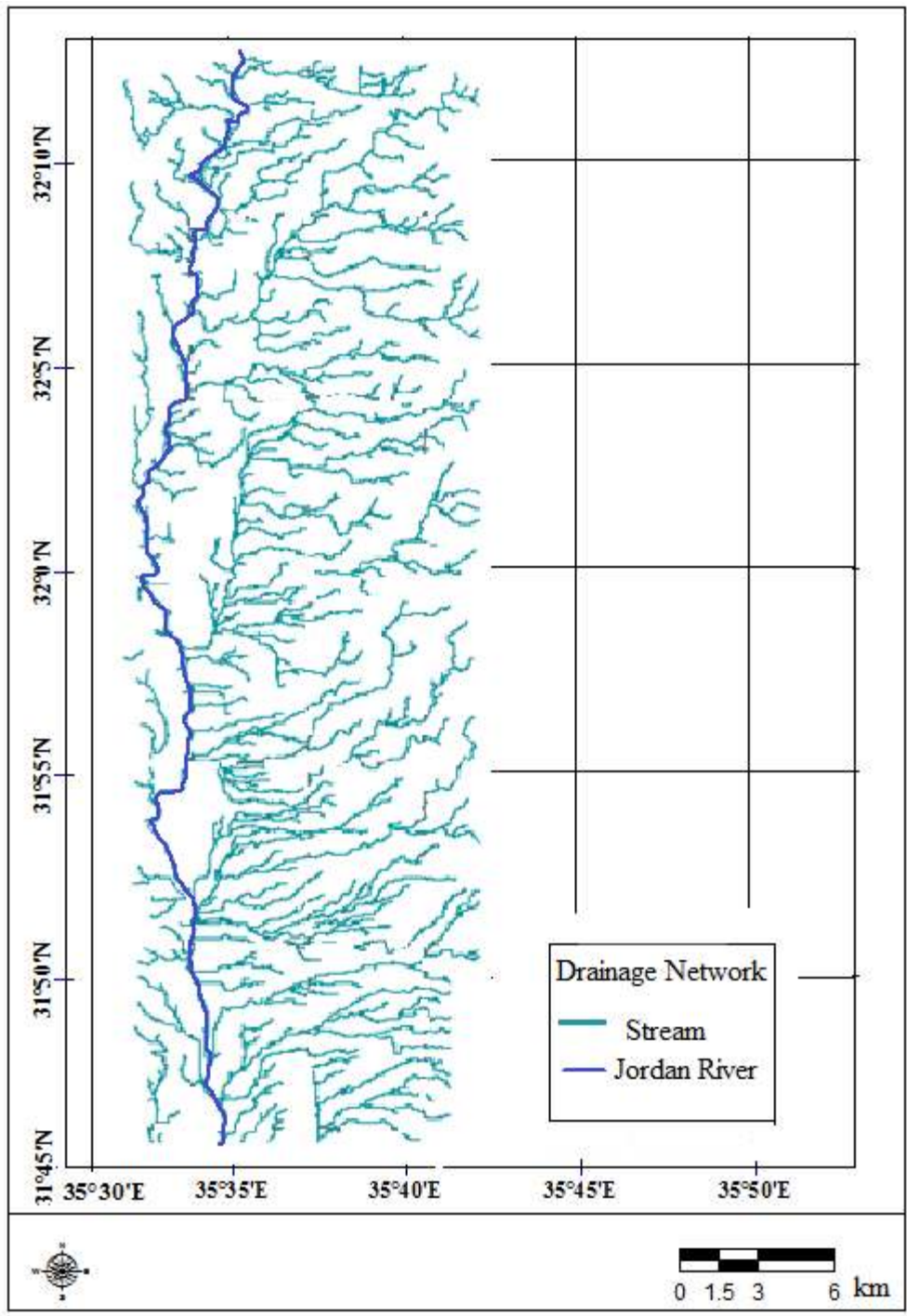
Figure 2.1: Drainage Network of the study area.

Extracted from CARTOSAT image, 2011.The pattern includes all permanent, temporarily or only episodically filled flow channels.

2.2.2 Geomorphology

On the territory of Jordan, it is possible to identify two main geomorphological unities: a rift system with the depression zone along the transform fault with the Gulf of Aqaba – Wadi Al-Araba – Dead Sea – Jordan valley, and the uplifted plate boundary with the escarpments, multi-staged plains and uplands and the trans-Jordan volcanic plateaus. The connecting link between the two units is provided by the eastern macro-slope (descent) of the Dead Sea's rift (Ufimtsev, 2008). The study area is classified from geomorphological point of view into: JV and Wadi channels, Terrace Plains in the Jordan Valley and the Jordan Valley escarpment.

1. JV and Wadi Channels: This is a flat area within the tectonic depression of the Jordan Rift Valley, with elevations varying from 210 m below sea level to 422 m below sea level. The Jordan Valley is filled by Upper Tertiary and Quaternary sediments (such as the lacustrine Lisan Marl, the alluvial fan sediments of Pleistocene age, and the recent fluvial sediments. The Jordan Valley is drained by the southward-flowing Jordan River and its western and eastern tributaries draining the surrounding mountain range (Sahawneh, 2011).

2. Jordan Valley Escarpment: This escarpment formed as a result of step faulting and flexure formations initiated during rifting and modified later by fluvial erosion during the fluvial periods of Upper Miocene to Recent time (Bender, 1974).

3. Terrace Plains in the JV: Two terraces are found in the valley: the low-lying flood plain of the Jordan River (Zor) and the Jordan Valley proper area (Ghor). These two zones are separated by a transition zone (Katar) (Arabic for 'badland') along most of the length of the valley. The Katar zone shows a dense drainage system within the Lisan Marl sediments, which indicates the role of rare rainfall and erosional processes in this arid area (Sahawneh, 2011). Figure 2.2 shows Geomorphology map of the study area.

Regions located in the escarpment are highly rated due to the characteristics of this area. In contrast with JV and wadi channels which is poorly rated area due to the presence of the lacustrine Lisan Marl formation, the alluvial fan sediments of Pleistocene age and the recent fluvial sediments. Terrace plains are moderately rated due to the presence of Zor, Katar and Ghor soils.
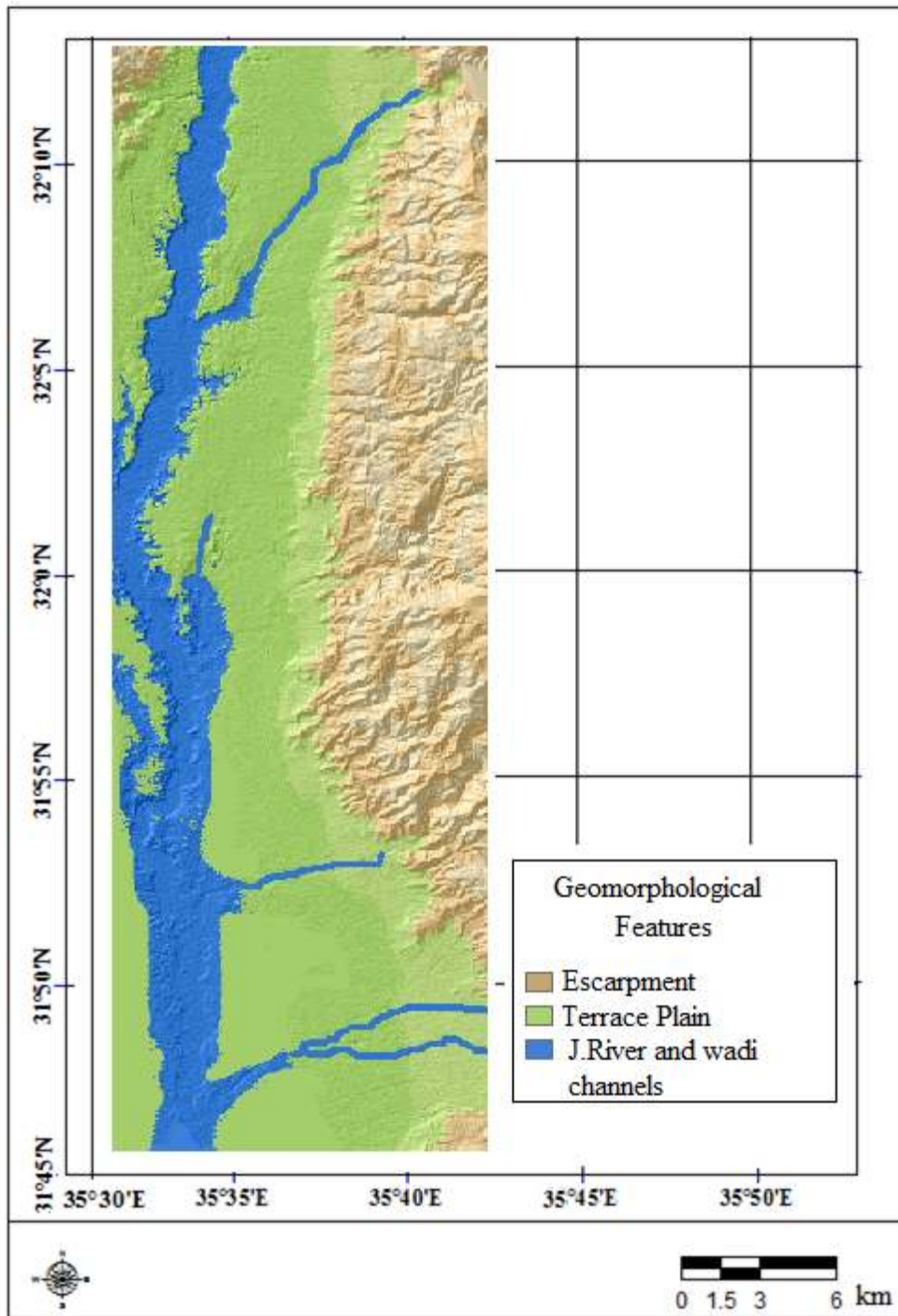
Figure 2.2: Geomorphology map of the study area.

Brown: Escarpment, Green: Ghor terrace plain+ Katar, Blue: Zor plain+ wadi channels

2.2.3 Lineaments density

Lineaments is simply defined as any feature appears as a line due to contrast in terrain or ground cover in an aerial or space image (Al Saud, 2010), it is also defined according to Shawabkeh (2001) as a simple or composite linear feature of a surface, whose parts are aligned in a rectangular or slightly curvilinear relationship and which differs distinctly from the patterns of adjacent features and presumably reflects a subsurface phenomenon. It is any feature appears as a line due to contrast in terrain or ground cover in an aerial or space image (Kocal et al, 2007). Lineaments are vital geological features that play the role of a key indicator for ground water and petroleum searching (Marghany, 2012). Presence of lineaments may act as a conduit for ground water movement which results in increased secondary porosity and therefore can serve as groundwater potential zone (Thirukumaran, 2011).

Lineaments are originated from two types of sources. Firstly, lineaments may occur due to tectonic activity, this kind of lineaments usually corresponds to faults, joints and/or lithological boundaries, the other type of lineaments is due to man-made features including roads, railroads, crop field boundaries or any kinds of variations in land use patterns (Ayten, 2005) .

Lineaments are very important from hydrogeological point of view and may provide the pathways for groundwater movement (Sankar, 2002), Lineaments are important in rocks where secondary permeability, porosity and intergranular characteristics together influence groundwater movements (Kumar and Bali, 2008). Lineaments map generated and used in this study is shown in Figure 2.3 below.
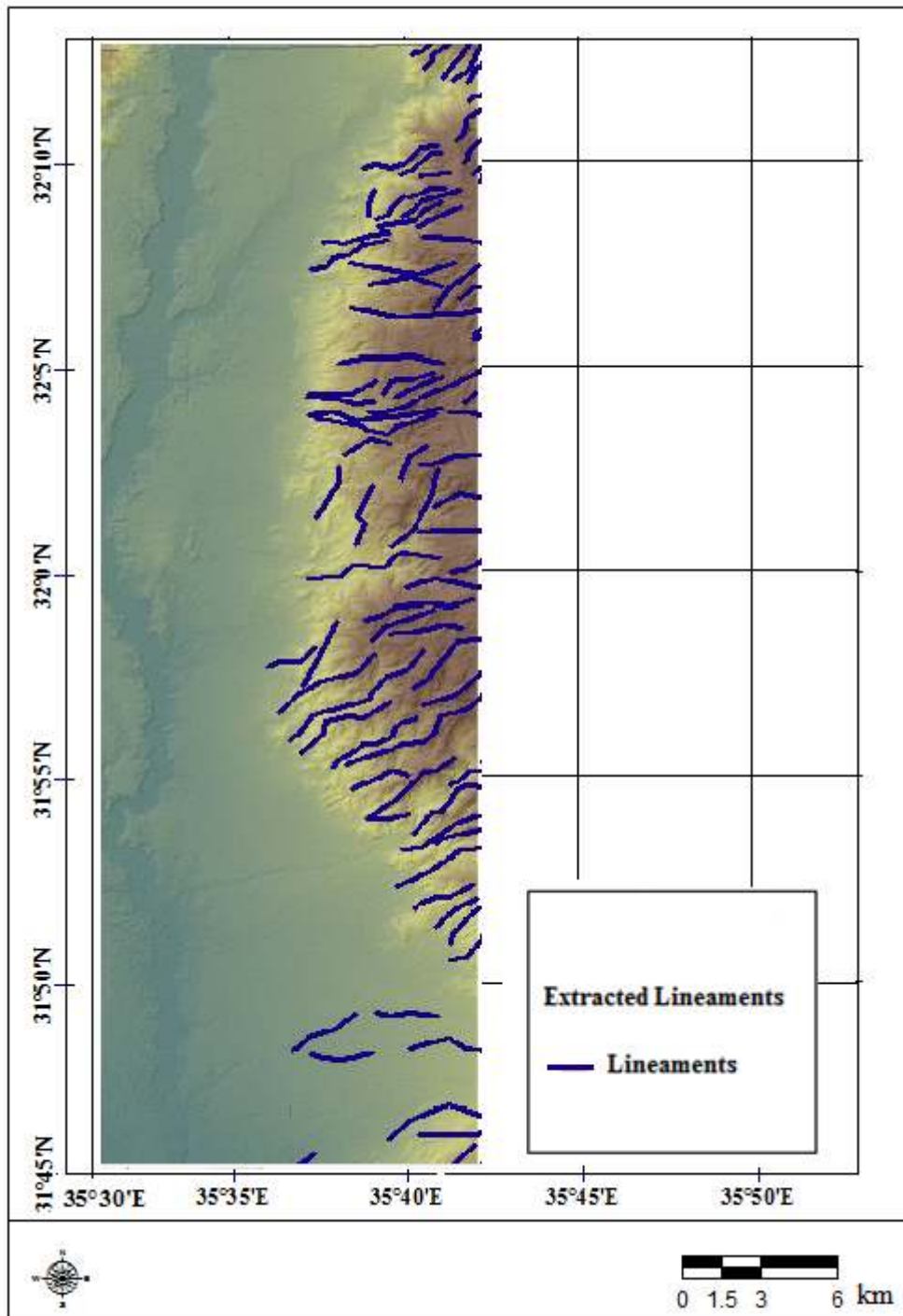
Figure 2.3: Lineaments Map of the study area

Extracted manually from CARTOSAT data 2011

2.2.4 Geology& Lithology

During the last decades, the area in general was studied by numerous researchers such as (Picards, 1931; Quennell, 1958; Daniel *et al*. 1963, Freund *et al.,* 1970; Neev and Hall, 1979; Garfunkel, 1981; Zak *et al*. 1981; ten-Brink *et al*., 1993 and 1999; Belitzky, 2002;Schultze *et al*., 2003, Al-Zoubi *et al*., 2001, 2002, 2006, 2007).

Picard (1931) was the first to describe the depression as a tectonically graben system bordered by two faults. The western boundary fault was noted as the oldest tectonic element in the study area. This fault lies along the western side of the Dead Sea Basin margin and it was assumed that it curves to the northwest away from the rift relaying with the Uja (Flexure) structure. Later the faults were recognized as to belonging to a rift system, which developed along a sinistral transform fault system, along which the Arabian plate (with Jordan) is moving northward (Freud *et al.* 1970; Garfunkel, 1981; ten-Brink *et al.*, 1999). The main strike-slip fault extends from Aqaba on the eastern side of the rift system till the southern end of the Dead Sea, where the transform movement is jumping to a the parallel fault on the western side of the Dead Sea and causing thereby in the past the opening of the pull-apart-basin of the Dead Sea. North of the Dead Sea the transform fault bend NE-ward and crossing the Jordan Valley up to Deir Alla, from where it follows the eastern margin of the rift system northward up to the Sea of Galilee. The study area (lies just east of the section where the transform fault bends to the northeast and due to the leftlateral movement causing in this area transpressional deformation patterns. This refers mainly to the deeper underground, where we have to assume an intensive block faulting of the Mesozoic rocks with elongated deformation pattern. However these rocks in the underground are covered in the study area with several hundred meters of Upper Tertiary and Quaternary sediments. According Bayer *et al*. (1989) the transform movement started in the Upper Miocene about 12 My ago and is still active today, reaching in the meantime a horizontal displacement of the Arabian Plate of about 107 km. The sedimentary section of the study area is subdivided into two parts. The pre-rift section from Paleozoic to lower Tertiary age and a syn-rift (syntectonic) section of Upper Miocene to recent age. Three relatively deep boreholes were drilled in the study area. Jericho 1 is the deepest borehole, located on the pre-rift Senonian chalk/chert in the western side of the basin and reaching Oxfordian limestone/shale at 1644 m depth, whereas the Jordan Valley 1 (JV-1), drilled in 1959 started in Pleistocene rift sediments and penetrated about 1000 m to reach the top of the Jurassic. The Jordan valley 2 (JV-2) borehole penetrated about 1400 m, where the top of the Early Cretaceous was found at a depth of

1367 m below ground. The topmost section of this well down to 560 m, including the young syntectonic sediments and late Pleistocene Lisan Marl Formation cropping out in the Jordan valley (Shawabkeh, 2001). The detailed geological description shown in Table 2.3.

The pre-rift sediments such as Triassic, Jurassic and Cretaceous formations are mainly distributed and exposed along the escarpment that defines the eastern boundary of the area. The rocks of Triassic, Jurassic and Cretaceous formations are generally distributed in the NE-SW direction. This system has folding axes in the same direction. The folds are gentle and are both synclines and anticlines (Muneizel *et al*., 1993). The system well bedded horizontally or gently dipping step down into the JV in a series of faults in the same direction as the major transform fault.

The Triassic and Jurassic systems consist of Zerqa Group, which subdivided into two formations Z1 and Z2. The Z1 formation is related to Triassic period and consists of sandstone, calcareous, limestone, shale and gypsum. The Jurassic formation Z2 mainly consists of limestone, marl, dolomite, sandstone and shale. This formation is partly outcropping in the JV side wadis (Toll, 2007).

The Cretaceous system consists of the Kurnub group K, which lies with conformity on the Azab formation Z2 of Zarqa group. The K group is a predominantly deposits at the base of Cetaceous and subdivided into two units. The lower one massive white sandstone with thin dolomite and shale bands, where the upper one is varicolored sandstone containing thin intercalations of limestone, shale, dolomite and marl.

The Kurnub group is overlain with conformity by deposits of Upper Cretaceous –Lower Tertiary. The Upper Cretaceous– Lower Tertiary systems have been divided into two groups. The lower one is termed Ajlun group and the upper part is named Belqa group.

The Ajlun group falls within the Cenomamian and Turonian epochs and outcrops extensively along the escarpment of the JV. The group is essentially a carbonate sequence and consists of seven litho-stratigraphic subdivisions (A1-7). These divisions based in water bearing characteristics of the sediments and separate the sequence in the aquifers and aquicludes.

The Belqa group ranges in age from Santonian to Lower Miocene. The carbonate rocks of this group are conformable with the underlying Ajlun group. In the study area the group subdivided into two formations B1 and B2 and its exposures occur mainly along the

escarpment in the Northern part of the JV. Both formation B1 and B2 could be recognized as an aquifer.

The Upper Tertiary system is an undifferentiated formation of the JV group, where it consists of mainly conglomerates and marls. The deposits of these formations associated with the tectonic activity which initiated the rift valley. The JV groups lie unconformable on the older systems and are overlain by Quaternary sediments.

The Quaternary system consists of the pre-Lisan terrestrial deposits, the Lisan formation and recent alluvial sediments. The Lisan formation represents lacustrine deposits and lies uncomfortably on the older system in the JV the Lisan formation appears not deformed by the tectonic activity.

The recent superficial deposits are composed of fan, talus and terrace river deposits. The terraces cut at various stages in the formation of the wadis and covered with the terrace alluvium (Toll, 2007).

The above geological descriptions show that the sediments in the study area are affected by the tectonic activity in the region. The rifting regime had a profound influence on the subsurface flow of groundwater, with the significant displacements of normal faults bringing lower aquiferous horizons in contact with shallower formations. This opened up flow paths between the deep seated aquifers of the escarpment and the shallow one in the Jordan Valley. At the same time the water still flows up along such routes, forming springs along the eastern escarpment.

The main boundary fault runs N-S parallel to the base of the eastern escarpment and over laden by different alluvial deposits. Where the E-W trending faults within the study area seems to be not appearing to inhibit the flow of groundwater and could be act as a conduit.

Geology map prepared by Natural Resources Authority (NRA, 1989) was used in this study, as shown in Figure 2.4 and summarized in table 2.3.
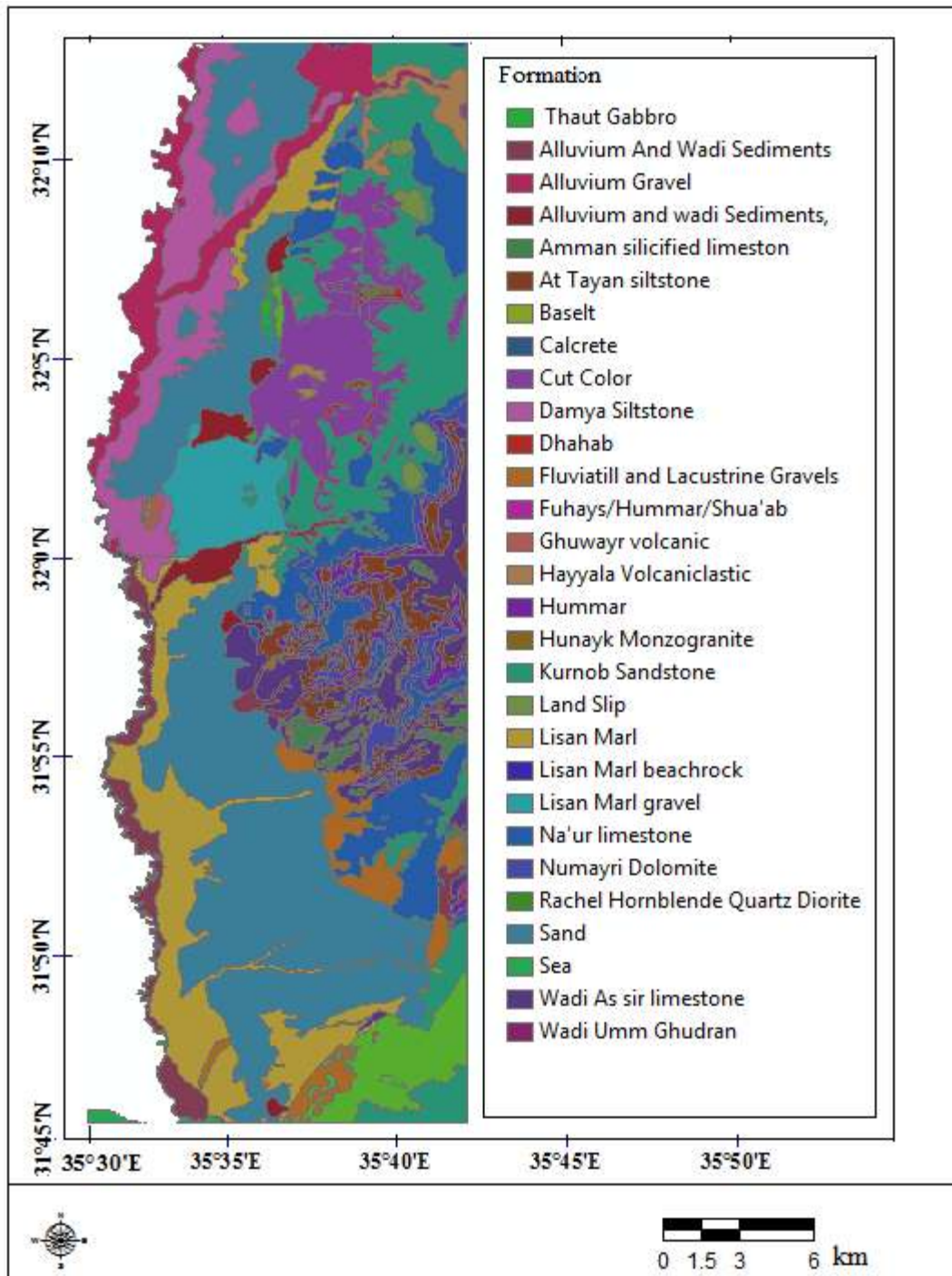
Figure 2.4: Geology map of the study area

(Reference: NRA, 1989)

Table 2.2: Geological description of the study area, (Reference: Shawabkeh, 2001)

PERIOD	EPOCH	GROUP	FORMATION	SYMBOL	LITHOLOGY
Quaternary	Holocene (Recent)		Fan, talus, terrace, river		**Sand, clay, gravel**
	Pleistocene	Jordan Valley	Lisan	J	**Marl, clay, gypsum, sand, gravel**
Tertiary	Pliocene		undifferentiated		**Conglomerate, marl**
	Miocene				
	Oligocene				
	Eocene	Belqa			
	Paleocene				
Upper Cretaceous	Maestrichtion				
	Campanion		Amman	B2	**Silicified limestone, chert**
	Santonian		Wadi Ghudran	B1	**Chalk, chalky marl**
	Turonian	Ajlun	Wadi Sir	A7	**Limestone**
	Cenomanian		Shueib	A5-6	**marly limestone**
			Hummar	A4	**Limestone**
			Fuheis	A3	**Marl**
			Naur	A1-2	**marly limestone**
Lower Cretaceous	Albian	Kurnub		K	**White sandstone with dolomite and shale; varicolored sandstone with limestone, shale, dolomite and**
	Aptian				
	Neocomian				

					marl
Jurassic		Zerqa	Azab	Z2	**Limestone, marl, dolomite, sandstone, shale**
Triassic			**Main**	**Z1**	**Sandstone, calcareous sandstone, limestone, shale, gypsum**

2.2.5 Soil type

Soil mapping and classification started in Jordan in the 1950s at a scale of 1:1,000,000, using the US soil classification system of 1938. Twelve great soil groups are recognized, the most common of them are grey desert soils, alluvial soils developed under desert climate, yellow soils developed under steppe conditions, and yellow and red Mediterranean soils developed where annual rainfall exceeds 250mm (Al-Qudah, 2000)

Soil map prepared by (Ministry of Agriculture, 1995) was used in this study, as shown in Figure 2.5, in the study area 10 different soil types are recognized as shown in Table 2.3.
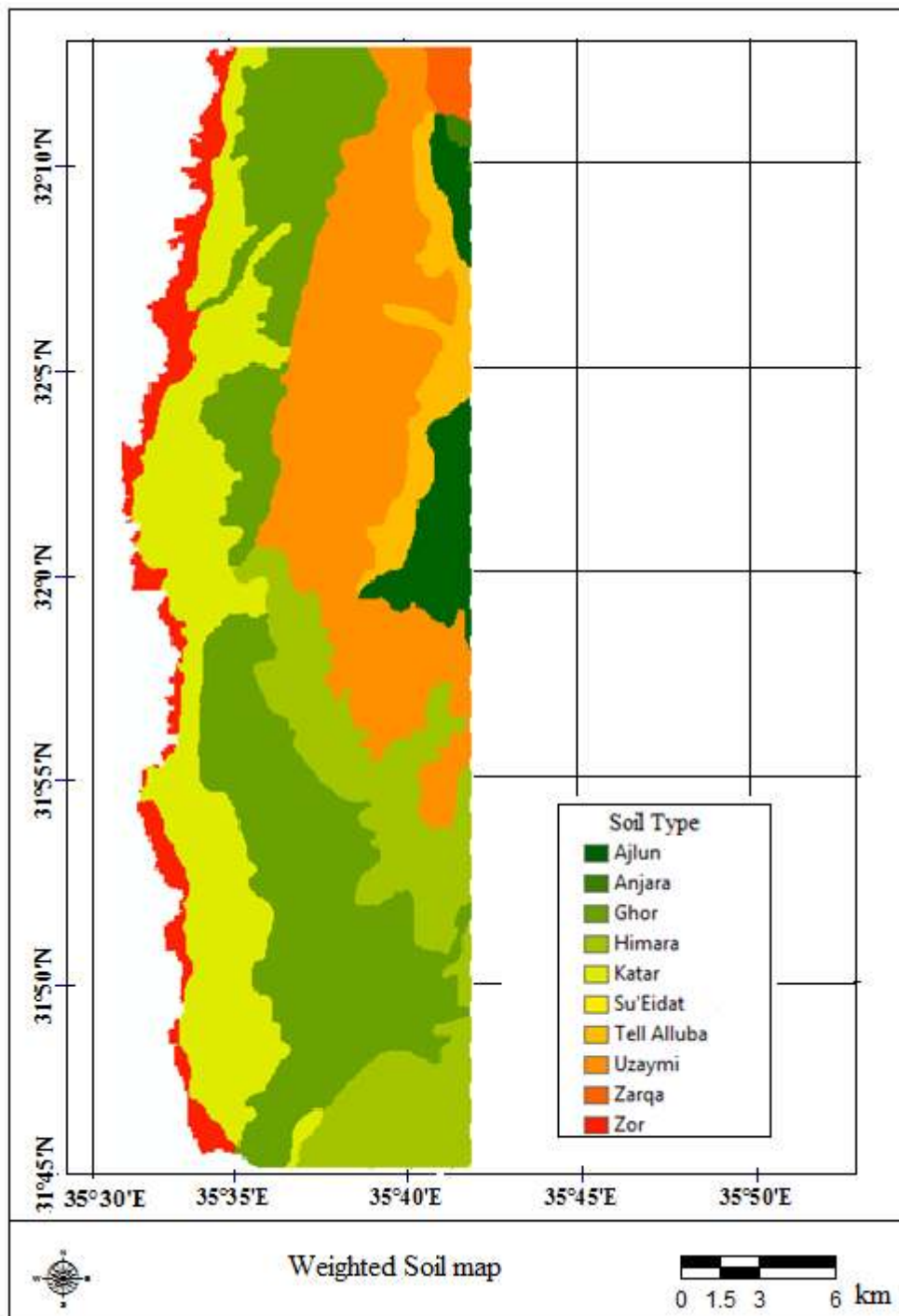
Figure 2.5: Soil map of the study area.

(Reference: Ministry of Agriculture, 1995)

Table 2.3: Characteristics of the study area soils, (Al-Mahamid, 2005)

Soil Unit	PHYSIOGRAPHY
Ajlun (AJL)	Deeply dissected limestone plateau with colluvial filled valleys and long, steep rocky slopes to valleys: undulating plateau edge and crests with rock outcrops and colluvial mantled landslip zones with Limestone boulders: altitude 500-1200 m: relative relief 250m.
Anjara (ANJ)	Deeply dissected uplands and gorges on Ajlun Group limestone, chalks and marls: very steep slopes and narrow convex crests: altitude 0 to 800m: relative relief 400m
Tell Alluba (ALL)	Deeply dissected upper part of escarpment on limestones, marls and cherts of the Ajlun and Balqa Groups: includes rock faces, landslip zones, colluvium and fans: altitude 300 to 1200m: relative relief 250-300m.
Zarqa (ZAR)	Very deeply dissected gorge and valley floor of Zarqa River cut into Kurnub sandstone: gentler upper slopes cut in Naur limestone with colluvial mantle: terrace alluvium and mixed colluvium of sandstone and limestone in valley bottom and lower slopes: xeric-aridic moisture regime and thermic and hyperthermic temperature regimes: altitude 500-650m.
Uzaymi (ZAY)	Deeply dissected middle section of escarpment in calcareous rocks of the Ajlun Group: very steep, rocky slopes on rock faces, interfluves and wadi sides with associated colluvial fans: xericaridic moisture regimes north of Dead Sea: thermic and hyperthermic temperature regime: altitude 100-900m: relative relief 300-400m.
Zor (ZOR	Narrow flood plain of the River Jordan which extends from the junction of the River Yarmuk in the north to the Dead Sea in the south, flat alluvial cover plain, cut-off meanders with sand bars of the river channel, older alluvial terraces and low lying saline plain around the Dead Sea. On the east, the Jordan River merges gently upslope into alluvium derived from erosion of the lisan marls of the Katar Unit. Altitude -387m to -210m.
Himara (HIM)	Dissected escarpment on Kurnub sandstone passing into Paleozoic sandstones. Lies downslope of the Tell Alluba and Su'eidat limestone units which are on the middle and upper part of the escarpment. Deeply dissected sandstone ridges and cliffs, have colluvial fans at their bottom slopes. Undulating sandstone plateau areas, interrupted by sandstone outcrops and dissected by wadis. Low level alluvial/colluvial fans, slope downwards towards the Dead Sea. Locally, steeper fans and dissected Lisan deposits occur. Altitude 200m to 450m.
Ghor (GOR)	Coalesced alluvial fans and terraces and pediment fans derived from the erosion of the highlands. The material is largely of calcareous origin, but there is sandstone admixture in the fans of the deeper wadis. Steep, eroded, high angle alluvial fans, give way downslope to moderately sloping stony, occasionally sandy, alluvial fans. On the margins with the Katar Unit, the fan alluvium is slightly eroded by minor wadis. Isolated hills on Lisan Formation protrude above the gently sloping fans.
Katar (KAT)	Thin strip running along the margins of the present channel of the River Jordan in the northern two thirds of the Garben, but widens out into more extensive blocks in the southern third. The unit occupies 168 Km2
Su'eidat (DAT)	Deeply dissected middle section of the escarpment to the Dead Sea in calcareous rocks of the Ajlun Group calcareous rocks. Very steep rocky scarps and free faces on limestone and convex interfluve crests with limestone pavement in places. Steep dissected upper slopes give way downslope to slightly convex colluvial fans. Near the bottom of the unit are high angle gravelly fans. Dissected slopes on tufa occur locally. Altitude 0-900m, relative relief 300m.

2.2.6 Slope Steepness

It is well known that high relief and steep slopes impart higher runoff, while the topographical depressions help in an increased infiltration (Shahid *et al*., 2000).

Slope steepness map (in degrees) was generated from high resolution DTM Using CARTOSAT-1 data of 2.5m spatial resolution from the year 2011 as shown in Figure 2.6.
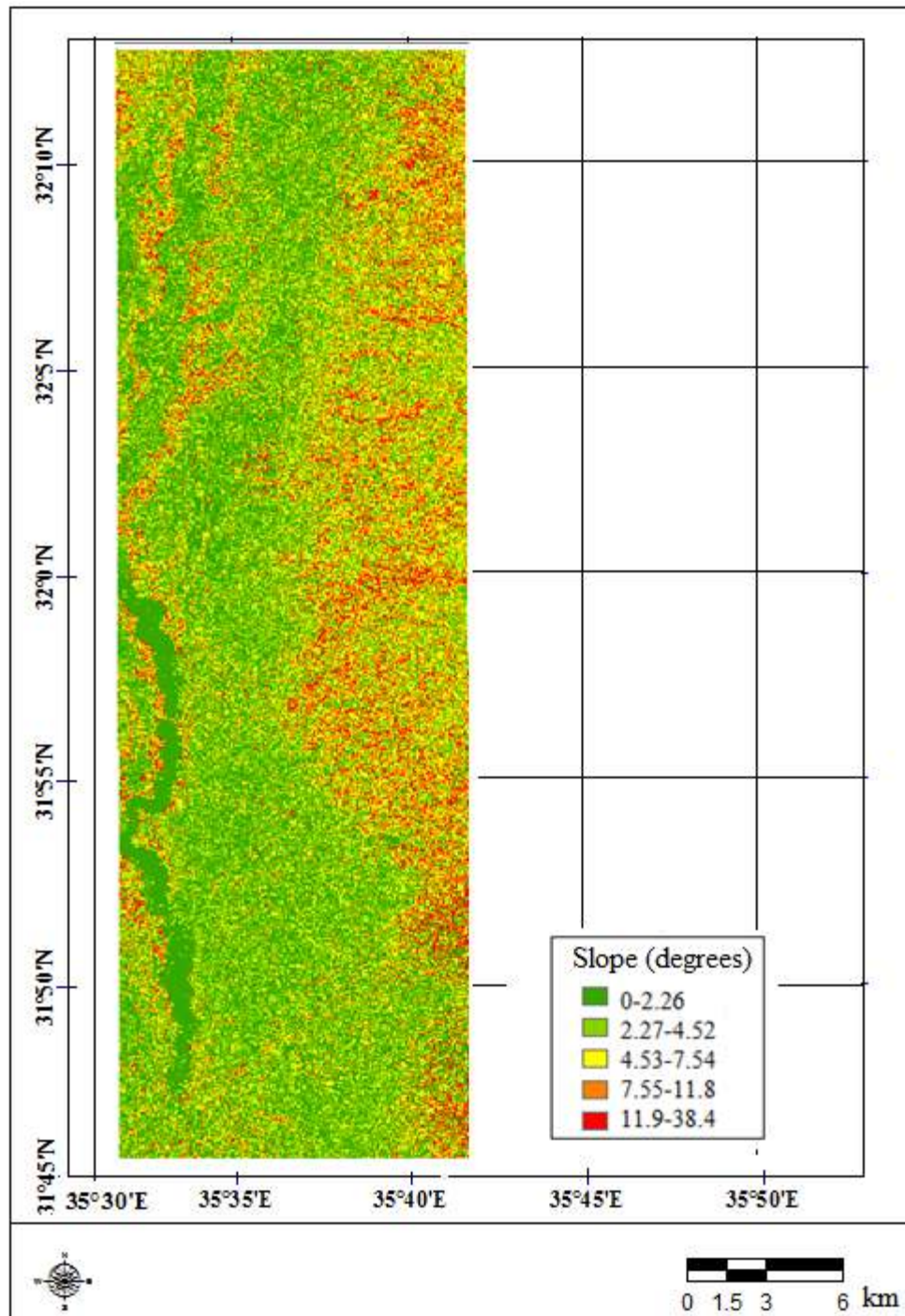
Figure 2.6: Slope steepness map of the study area

(Extracted from CARTOSAT DTM, 2011)

2.2.7 Elevation

DTM was generated using CARTOSAT-1 data of 2.5m spatial resolution from the year 2011, the elevation in the study area varies from 378m below sea level to 1020 m above sea level as shown in figure 2.7
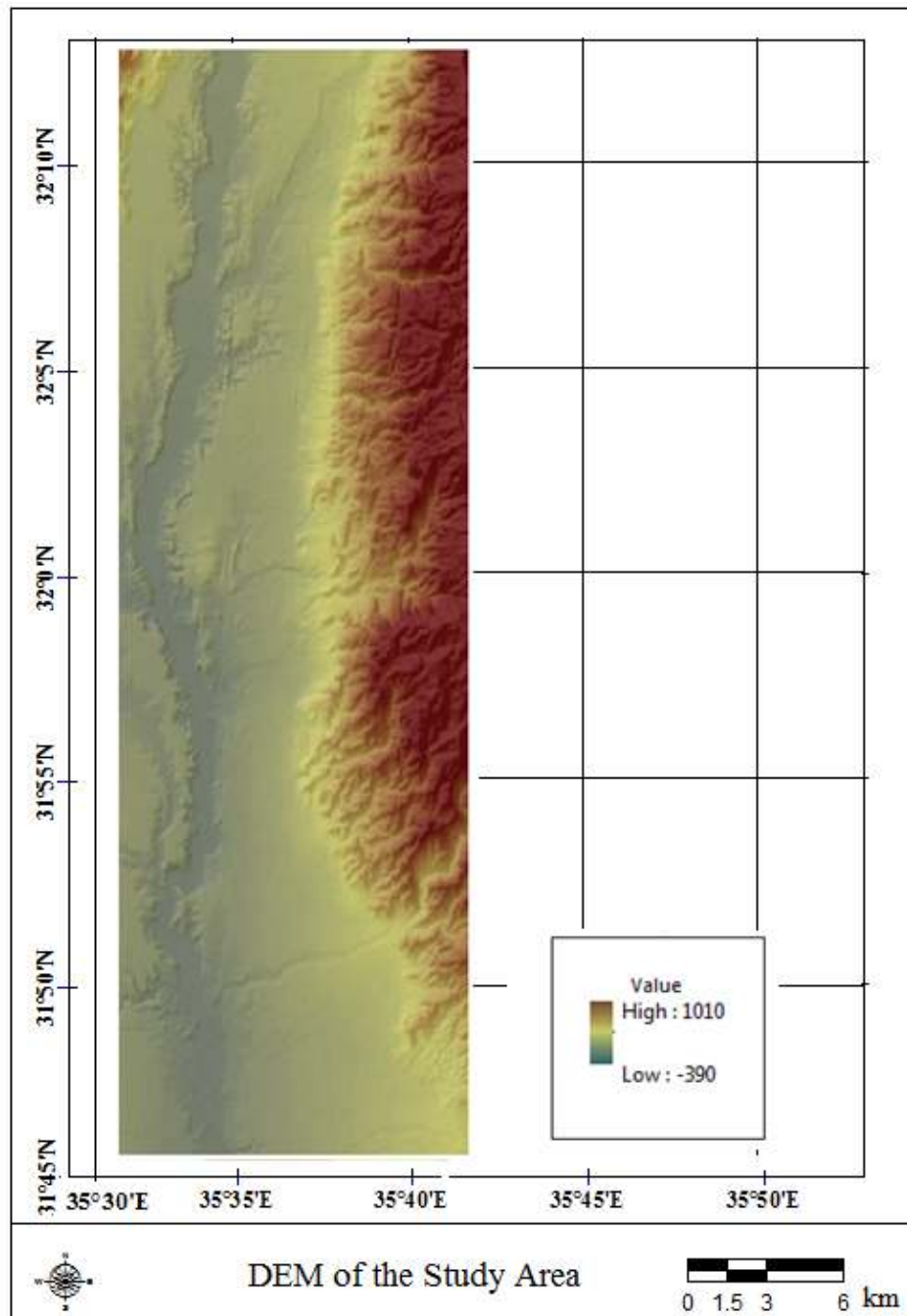
Figure 2.7: Digital elevation model of the study area

(Generated from CARTOSAT data, 2011)

2.2.8 Land cover/ Land use

The importance of land cover/ land use in the exploration of groundwater comes from its role in controlling surface runoff and infiltration it governs the behavior of water flow on terrain surface vertically and horizontally (Al-Saud, 2010), for example urban areas which have a lot of paved roads infiltrating less water than forest and green areas, in addition to that the groundwater is more preserved in the areas far from the main roads (Chuma *et al.,* 2013). Sub surface runoff is also influenced by land cover / land use. Land cover / land use also influence the percolation of precipitation from the top soil to the subsurface aquifer zones, forest cover and agriculture area represents good recharge condition as compared to the scrubland and wastelands (Thapa *et al*., 2008).

The effect of land use / cover is expressed either by reducing runoff, or by trapping water on their leaf, water droplets trapped in this way go down to recharge groundwater. Land use/cover may also affect groundwater negatively by evapotranspiration, assuming interception to be constant (Libasse, 2007), in general irrigated crops affect the groundwater recharge positively because irrigation increases the amount of water applied to the system, generally enhancing groundwater recharge (Roark & Healy, 1998)

Thematic map representing land cover/ land use of the study was extracted from LANDSAT 5 (2010) and LANDSAT 7 ETM+ of the year 2011, the thematic map identified 13 classes, these classes are mainly: different soil types, crops, trees, settlement, and green houses as shown in Figure 2.8.
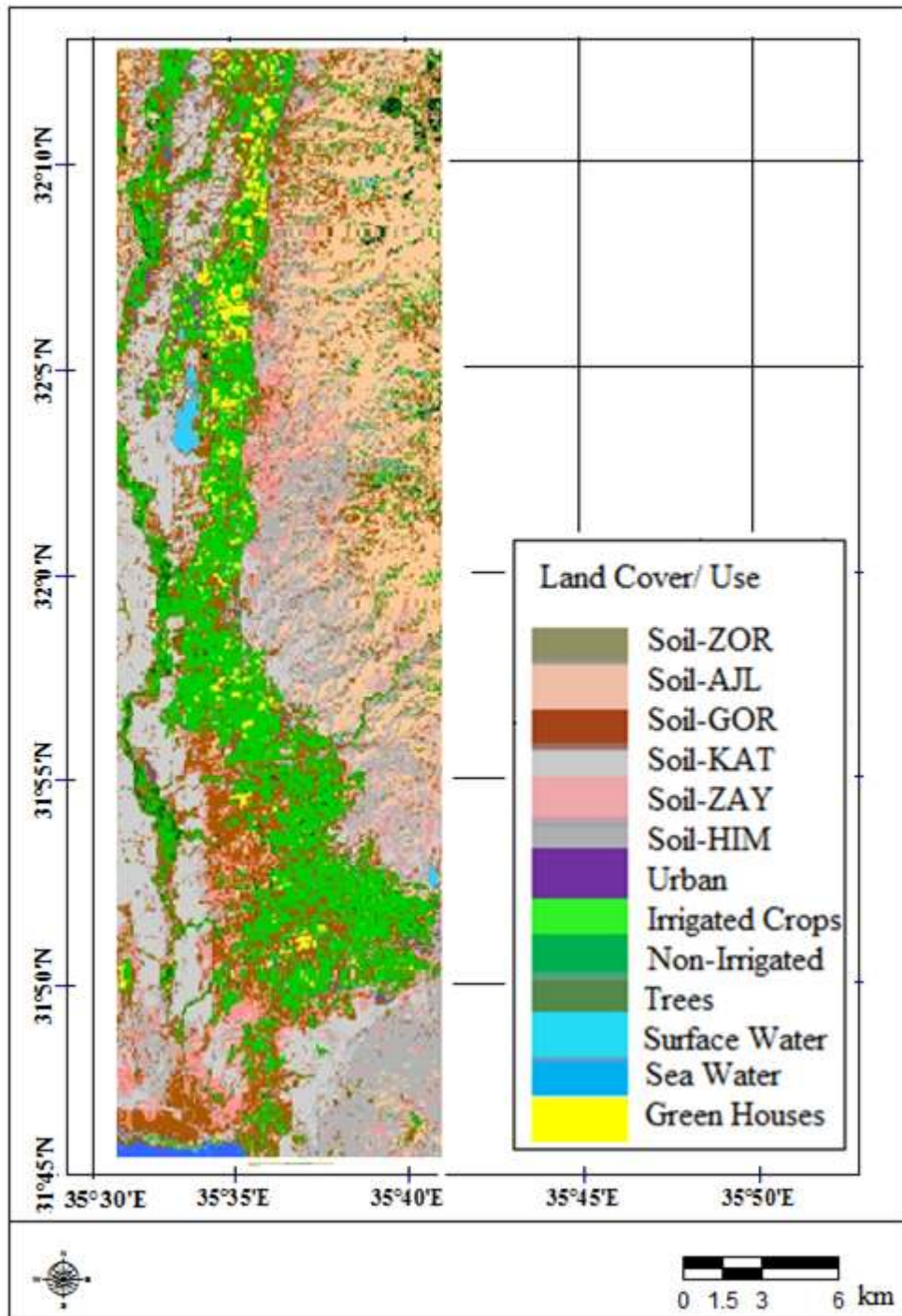
Figure 2.8: Land Cover/Use thematic map of the study area

Generated from combining LANDSAT7 June 2011 and LANDSAT5 December 2011 images.

2.2.9 Rainfall

Normally high annual rainfall distribution indicates the presence of high groundwater potential zones (Sener *et al.*, 2005), but it also depends on many other factors such as soil type and land cover. In Jordan rainfall usually starts in November and continues until the end

of April, a Thiessen polygon for the mean annual rainfall distribution is prepared as shown in Figure 2.9.
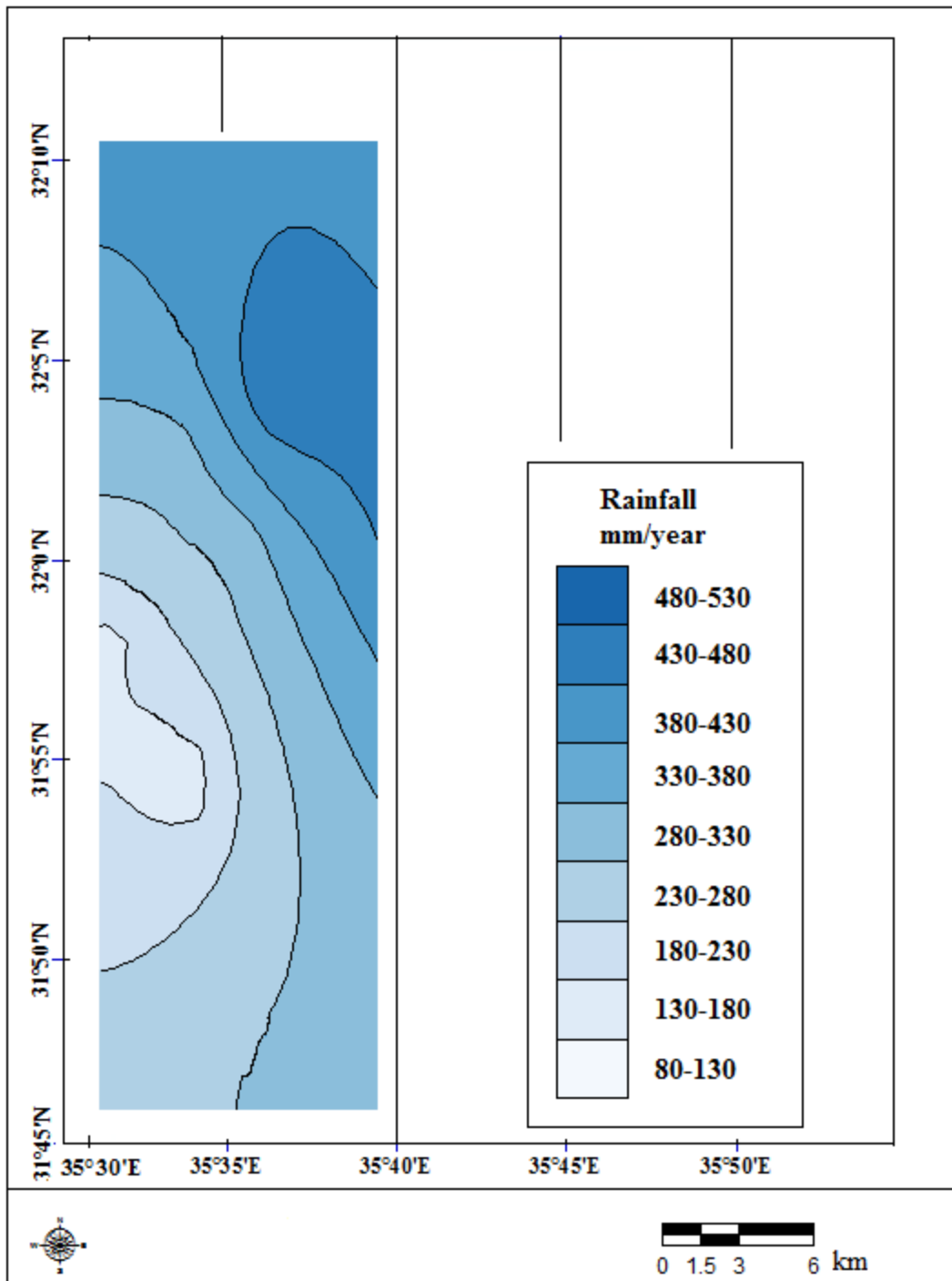
Figure 2.9: Mean annual Rainfall distribution over the study area

(Normal year average for the water years from 1937/38 to 2008/09). (Reference: Ministry of water and irrigation, 2009)

2.3 Image classification

Image Classification is the use of spectral information in a multispectral image to classify each pixel in order to produce thematic maps that represent different kinds of land cover (Lillesand & Kiefer, 2004). Remotely sensed imagery can be digitally classified through two means: the unsupervised and the supervised. Unsupervised classification is useful for preliminary spectral class discrimination. It is considered to be an exploratory procedure where the classification algorithm determines the spectral categories without supervision by the user. A supervised classification utilizes user inputted training sites to classify each pixel in the image into the various corresponding training sites (Gaber *et al.*, 2010; Gercek, 2002).

In this study supervised classification is used to generate land cover /land use thematic map of the study area using LANDSAT-5 and 7 ETM images from the year 2010 and 2011, as shown in Table 2.4, the used data basically represents two sequential seasons; winter season (December 2010) and summer season (June 2011) to show the temporal changes of land cover and its spectral characteristics, all bands of these data sets were merged to enhance the quality of the classification, except the thermal band (band-6) which has only a coarse spatial resolution of 120m.

Table 2.4: Used LANDSAT data in image classification

No	Data Source	Source	Aquision Date	Used Bands	Spatial resolution
1	LANDSAT 5	USGS	3-12-2010	1,2,3,4,5,7	30m
2	LANDSAT 7	USGS	21-6- 2011	1,2,3,4,5,7	30m

2.4 Generation of High resolution DTM

2.4.1 Introduction to CARTOSAT Imagery

A digital elevation model (DEM) is a 3D digital representation of the Earth's topography. It is often known as digital terrain model (DTM) in case vegetation and buildings are removed, while it is specified as digital surface model (DSM) if the visible surface is modeled. In this work, we simply refer to DEMs, since vegetation and buildings play a minor role. Both raster and triangular irregular network (TIN) are ways for digital representation of DEM. Traditionally DEMs/DTMs are generated from land surveying but - especially for large areas - they are also built by optical remote sensing techniques using stereo or multi-view analysis

and appropriate filtering (El-Sammany *et al.*, 2011), Synthetic Aperture Radar (SAR) or laser scanning from airborne platforms (LiDAR). (Jacobsen, 2004)

CARTOSAT-1 which is a sun synchronous satellite was launched in 2005. This satellite carries two panchromatic cameras that capture stereoscopic images over a 30 km swath at 2.5m ground resolution, enabling the creation of 3D maps (Bhardwaj, 2013) .In this study two CARTOSAT-1 stereo pairs of the lower Jordan Valley area of October 2011were used in order to extract a high resolution DEM which is used subsequently to generate an accurate and representative morphometric and hydrological parameters of the study area. These parameters are very important in the hydrological modeling and in water resources management; they provide a wealth of information regarding catchment geomorphology and hydrology. (Hancock *et al.*, 2006)

The Details of CARTOSAT-1stereo pair used for DEM generation are summarized in Table 2.5 as per the provided data with the CARTOSAT-1 mages by EuroMap 2011.

Table 2.5: Details of CARTOSAT-1stereo pair used for DEM generation

Scene	fore +26 deg	aft -5 deg
Sat ID	CARTOSAT-1	CARTOSAT-1
Sensor	PAN_FORE	PAN_AFT
Path	0304	0304
Row	0250	0250
Date Of Pass	20Oct11	20Oct11
Pass Type	SSD	SSD
Orbit No	34513	34513
Resolution Along	2.5	2.5
Resolution Across	2.5	2.5
Processing Level	STD	STD
No Scans	12000	12000
Map Projection	NONE	NONE
Datum	WGS_84	WGS_84
Ellipsoid	WGS_84	WGS_84

CARTOSAT-1 has two cameras known as: the 'Fore' camera which points 26 degrees ahead of nadir and the 'Aft' camera which points back 5 degrees behind nadir which gives excellent stereo viewing geometry, with an average base-to-height ratio of approximately 0.62 at the satellite altitude. Like many other remote sensing platforms CARTOSAT-1 operates in a near-polar, circular sun synchronous orbit at an average altitude of 618 km. Table 2.6 presents some key orbit characteristics (Willneff *et al.*, 2008).

Table 2.6: CARTOSAT-1 Specifications

Orbital altitude		618 km
Swath	Fore	29.42 km
	Aft	26.24 km
Along-track view angle	For	+26 deg
	Aft	-5 deg
Across-track resolution (at Nadir)	Fore	2.452 m
	Aft	2.187 m
Ground sampling distance(along track)		2.54 m
B/H ratio		0.62
Image size		12000*12000
Pixel size		7*7 microns
Focal Length		1945 mm

2.4.1.2 Rational Polynomial Coefficients (RPC)

The Shuttle Radar Topography Mission (SRTM) height models can be used for several applications, but it has gaps in mountainous regions, caused by the radar layover, and is not so accurate in steep areas. In addition the grid width of 3 arcsec, corresponding to approximately 92m at the equator, is limiting the morphologic details. Stereo pairs from IKONOS, QuickBird and the former OrbView-3 are expensive. The stereo pairs from the SPOT HRS only have been available for test purposes, usually only the derived height models can be bought, but they may be critical in forest areas (Büyüksalih and Jacobsen, 2008). As alternative solution the stereo sensors Cartosat-1 and ALOS/PRISM are now available; both systems with 2.5m ground sampling distance (GSD).

Generating DEMs from stereo images requires two things: a) the use of a geometric model b) the use of ground control points (GCPs). Due to non-availability of GCPs the collection of GCPs presents a significant problem, therefore a method of generating DEMs which doesn't need any GCPs is considered quit interesting for users (Krishna *et al.*, 2008). Consequently, the use of the RPC's is becoming a new standard with high resolution satellite imagery, and it has already been implemented for various high resolution sensors such as IKONOS II and QuickBird (Croitoru *et al.*, 2004).

Rational Polynomial Coefficient (RPC) can be defined as a sensor model used to determine the ground coordinates of pixels in high resolution satellite imagery. This model transforms three-dimensional object-space coordinates into two-dimensional image- space coordinates. (Grodecki & Dial, 2003) .The RPC model relates image space to latitude, longitude and height above the ground, and because this model expressed as the ratio of two cubic polynomial expressions the name (rational polynomial) came from. (Ravibabu *et al.*, 2009)

Models based on Rational Polynomial Coefficients (RPC) have recently sparked considerable interest within the remote sensing community because of their simplicity and accuracy. Indeed, some commercial, high-resolution, satellite imagery data are now supplied with RPC even though they do not disclose their physical sensor model. RPC, with stereo pairs, enable full photogrammetric processing including 3-D reconstruction, generation of digital elevation models (DEMs), ortho-rectification, block adjustment and feature extraction (Kamal *et al.*, 2009).

2.5 Groundwater Potential Zone Mapping Methods

Two methods were used in this study to organize and analyze complex decisions to determine the Groundwater potential zones (GWPZ) in the study area. The first used method is: a) Analytical Hierarchy Principle (AHP) in which weights are assigned to each parameter to reflect its relative importance. The second method is: b) Fuzzy logic approach by which membership functions are defined to reach a certain aim which is the determination of the GWPZ.

2.5.1 Analytical Hierarchy Principle (AHP)

The Analytic Hierarchy Process (AHP) is defined as a theory of measurement through pairwise comparisons which relies on the judgments of experts to derive priority scales. The comparisons are made using a scale of absolute judgments that represents how much more one element dominates another with respect to a given attribute. AHP employs a consistent

way of converting such pair-wise comparisons into a set of numbers representing the relative priority of each criterion (Saaty, 1980, 2008).

Every class depending on its ground water potential level is given a specific weight ranging from 10 to 100 and then each value is scaled depending on its weight in the matrix. These weights were assigned depending on the judgment of experts from the field of geology, agriculture, hydrogeology, metrology, hydrology and geophysics, in addition to that some weights were assigned according to the previous studies on similar areas.

In order to quantify pairwise importance nine points scale is provided as shown in Table 2.7. These numbers indicate how many times more important or dominant one element is over another element with respect to the criterion or property with respect to which they are compared (Saaty, 2008).

Table 2.7: The fundamental scale of absolute numbers for the applied factors

1/9	1/7	1/5	1/3	1	3	5	7	9
Extremely	Very Strongly	Strongly	Moderately	Equally	Moderately	Strongly	Very Strongly	Extremely
Less important								More important

Calculation of Consistency Ratio (CR) is the last step in the AHP analysis to measure how consistent the judgments have been relative to large samples of purely random judgments. If the CR is much in excess of 0.1 the judgments are untrustworthy because they are too close for comfort to randomness and the exercise is valueless or must be repeated (Coyle, 2004).

In conclusion AHP analysis is summarized in the following steps:

1: Principal Eigenvalue (λ_{max}) is computed by eigenvector technique.

2: Consistency Index (CI) is calculated using the following equation (Saaty, 1980):

$$CI = (\lambda max - n)/(n - 1)$$

Where n is the number of factors

3: Consistency Ratio (CR) is calculated as (Saaty, 1980):

$$CR = (CI)/(RCI)$$

Where, RCI = random consistency index obtained from Table 2.7.

2.5.2 Fuzzy Logic Approach for Generating GWPZ

The theory of fuzzy sets was first introduced by (Zadeh, 1965) to model uncertainty in subjective information. Fuzzy sets are defined as sets whose members are vague objects. Data can generally be received in terms of linguistic judgments and beliefs (natural language), which can then be converted to the form of fuzzy sets in order to provide a base for logical and mathematical reasoning (Zadeh, 1975).

Developing an index based on the fuzzy logic necessitates comprehension of three important parts of the fuzzy inference system, including **membership functions, fuzzy set operations and inference rules**, which are briefly described below. Each selected input or input set has a domain called the universe of discourse that is divided into subsets which are expressed by linguistic terms. The relationships between the subsets of inputs and outputs, as well as those among the subsets of inputs, are defined by if-then rules and fuzzy set operators. (Gharibi *et al.*, 2012)

Fuzzification of the entries: In this step all variable are assigned to a membership function in order to be transformed from numerical to linguistic subsets such as small, poor, excellent or high. A membership function (MF) is a function that defines how each point in the input space is mapped to a membership value between 0 and 1 (Riad *et al.*, 2011). The individual classes for each map might be defined according to their degree of membership. The classes in any map can be associated with fuzzy membership values in an attribute table. There are no practical constraints on the choice of fuzzy membership values. Values are simply chosen to reflect the degree of membership of a set, it is necessary to know that not only can a single map have more than one fuzzy membership function, but also several different maps can have membership values for the same proposition or hypothesis (Bonham-Carter, 1994).

The nature of the curve for particular type of feature varies according the potential of the Groundwater occurrence of that feature (Shahid, 2002).

Definition of the rules: Defining the rules is an important step in Fuzzy logic approach by which we link the hypothesis with the conclusion through a certainty factor. These rules are based on the form "if …then and". The knowledge in a problem-solving area can be represented by a number of rules. The task of rules definition is usually accomplished by experts with general knowledge on the specific field. There is no need for assigning weights in the criteria used.

Processing of the rules (inference): The inference step in Mamdani's approach consists of three stages (Mantelas *et al.*, 2007):

a) Aggregation: returns the fulfillment of hypothesis for every rule individually (max, sum).

b) Implication: combines aggregation's results to the rule's certainty factor (min, prod).

C) Accumulation: brings together the individual results of the variables.

Five operators can be used to combine fuzzy membership functions; the fuzzy AND, fuzzy OR, fuzzy algebraic product, fuzzy algebraic sum and fuzzy gamma operator (Bonham-Carter, 1994). All of these operators were tested in order to find the most suitable operator that could link the membership functions of this study, for example fuzzy OR is usually used to identify the highest membership values for any of the input criteria.

In general, fuzzy OR is equivalent to the Boolean OR (logical union), defined as:

$$\mu_{combination}= \max (\mu_A, \mu_B, \mu_C, \dots)$$

Where $\mu_{combination}$ is the combined fuzzy membership function, μ_A is the membership value for map A at a particular location, μ_B is the value for map B, etc. (Kayastha *et al.*, 2013)

One of the other common operators is fuzzy AND, this operator is not used in this study because it returns the least common denominator for the membership of all the input criteria. And that is not the aim of this work. According to (Zimmerman, 1996) fuzzy AND operator defined as:

$$\mu_{combination}= \min (\mu_A, \mu_B, \mu_C, \dots)$$

Many other operators could be used such as: fuzzy algebraic product which multiplies each of the fuzzy values for all the input criteria, fuzzy algebraic sum which add the fuzzy values of each set the cell location belongs to, and fuzzy gamma operation which is an algebraic product of Fuzzy Product and Fuzzy Sum, which are both raised to the power of gamma. Table 2.8 shows the whole linking fuzzy operators (Zimmerman, 1996).

Table 2.8: Fuzzy logic Operators

No	Fuzzy Operator	Expression
1	Fuzzy AND	$\mu_{combination}= \min (\mu_A, \mu_B, \mu_C , \dots)$
2	Fuzzy OR	$\mu_{combination}= \max (\mu_A, \mu_B, \mu_C , \dots)$
3	Fuzzy Algebraic Product	$\mu_{combination}= \prod_{n=1}^{n} \mu i$
4	Fuzzy Algebraic SUM	$\mu_{combination}= 1- \prod_{n=1}^{n}(1 - \mu i)$,
5	Fuzzy Gamma Operation	$\mu_{combination}= (\prod_{n=1}^{n} \mu i)^{\gamma} (1-\prod_{n=1}^{n} (1- \mu_i))^{1-\gamma}$, $0 \leq \gamma \leq 1$

Selection of Fuzzy operator depends on the type of applications and the complexity of the problem, for example using fuzzy algebraic product for large number of maps the result will be close to zero, on the other hand the same occurs but in the other extreme with Fuzzy algebraic sum ; where the result is close to 1 (Beek, 2000).

Fuzzy gamma operation is used in this study, which is defined in terms of the fuzzy algebraic product and the Fuzzy algebraic sum by the expression:

$$\mu combination= (\text{Fuzzy algebraic sum})^{\gamma} (\text{Fuzzy algebraic product})^{1-\gamma} , 0 \leq \gamma \leq 1$$

where (γ) is a parameter chosen in the range (0 , 1). Wise choice of the (γ) produces output values that ensure a flexible compromise between the "increasing" tendencies of the Fuzzy algebraic sum and the "decreasing" effects of the Fuzzy algebraic product where (γ) is a parameter chosen in the range (0, 1). When (γ) is 1, the combination is the same as the fuzzy algebraic sum; and when (γ) is 0, the combination equals the fuzzy algebraic product (Rathar et al, 2012).

Defuzzification of the output fuzzied values: is the transformation of the fuzzy set (results) into a linguistic expression or a crisp value (Bezdek, 1981). This transformation can be done by several methods such as centroid, bisector, Middle, Smallest, and Largest of Maximum; the used method in this study is the Centroid defuzzification.

Centroid defuzzification returns the center of area under the curve; this method selects the output crispy value corresponding to the center of gravity of the output membership function, the only disadvantage of this method is that it is computationally difficult for complex membership functions. The centroid defuzzification technique can be expressed as (Naaz *et al.*, 2011):

$$Z^* = \frac{\int \mu c(z).z\, dz}{\int \mu c(z)\, dz}$$

Where Z^* is the crisp output, $\mu c(z)$ is the aggregated membership function and z is the output variable.

3. METHODOLOGY AND CONCEPT

3.1 Flow-chart

The Methodology of this work consists of two parts; one part deals with the construction of the data base including the preparation of GIS and remote sensing maps, the other part includes the generation GWPZ maps by AHP and fuzzy logic approaches.

In order to achieve the objectives of this study the following general methodology is applied as shown in Figure 3.1, this methodology consists of four main steps: Database construction, Rating and modeling, Generation of groundwater potential zone map and verification of the results.
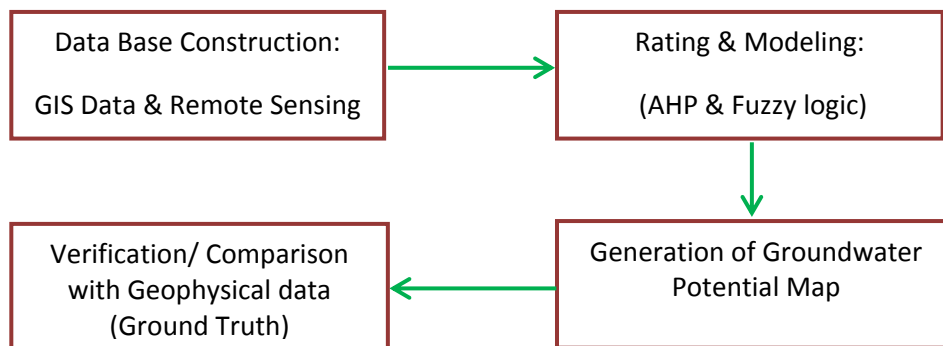
Figure 3.1: General Methodology of the work

1. **Database construction (GIS and Remote sensing data)**: data base was constructed by collecting data from different sources as shown in Table 2.1, this data consists of: a) Spatial database and b) Attribute database, the collected data was in form of tables, maps and digital maps; some of these maps were digitized, rectified, edited and processed to have digital form suitable for this kind of work.

3.2 Generation of land-cover/land-use thematic map

During the construction of the database the following maps were generated and used in the modeling:

     I.   Generation of land-cover/land-use thematic map.

    II.   Generation of Lineaments map.

   III.   Generation of high resolution digital elevation model.

The used methodology for image classification and generation of land-cover thematic map is listed below as shown in Figure 3.2:

1. Satellite Images preperation: this step consisted of : clipping the satellite image to define the study area, combining the bands , stacking the images and filling the gaps of the satellite images.

2. Defining training sites, classification and generating classification report.

3. Post processing /Accuracy Assessment.
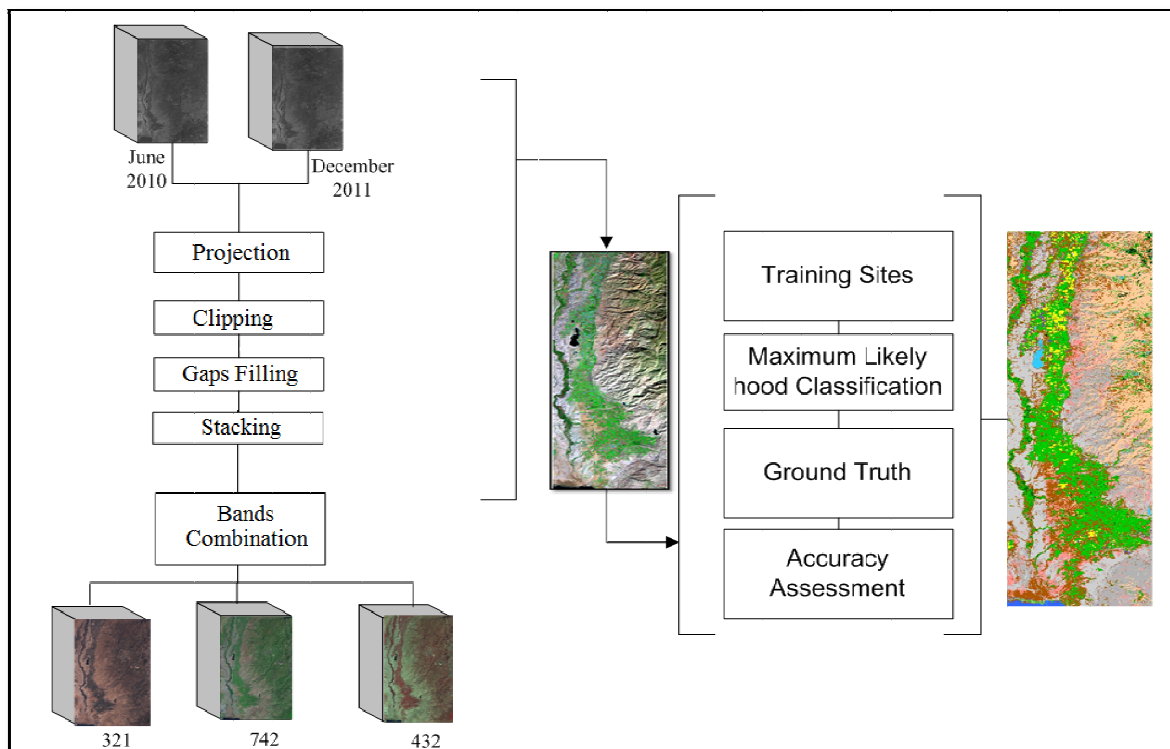
Figure 3.2: General Processes of supervised classification

3.2.1 Gaps Filling

On 31 May 2003 the Landsat 7 Enhanced Thematic Mapper (ETM) sensor had a failure of the Scan Line Corrector (SLC). Since that time all Landsat ETM images have had wedge-shaped gaps on both sides of each scene, resulting in approximately 22% data loss. (YCEO, 2011)

Different techniques could be used to solve this problem such as using mask to exclude these gaps from the classification, or using image-processing packages which have capabilities to fill the gaps. (Scaramuzza *et al.*, 2004) developed a technique to fill the gaps using data from other scenes, in this method a linear transformation is applied to the filling image to adjust it based on the standard deviation and mean values of each band of each scene. For optimal

results, the chosen images to generate a gap-filled product should be from the same season and contain minimal transient data such as clouds, snow cover or fires (AUSGEO, 2005). This technique is applied here using an add-on module in the ENVI software, the results of this process is shown below in Figure 3.3.a.
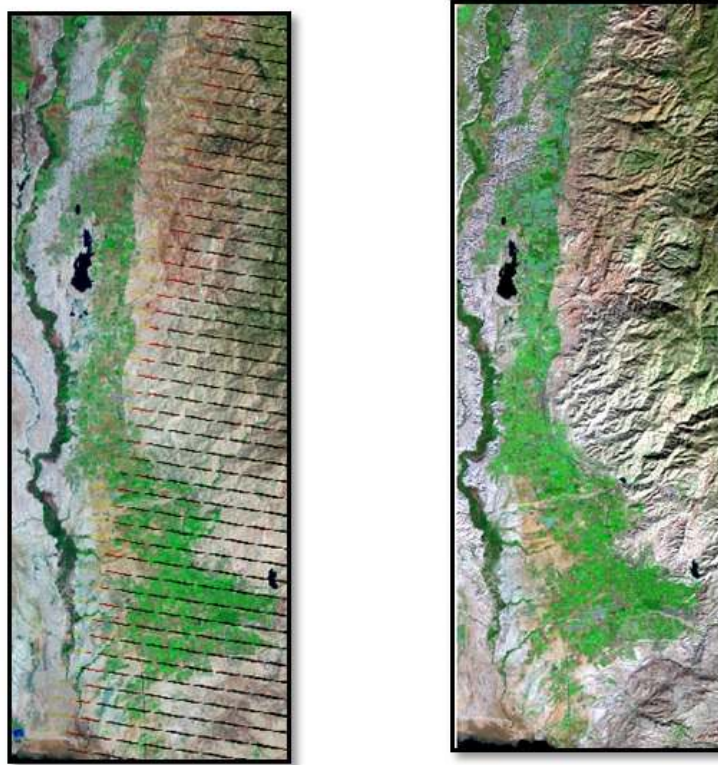
Figure 3.3: Gaps Filling of LANDSAT Image

Image (Left): LANDSAT7, June 2011, Image (Right): filled with, LANDSAT7 April 2010

3.2.2 Supervised Classification

Supervised classification unlike unsupervised classification involves the user creating training samples from land use/land cover classes that are determined to be present in the imagery, which is achieved by calculating a statistical distance based on mean values and the covariance matrix of the classes. The statistical distance expresses a probability value: an unknown pixel is assigned to a class to which it has the highest probability (Meijerink *et al.*, 2007; Biediger, 2012).

Generally there are three major steps involved in the typical supervised classification procedures as follows (Bharti, 2004):

1. Training Stage: The analyst identifies representative training areas and develops a numerical description of the spectral attributes of each land cover type of interest in the scene.

2. Classification Stage: Each pixel in the image is categorized into the land cover class it most resembles. If the pixel is not matching to any predefined class then it is labelled as rejection.

3. Accuracy Assessment: The classified image is compared with reference data to check the accuracy of the classification.

3.2.3 Training Stage (Selecting Training Samples)

It is important that the training areas be representative of the full variability of spectral response in that class (not only uniform, extreme cases), the training sites must be large enough to allow a significant and reliable determination of the spectral signatures. Lillesand *et al.* (2004) recommend that a minimum of 10 N to 100 N pixels be part of training areas, where N is the number of spectral bands and King (1999) recommended for Landsat data 70 to 700 pixels per class.

Swain and Davis (1978) recommend as a practical minimum that 10N training pixels per spectral class be used, with as many as 100N per class if possible. For data with low dimensionality those numbers can usually be achieved, but for hyperspectral data sets finding enough training pixels per class is extremely difficult.

In this study 13 classes were defined as shown in Table 3.1. Feature space decision rule determines whether or not a candidate pixel lies within the nonparametric signature in the feature space image. When a pixel's data file values are in the feature space signature, then the pixel is assigned to that signature's class (Sharma *et al.*, 2013), in Figure 3.4 overlapping of 5 classes in feature space is shown.

Table 3.1: Land-cover/Land use classes

ID	Class
1	Soil-ZOR
2	Soil-AJL
3	Soil-GOR
4	Soil-KAT
5	Soil-ZAY
6	Soil-HIM
7	Urban
8	Irrigated Crops
9	Non-Irrigated Crops
10	Trees
11	Surface Water
12	Water
13	Green House
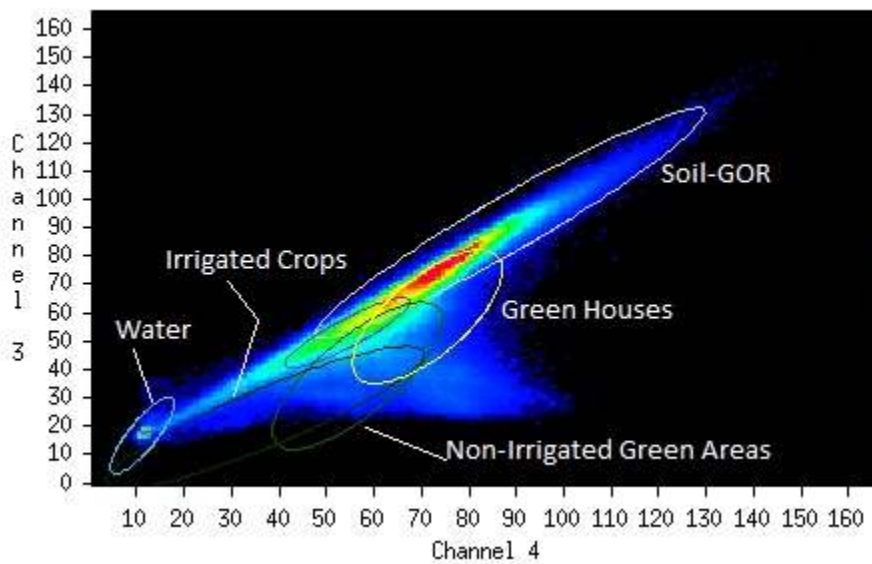
Figure 3.4: Overlapping of 5 Classes in Feature space

(Band 4: NIR vs. Band 3: R)

Bands 3 (R) and 4 (NIR) were chosen to display because they have dissimilar spectral responses, thus spreading the ellipses of the classes spectral ranges over a larger area allowing for easier interpretation (Schnetzer, 2007).

3.2.4 Classification Stage

In the classification stage, the image is classified according to classification method such as: minimum distance, parallelepiped and maximum likelihood. In the current study, the maximum likelihood classifier is used. The use of this classification method assumes that the spectral response of each class is normally distributed. The spectral response of each class can be described by two parameters: the mean vector and the covariance matrix. Maximum Likelihood assumes that the statistics for each class in each band are normally distributed and calculates the probability that a given pixel belongs to a specific class. Each pixel is assigned to the class that has the highest probability (Richards, 1999). The result is a series of bell shaped distributions on a three dimensional surface called the probability density function (Lillesand *et al.*, 2004).

3.3 Extraction of Lineaments Map from Remote Sensing Data

There are basically three methods for obtaining lineament maps from remotely sensed images, the first method is spatial convolution filtering methods for lineament extraction, the second method is called multiband analysis and finally the third one is automatic lineament extraction methods (Kocal, 2004), extracting lineaments from remote sensing data is also classified as:

- Manual Lineament Extraction: by visual interpretation.

- Semi-Automatic Lineament Extraction: using computer assisted techniques based on some digital image analyses techniques and visual interpretation.

- Automatic Lineament Extraction: using computer assisted techniques.

Work methodology used in this study for lineament extraction is a combination of the above methods; the working scheme is summarized in Figure 3.5
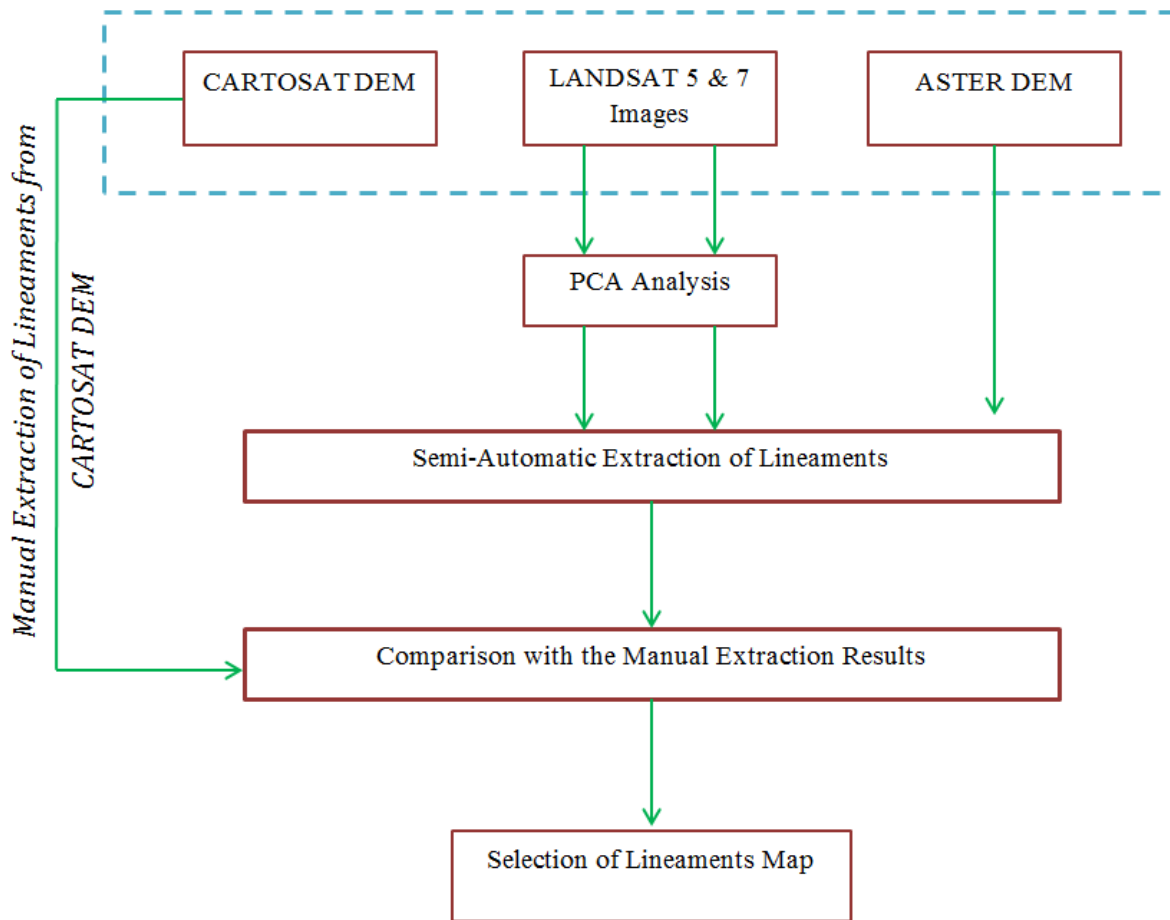
Figure 3.5: Work Methodology for extracting lineaments map

In this study different data sets were used to extract lineaments map of the study area; LANDSAT-7 images from the year 2011, LANDSAT-5 from the year 2010, ASTER DEM from the year 2011 and CARTOSAT DEM from the year 2011.

Principal component analysis (PCA) were carried out to select influential TM bands of LANDSAT-5 and 7 images for lineaments extraction, PCA is used in order to get rid of the redundancy present through the bands of the image and also to represent nearly the whole of the available information in three bands(Suzen and Toprak, 1998). In general the first component of the PCA consists of both near and middle-infrared information (Bands 4, 5 and 7), and the color composite of the PCA provide a good option for visual interpretation, thus lineaments is easily identified using PCA of the Landsat ETM image, which removes redundant information from visible and NIR multi-spectral data (Jensen, 1996; Nama, 2004; Sarp, 2005).

Table 3.2 shows the determined Eigenvalues of LANDSAT-5 and 7, the three highest values of each set were selected for this work. According to the results the used false color combination for LANDSAT 5 is: 5,4,1 and for LANDSAT7 is : 7,5,4.

Table 3.2: Eigenvalues of the used LANDSAT bands

LANDSAT-5 TM Band	Eigenvalue	LANDSAT-7 TM Band	Eigenvalue
1	856	1	39
2	21	2	164
3	68	3	143
4	350	4	198
5	321	5	197
7	6	7	490

3.3.1 Manual Extraction Procedure

The main advantage of manual extraction is that it is easy to detect the non-geological lineaments such as roads, fences, field boundaries with human eye. Deleting the vectors that correspond to the non-geological features will increase accuracy and enhance the applicability of the methodology in terms of detecting the discontinuities. (Kocal, 2004)

The manual extraction can be summarized as shown in Figure 3.6 into the following steps:

1. Selection of the image to be used in the extraction.

2. Applying enhancement filters.

3. Visual lineament tracing (digitization).

4. Assessment of the resulted lineaments.
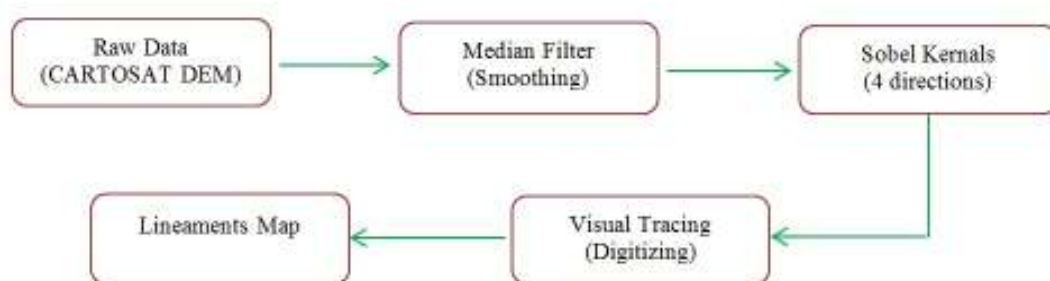
Figure 3.6: Flow chart of the used manual extraction of the lineaments

Raw data (CARTOSAT DEM) is smoothed with an average low pass filter in order to eliminate the noise, median filter is used for this purpose by which the neighboring pixels are ranked according to brightness (intensity) and the median value becomes the new value for the central pixel.

In particular, median filters offer three advantages (Rajeswari and Jeyaselvi, 2012):

a. No reduction in contrast across steps, since output values available consist only of those present in the neighborhood (no averages).
b. Median filtering does not shift boundaries, as can happen with conventional smoothing filters (a contrast dependent problem).
c. Since the median is less sensitive than the mean to extreme values (outliers), those extreme values are more effectively removed.

Many different enhancement filters could be applied to enhance the visual tracing of the lineaments such as Laplacian, Sobel and Prewitt filters. Four directional-filters were used to delineate the lineaments in the study area using Sobel filter. The used directional filters are shown in Table 3.3:

Table 3.3: Sobel directional filters for the delineation of lineaments

N-S(Vertical)			NE-SW (Diagonal)		
-1	0	1	-2	-1	0
-2	0	2	-1	0	1
-1	0	1	0	1	2
E-W (Horizontal)			NW-SE (Diagonal)		
-1	-2	-1	0	1	2
0	0	0	-1	0	1
1	2	1	-2	-1	0

Using Sobel enhancement filter the out-coming result is more satisfactory than the Prewitt kernels but the lineaments have a segmented appearance due to the increased spatial frequency. (Suzen and Toprak, 1998).

3.3.2 Semi-Automatic Extraction of lineaments Map

Automatic extraction of lineaments is basically computer-aided method for lineament extraction; if there is manual interference in the processes such as (removal of non-geological lineaments like roads, field boundaries, etc…) the method is called as semi-automatic. A comparison between manual and automatic methods for lineament extraction is shown in Table 3.4 (Hung, 2001).

Table 3.4: Comparison between Manual and the Automatic lineament extraction methods

Manual lineament extraction methods	Automatic lineament extraction methods
Depend on the quality of the performance of the image (on paper and/or screen)	Depend only on the quality of the image
Partly depend on the complexity of the research area	Totally depend on the complexity of the research area
Strongly depended on human experience and ability	Totally depend on the mathematical function of software
Takes a lot of time	Very quick method
Strong effect of human subjectiveness	Little effect of human subjectiveness
Easy to distinguish the kind of lineament (tectonic setting, manmade, …)	Can't recognize the kind of lineament, so the result may be confused.
Simple but subjective method	Complex but objective method

LINE algorithm in PCI Geomatica-10 software was used to extract lineaments automatically from remote sensing data, LINE algorithm has 6 parameters for lineament extraction process, and these parameters are mentioned in table 3.5 below.

Table 3.5: PCI Geomatica LINE algorithm parameters

Parameter	Description	Default Value	Optimal Value
RADI	Radius of filter in pixels	3	10
GTHR	Threshold for edge gradient	15	60
LTHR	Threshold for curve length	15	30
FTHR	Threshold for line fitting error	2	3
FTHR	Threshold for angular difference	10	30
DTHR	Threshold for linking distance	30	3

LINE algorithm consists of three stages: Edge Detection, Thresholds, and Curve Extraction, these steps are summarized in the PCI Geomatica 10.1 Online User's manual as follows:

1. The edge detection algorithm is applied to produce an edge strength image where the input image is filtered with a Gaussian function whose radius is given by the RADI parameter.

2. Threshold is applied to the edge strength image to obtain a binary image by the GTHR parameter.

3. Curves are extracted from the binary edge image by several steps: a thinning algorithm is applied to the binary edge image to produce pixel-wide skeleton curves. Next, a sequence of pixels for each curve is extracted from the image. Any curve with the number of pixels less than LTHR is discarded. The extracted curve is then converted to vector form by fitting piecewise line segments to it. The resulting polyline is an approximation to the original curve where the maximum fitting error (distance between the two) is specified by the FTHR parameter. Finally, the algorithm links pairs of polylines that satisfy the following criteria. (PCI Geomatica Online User's manual, 2001)

Different trials were done to set proper thresholds of the lineament extraction algorithm parameters, the selection of the parameters depended on trial and error, and according to previous studies as shown in Table 3.6.

Table 3.6: Used LINE algorithm parameters in previous studies

Parameter	ASTER (Hung et al,2005)	TM (Hung et al,2005)	SPOT (Abdullah et al, 2009)	IKONOS (Kocal et al,2007)	BAND-4 of LANDSAT-5 used in this study
RADI	5	5	12	5	10
GTHR	10	10	90	20	25
LTHR	7	3	30	10	20
FTHR	3	3	10	2	3
FTHR	7	7	30	20	20
DTHR	3	3	20	1	5

In this research the importance of LANDSAT bands and Advanced Spaceborne Thermal Emission and Reflection Radiometer (ASTER) DEM was studied to determine the best remote sensing data for Semi-Automatic extraction of lineaments, a comparison between the variables of the extracted lineaments form these data are shown in Table 3.7.

Table 3.7: Comparison between the extracted lineaments from different sources

Parameter	Number of lineaments	Min. length (km)	Max. length (km)	Total length (km)
LANDSAT5, Band 4	203	0.5	4.8	145
LANDSAT5, Band 5	145	0.6	3.1	112
LANDSAT5, Band 1	63	0.5	2.2	49
LANDSAT7, Band 7	198	0.4	3.5	129
LANDSAT7, Band 5	111	0.5	3.1	32
LANDSAT7, Band 4	183	0.6	4.1	121
ASTER DEM	73	0.3	3.7	56

It is clear from Table 3.7 that band4 of LANDSAT-5, band-7& band-4 of LANDSAT-7 have the largest number of lineaments followed by band-4 of LANDSAT-7, also these bands have the longest lengths of lineaments among the all other extracted lineaments. All the data were scaled in order to compare the revealed results (Abdullah *et al.*, 2009), and to select the best data that could describe the situation of lineaments in the study area as shown on table 3.8.

Table 3.8: scaled extracted lineaments parameters from different sources

Parameter	Number of lineaments	Min. length	Max. length	Total length	Score (SUM)
LANDSAT5, Band 4	1.00	0.67	1.00	1.00	3.67
LANDSAT5, Band 5	0.59	1.00	0.35	0.71	2.64
LANDSAT5, Band 1	0.00	0.67	0.00	0.15	0.82
LANDSAT7, Band 7	0.96	0.33	0.50	0.86	2.66
LANDSAT7, Band 5	0.34	0.67	0.35	0.00	1.36
LANDSAT7, Band 4	0.86	1.00	0.73	0.79	3.38
ASTER DEM	0.07	0.00	0.58	0.21	0.86

Band-4 of LANDSAT-5 has the largest score compared to the other bands; therefore this band is selected for the comparison with the results from manual extraction method.

3.4 Generation of DTM and Geomorphological parameters

3.4.1 Generation of High resolution DTM and Extraction of Morphometric Parameters

Working with High resolution space-borne remote sensing image data presents many alternatives which could be integrated into remote sensing applications with high level of details (Krishna *et al.*, 2008). As shown in Figure 3.7, generation of high resolution DTM from satellite images requests several working steps summarized as:

1. Collection of Ground control points (GCP's).

2. Generation of Digital surface model (DSM).

3. Filtering and Refinement of the generated Digital terrain model (DTM).
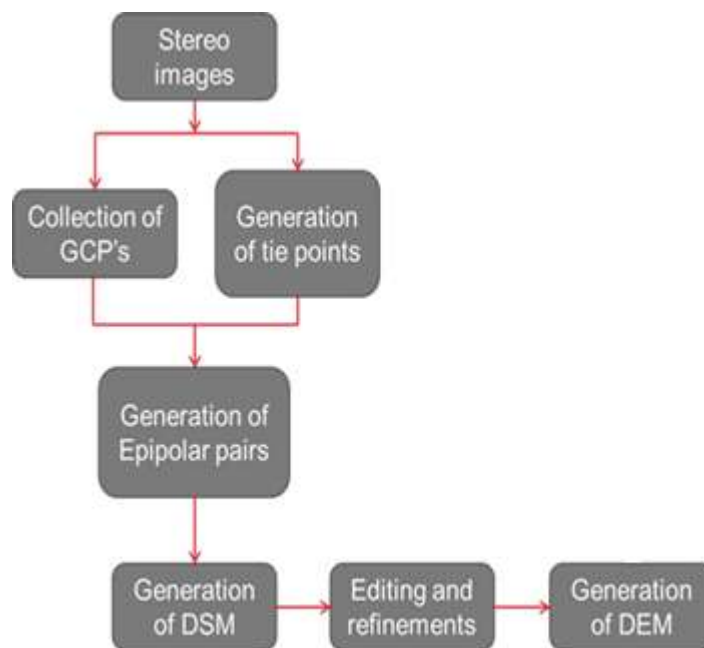
Figure 3.7: Generation of DEM processes

3.4.2 Collection of Ground Control Points (GCP's)

The collection of GCP's was done using differential Global Positioning System (DGPS), 28 ground control points (GCP's) were collected from the field covering the two stereo pairs of the study area as shown in Figure 3.8, these GCP's are used during the generation of the DTM as seed vertices to enhance the relative position of the model. In general the number of GCPs is a function of different conditions such as: the method of collection, the sensor type and resolution, the image spacing, the geometric model, the study site, the physical environment, GCP definition and accuracy and the final accuracy of the DTM (Aguilar, 2008).
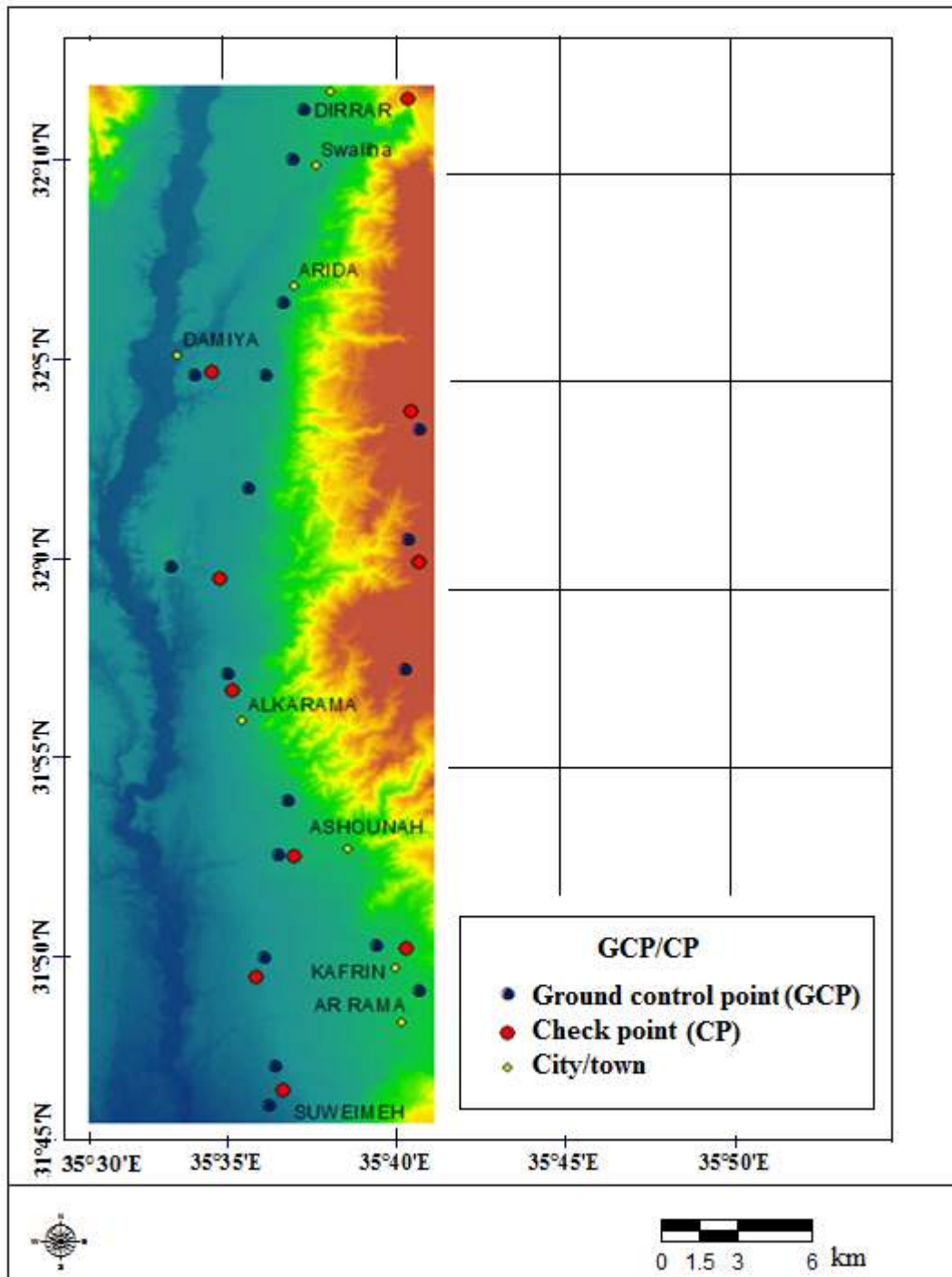
Figure 3.8: GCP's and CP's collected from the field

3.4.3 Extraction of DSM

After collecting the GCP's ENVI-5 software was used to generate the DTM from the two CARTOSAT-1 stereo pairs, tie points were automatically extracted and then epipolar pairs were generated to remove one dimension of variability and increasing the speed and reliability of image matching processes (ENVI DEM Extraction User's Guide, 2008)

The generated raster which has many buildings, roads and trees canopy is called Digital Surface Model (DSM), for the purpose of this study these unwanted features and any other outliers should be removed by means of filtering.

3.4.4 Filtering and improving the quality of DEM

In general, there are several methods for interpolation and filtering such as a) Splines approximation b) Shift Invariant Filters c) Linear Prediction d) Morphological Filters, which are most frequently applied (Passini *et al.*, 2002). In this study ENVI-5 Editing tool box is applied first for smoothing the DSM ,followed by interpolate filter, Median filter, and smooth filter using PCI Geomatica 10.3 Ortho-Engine. The Interpolate filter replaces failed values with an estimate weighted by distance calculated from the valid pixels surrounding the failed pixel(s), the Median filter ranks the pixel values within a five-by-five pixel frame according to brightness. The median is the middle value of those image pixel values, which is then assigned to the pixel in the center of the frame, while The Smooth filter is a Gaussian filter that calculates the weighted sum of all the pixels in a three-by-three pixel frame and assigns the value to the center pixel in the frame (Geomatica OrthoEngine User Guide, 2003). As a further step for smoothing and filtering Low pass filter is applied followed by Morphology filters –opening (Erode and Dilate of 12 Cells Radius = 30 m). As shown in Figure 3.9 these processes are followed by applying Neighborhood statistics using ArcMap 10 to enhance the quality of the DTM.
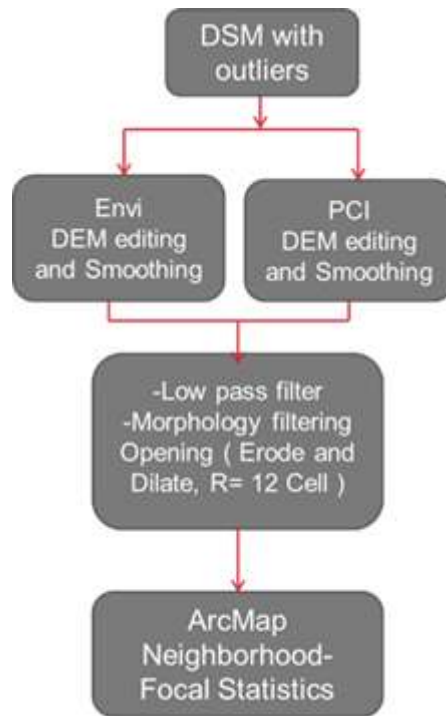
Figure 3.9: DSM flowchart with different filter processes

3.5 Extraction of Morphometric Parameters

The importance of (DTMs) in hydrological modeling and in water resources management comes from its potential in providing many hydrological parameters such as drainage networks and catchment boundaries. (Feng *et al.*,2005) The hydrologic modeling functions in ArcGIS-10 Spatial Analyst are used in this study for identifying sinks, determination of flow direction, calculating flow accumulation, delineation of watersheds, and creating stream networks. The elevation raster or digital elevation model (DEM) is used for automatically delineating a drainage system and quantifying the characteristics of the system. Figure 3.10 shows the extracted morphometric parameters of the study area.

a) Elevation   b) Hillshade   c) Slope   d) Aspect
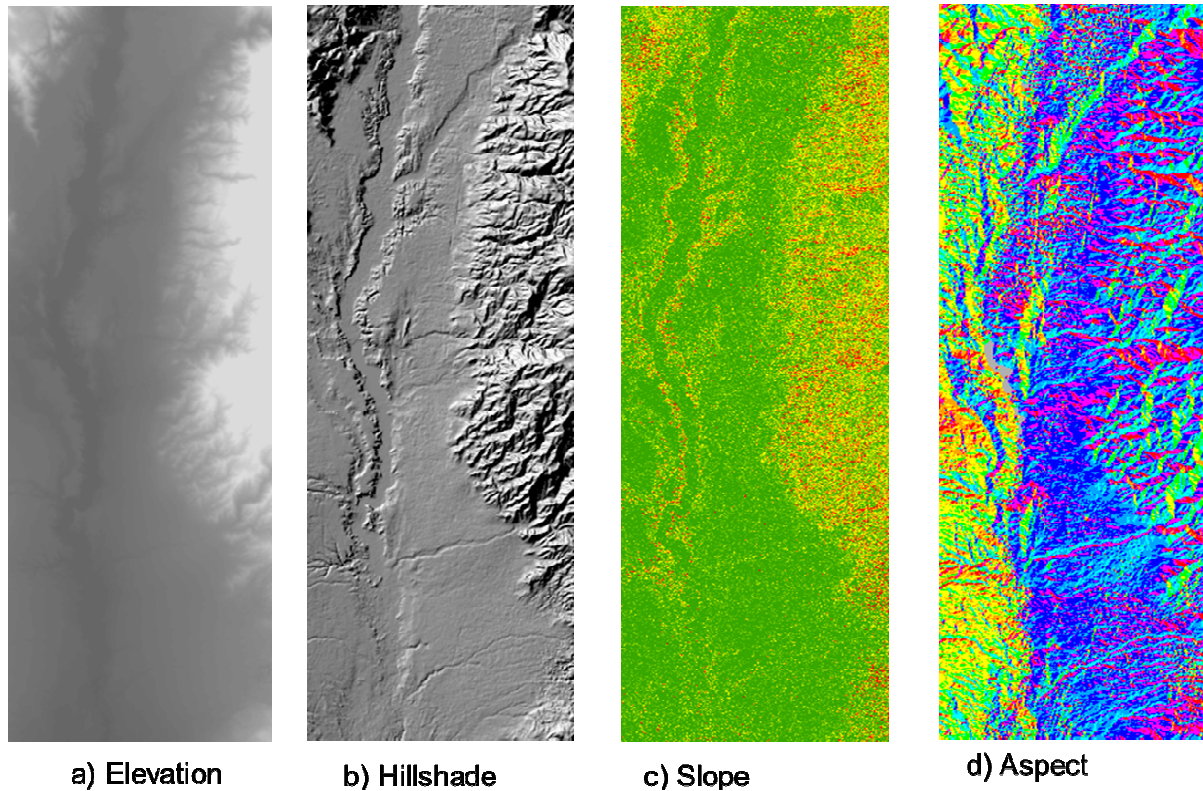
Figure 3.10: the morphometric parameters of the study area.

a) Elevation, white is high, grey is low .b) Hillshade. c) Slope, Red: steeper Green: flatter. d) Aspect: Red: North, Blue: West, Yellow: East.

Not all the above morphometric parameters are used in this study; only elevation and slope in addition to drainage network are used. Extraction of drainage networks is one of the important applications of DEM. However, derived networks have to be extracted at the correct length scale or drainage density. (Tarboton *et al.*, 1991) Figure 3.11 shows the extracted drainage network from CARTOSAT-1 data compared with extracted network from ASTER data of October 2011. Further discussion and comparison between CARTOSAT and ASTER drainage networks is presented in details in the next chapter.

59
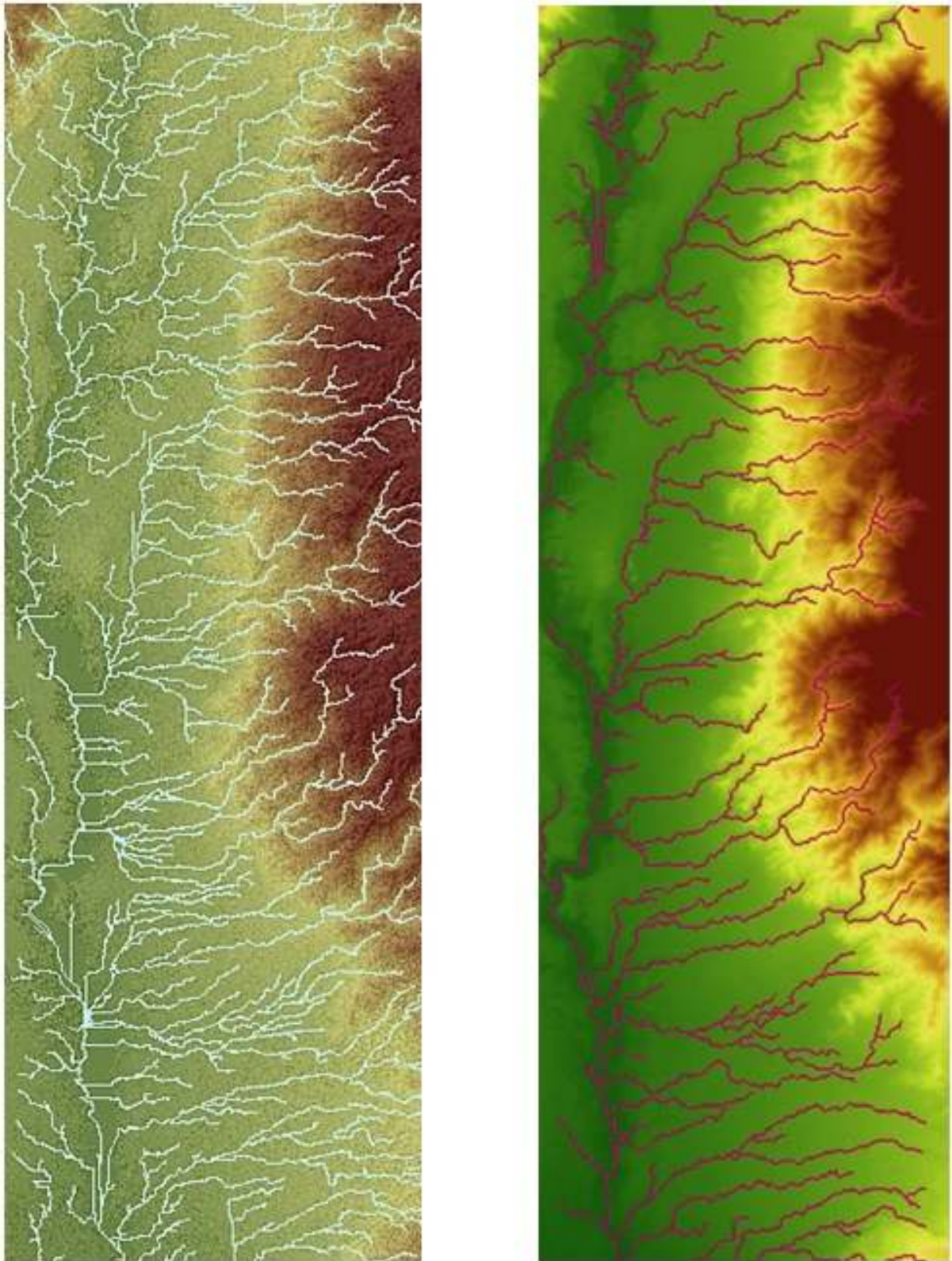
Figure 3.11: Extracted drainage network from CARTOSAT-1 and ASTER data.

Left: extracted drainage network from CARTOSAT DATA, Right: extracted drainage network from ASTER Data

3.6 Generation of Groundwater Potential Zones map

Two methods were used in this study to organize and analyze complex decisions to determine the Groundwater potential zones (GWPZ) of the study area. The first used method is: a) Analytical Hierarchy Principle (AHP) in which weights are assigned to each parameter to reflect its relative importance. The second method is: b) Fuzzy logic approach by which membership functions are defined to reach a certain aim which is the determination of the GWPZ.

3.6.1 Classification, weighting, and analysis of the parameters using Analytical Hierarchy Principle (AHP)

The procedure of the used AHP analysis is summarized in Figure 12.3.
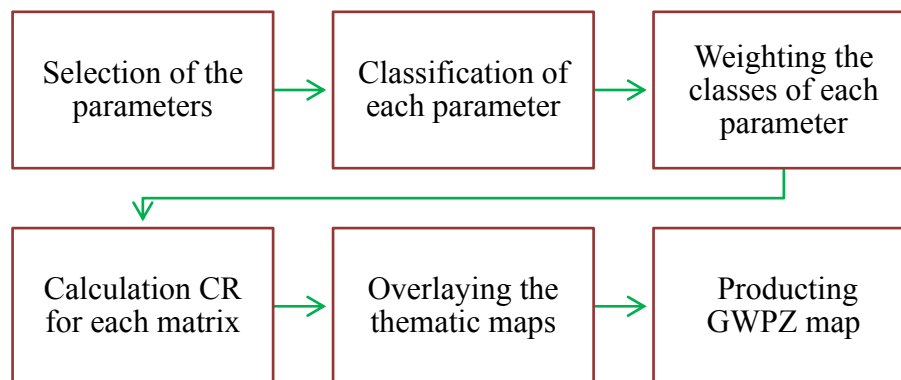
Figure 3.12: AHP work procedure

3.6.1.1 Drainage density (km/km^2)

Drainage density was calculated in ArcMap using Arc-Hydro10 tools. The drainage density with respect to the structural map of the study area shows: that the structural pattern has no big influence on the drainage system especially in the N-S direction, while it dominates in the E-W direction. In other words in the hard rock area; hydrologic sinks dominate the drainage of the system, and in the Jordan Valley plain the homogeneous permeability dominates the drainage. The study area according to the drainage density was classified into 5 categories as shown in Table 3.9.

Table 3.9: Classes of the Drainage Density

Drainage Density Class	Drainage Density (km/km^2)	Assigned Weight
Very low	0-0.0068	100
Low	0.0068-0.0130	80
Moderate	0.0130- 0.0300	60
High	0.0300-0.0470	40
Very High	0.0470-0.0640	20

Paired comparison matrix of the drainage density was prepared as shown in Table 3.10, high weights were assigned to the low drainage density class and vice versa, the calculated weight as shown in this matrix represents the relative importance of each class. Consistency ratio CR of the matrix was computed and found 0.049 which is acceptable according to (Saaty, 1980); Classification map of the drainage density is generated as shown in Figure 3.13.

Table 3.10: Paired comparison matrix of the drainage density

Class	Very Low	Low	Moderate	High	Very High	Weight
Very Low	1	3	4	7	9	50
Low	1/3	1	3	4	7	27
Moderate	¼	1/3	1	3	4	14
High	1/7	1/4	1/3	1	3	6
Very High	1/9	1/7	1/4	1/3	1	3
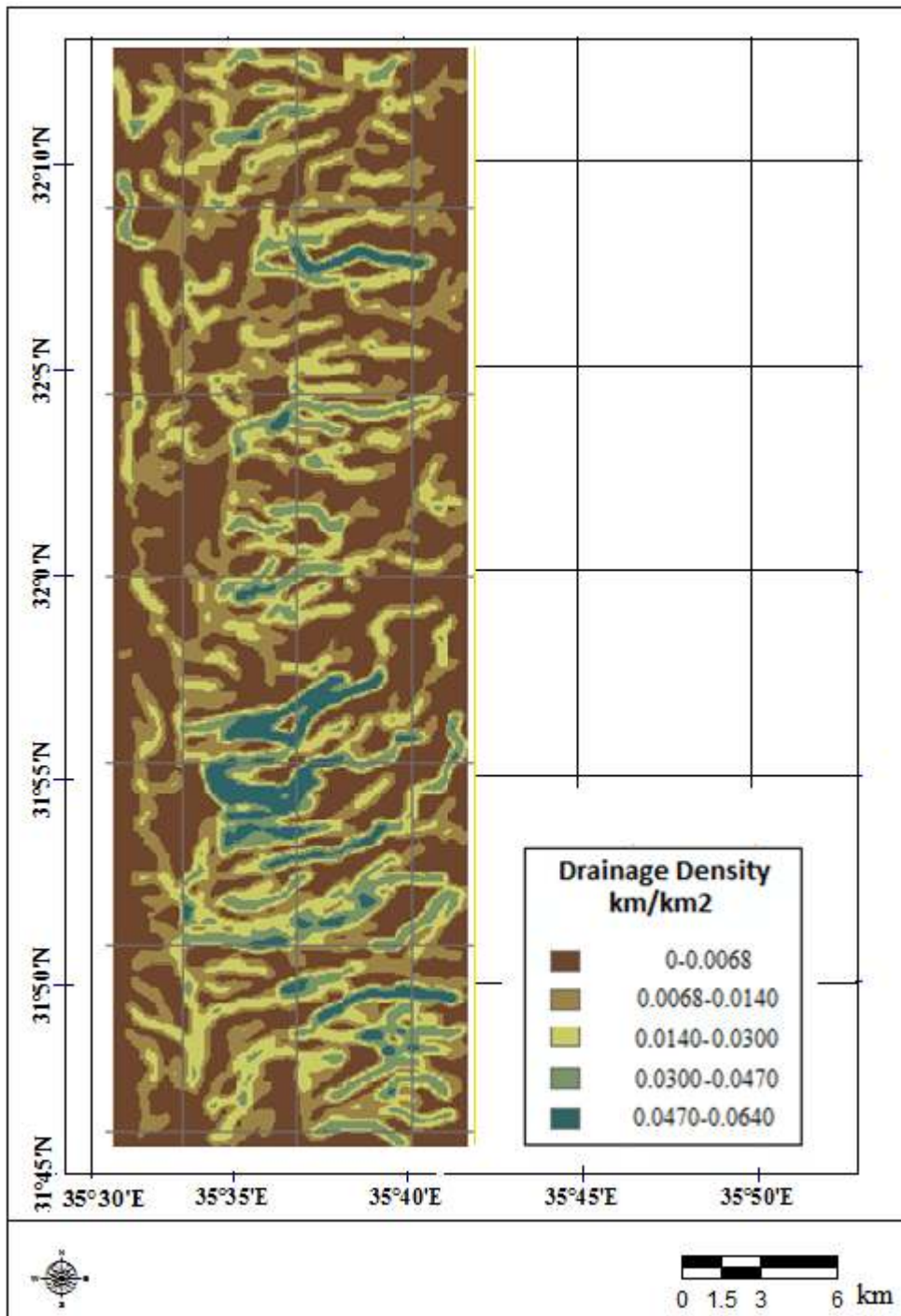
Figure 3.13: Weighted Drainage Density map

3.6.1.2 Geomorphology

Geomorphology map of the study area was digitized using ArcMap10 showing the three major geomorphologic classes as shown in Figure 3.14. The study area according to the Geomorphology was classified into 3 categories as shown in Table 3.11.

Table 3.11: Geomorphologic features of the study area

Class	Assigned Weight
Escarpment	85
JV and Wadi Flow	20
Terrace Plains in the JV	70
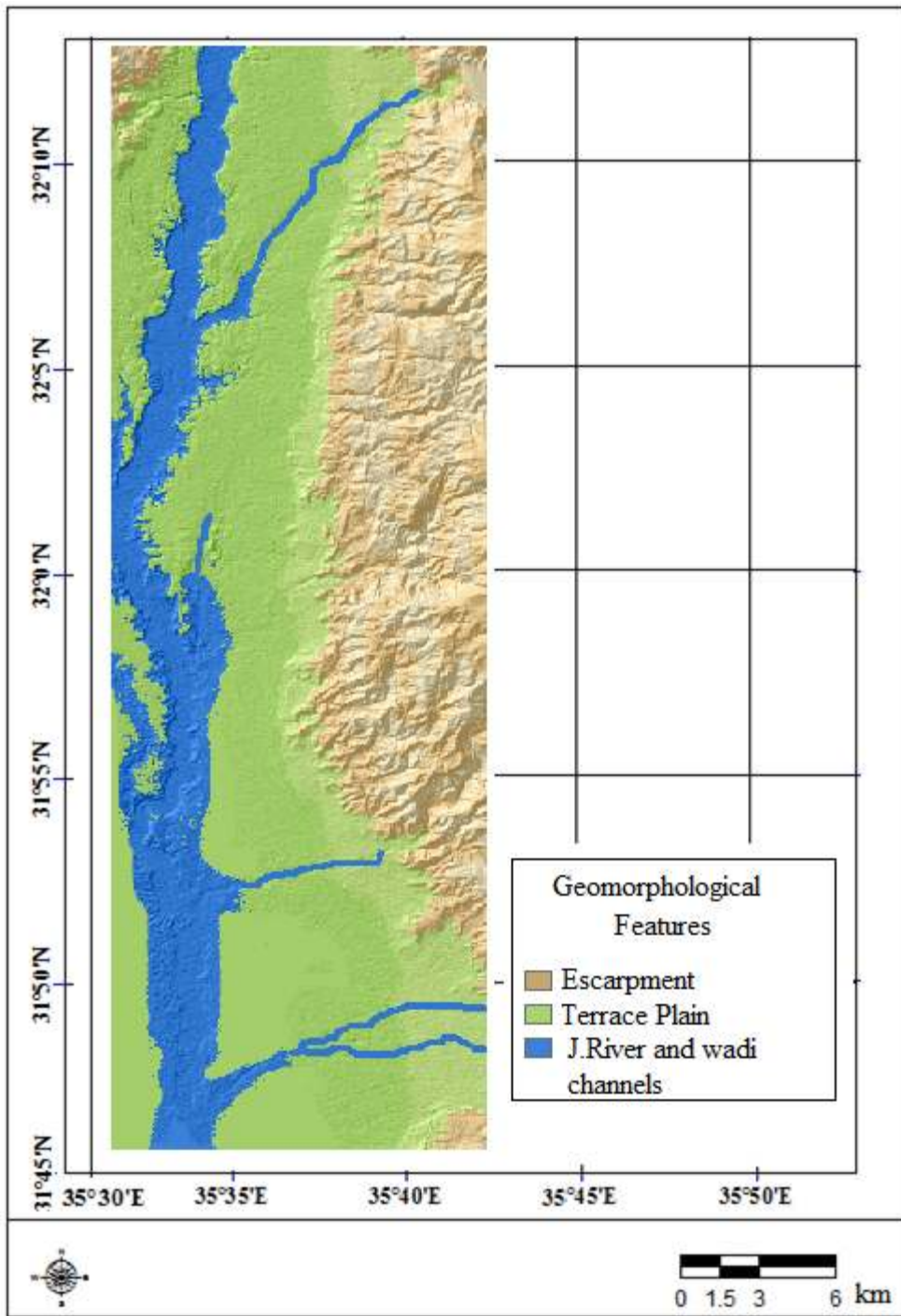
Figure 3.14: Geomorphology map of the study area.

Brown: Escarpment, Green: Ghor terrace plain+ Katar, Blue: Zor plain+ wadi channels

Paired comparison matrix of the Geomorphological features was prepared as shown in Table 3.12, the highest weight was assigned to Escarpment class while the lowest weight assigned to Wadi flow class. Consistency ratio CR for this matrix was computed and found 0.033.

Table 3.12: Paired comparison matrix of the Geomorphological features

Class	Escarpment	Terrace Plains in the JV	JV and Wadi Flow	Assigned Weight
Escarpment	1	3	5	64
Terrace Plains in the JV	1/3	1	3	26
JV and Wadi Flow	1/5	1/3	1	10

3.6.1.3 Lineaments density

According to the density of the lineaments in the study area 5 classes were defined representing the density in km/km^2 as shown in Table 3.13, the resultant lineaments density map is shown in Figure 3.15.

Table 3.13: lineaments classes of the study area

Class	Lineament Density (km/km^2)	Assigned Weight
Very low	0-0.48	20
Low	0.49-1.1	40
Moderate	1.2-1.8	60
High	1.9-2.7	80
Very high	2.8-4.9	100
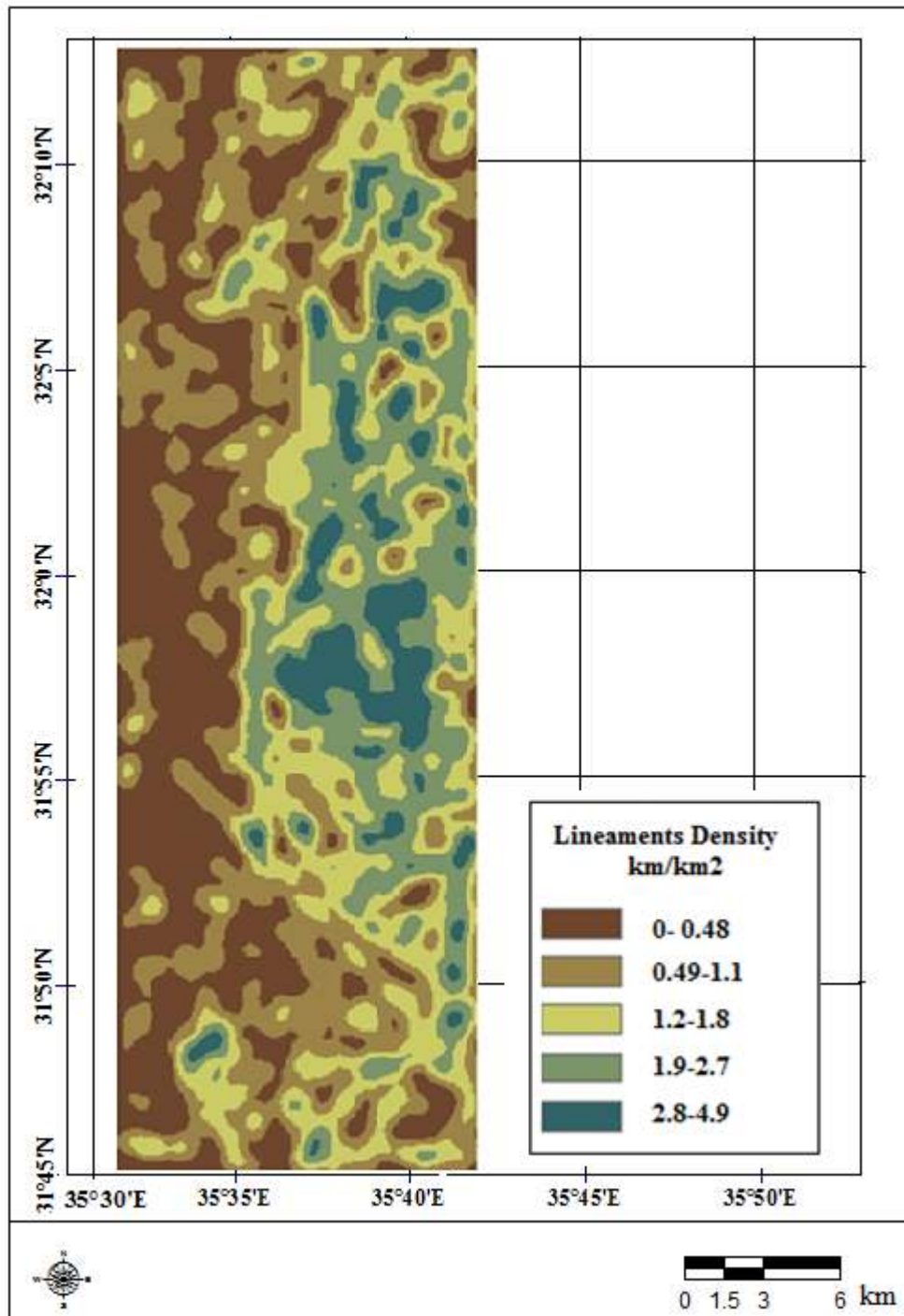
Figure 3.15: Weighted Lineaments Density map

Paired comparison matrix of the Geomorphological features was prepared as shown in Table 3.14 the consistency ratio of this matrix was 0.051 , the higher lineament density area the higher porosity and permeability which means higher potential to have groundwater, thus highest score was assigned to highest lineament density and minimum to lowest lineament density.

Table 3.14: Paired comparison matrix of the Lineaments Density km/km2

Class	Very Low	Low	Moderate	High	Very High	Weight
Very Low	1	3	5	8	9	53
Low	1/3	1	3	5	8	28
Moderate	1/5	1/3	1	3	5	13
High	1/8	1/5	1/3	1	3	6
Very High	1/9	1/8	1/5	1/3	1	3

3.6.1.4 Geology and Lithology

The study area divided into 10 classes as shown in Table 3.15 according to the importance of each geological formation in infiltrate and holding groundwater.

Table 3.15: Geological formations in the study area

Group	Class	Assigned Weight
Jordan River and wadi Deposits	Fluviatile and lacustrine gravels	15
	Alluvium and wadi sediments	60
	Alluvial fan	80
	Alluvium gravel	90
	At Tayan siltstone / Soil over bedrock	50
Jordan Valley	Lisan marl	10
	Lisan marl gravel/ Lisan beachrock	15
	Basalt/Thaur Gabbro	50
	Damya Siltstone	15
	Travertine and calcrete	50
	Ghuwayr - volcanic tuff -	80
Balqa	Amman silicified limestone	80

	Wadi Umm Ghudran – chalk, marl	30
Ajlun	Wadi As Sir - limestone	100
	Fuhays/Hummar/Shueib – limestone, dolomite	100
	Na'ur – marly limestone	20
Kurnub	Kurnub – sandstone, shale	50
Zarqa Azab	Ramla & Hamman - marlstone	30
	Dhahab – limestone, marl	30
	Hayyala - volcanoclastic /	30
	Rachel Hornblende Quartz Diorite Numayri Dolomite/Hihi	15

Paired comparison matrix of the Geological formations was prepared as shown in Table 3.16 the highest weight was assigned Wadi As sir, Fuhays,Hummar and Shua'ab limestone while the lowest weight assigned to Lisan Marl. Consistency ratio CR for this matrix was computed and found 0.04; geological formations were

Table 3.16: Paired comparison matrix of the Geological formations

Class	Group10	Group9	Group8	Group7	Group6	Group5	Group4	Group3	Group2	Group1	Weight
Group10	1	2	3	4	5	6	7	8	9	10	29
Group9	1/2	1	2	3	4	5	6	7	8	9	22
Group8	1/3	1/2	1	2	3	4	5	6	7	8	16
Group7	1/4	1/3	1/2	1	2	3	4	5	6	7	11
Group6	1/5	1/4	1/3	1/2	1	2	3	4	5	6	8
Group5	1/6	1/5	1/4	1/3	1/2	1	2	3	4	5	5
Group4	1/7	1/6	1/5	1/4	1/3	1/2	1	2	3	4	4
Group3	1/8	1/7	1/6	1/5	1/4	1/3	1/2	1	2	3	3
Group2	1/9	1/8	1/7	1/6	1/5	1/4	1/3	1/2	1	2	2
Group1	1/10	1/9	1/8	1/7	1/6	1/5	1/4	1/3	1/2	1	1
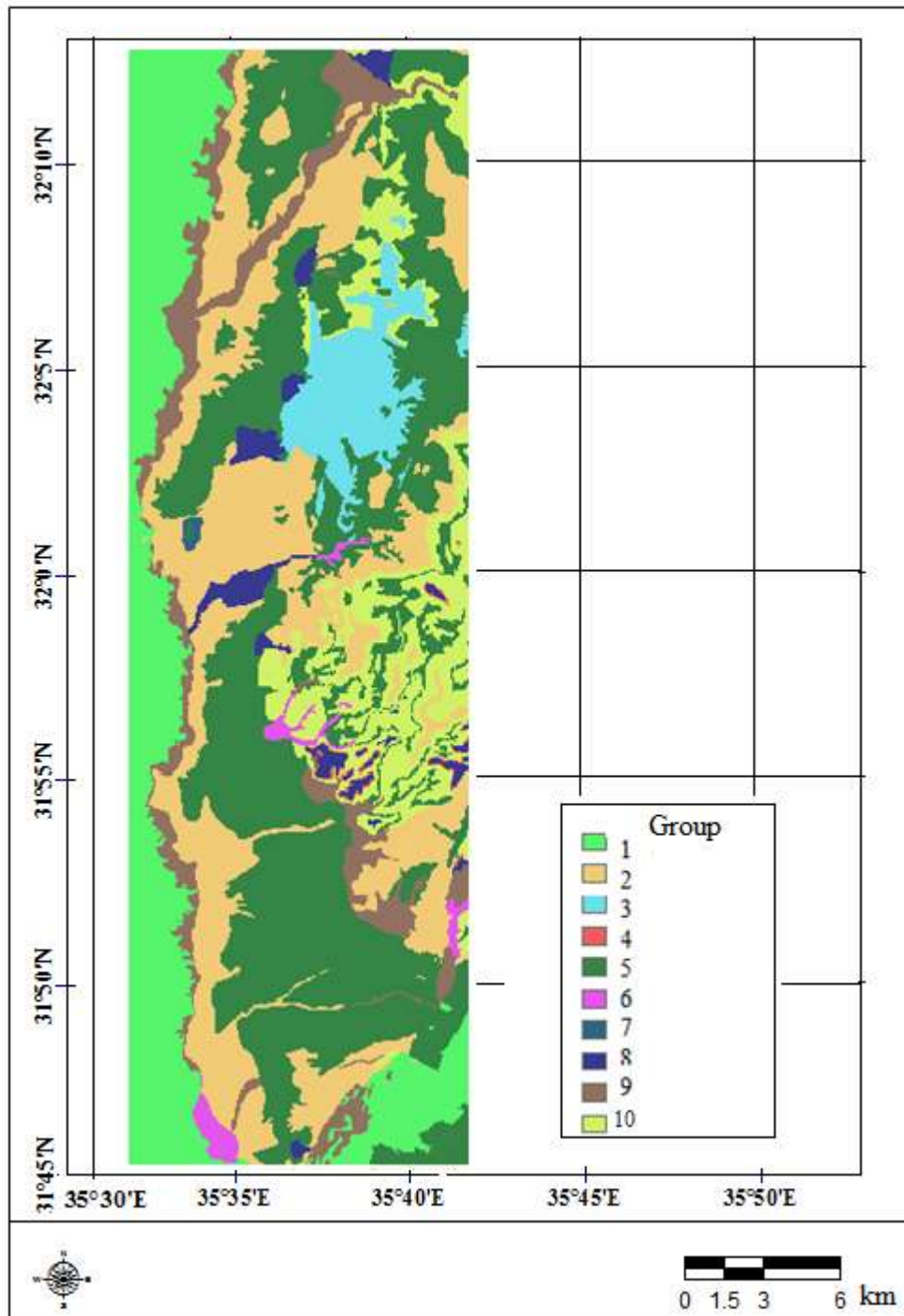
Figure 3.16: Weighted Geology map of the study area

This figure shows the importance of the geologic sequence together with the relevant lithology for the infiltration of the rain into the underground, and therewith for the recharge of groundwater

3.6.1.5 Soil type

The study area divided into 10 classes as shown in Table 3.17 according to the importance of each soil type impermeability and infiltration.

Table 3.17 Soil types in the study area

Soil Type	Assigned Weight
Ajlun (AJL)	90
Zarqa (ZAR)	80
Himara (HIM)	70
Anjara (ANJ)	50
Uzaymi (ZAY)	50
Su'eidat (DAT)	40
Tell Alluba (ALL)	40
Ghor (GOR)	30
Katar (KAT)	20
Zor (ZOR)	10

Paired comparison matrix of the Soil types was prepared as shown in Table 3.18 the highest weight was assigned Ajlun soil (AJL), while the lowest weight assigned to Zor soil (ZOR). Consistency ratio CR for this matrix was computed and found 0.044; classification map of Soil types is generated as shown in Figure 3.17.

Table 3.18: Paired comparison matrix of the Soil Types

Class	(AJL)	(ZAR)	(HIM)	(ANJ)	(ZAY)	(DAT)	(ALL)	(GOR)	(KAT)	(ZOR)	Weight
(AJL)	1	2	3	4	4	5	5	7	8	9	28
(ZAR)	1/2	1	2	3	4	4	5	5	7	8	21
(HIM)	1/3	1/2	1	2	3	4	4	5	5	7	15
(ANJ)	1/4	1/3	1/2	1	2	3	4	4	5	5	11
(ZAY)	1/4	1/4	1/3	1/2	1	2	3	4	4	5	8
(DAT)	1/5	1/4	1/4	1/3	1/2	1	2	3	4	4	6
(ALL)	1/5	1/5	1/4	1/4	1/3	1/2	1	2	3	4	4
(GOR)	1/7	1/5	1/5	1/4	1/4	1/3	1/2	1	2	3	3
(KAT)	1/8	1/7	1/5	1/5	1/4	1/4	1/3	1/2	1	2	2
(ZOR)	1/9	1/8	1/7	1/5	1/5	1/4	1/4	1/3	1/2	1	2
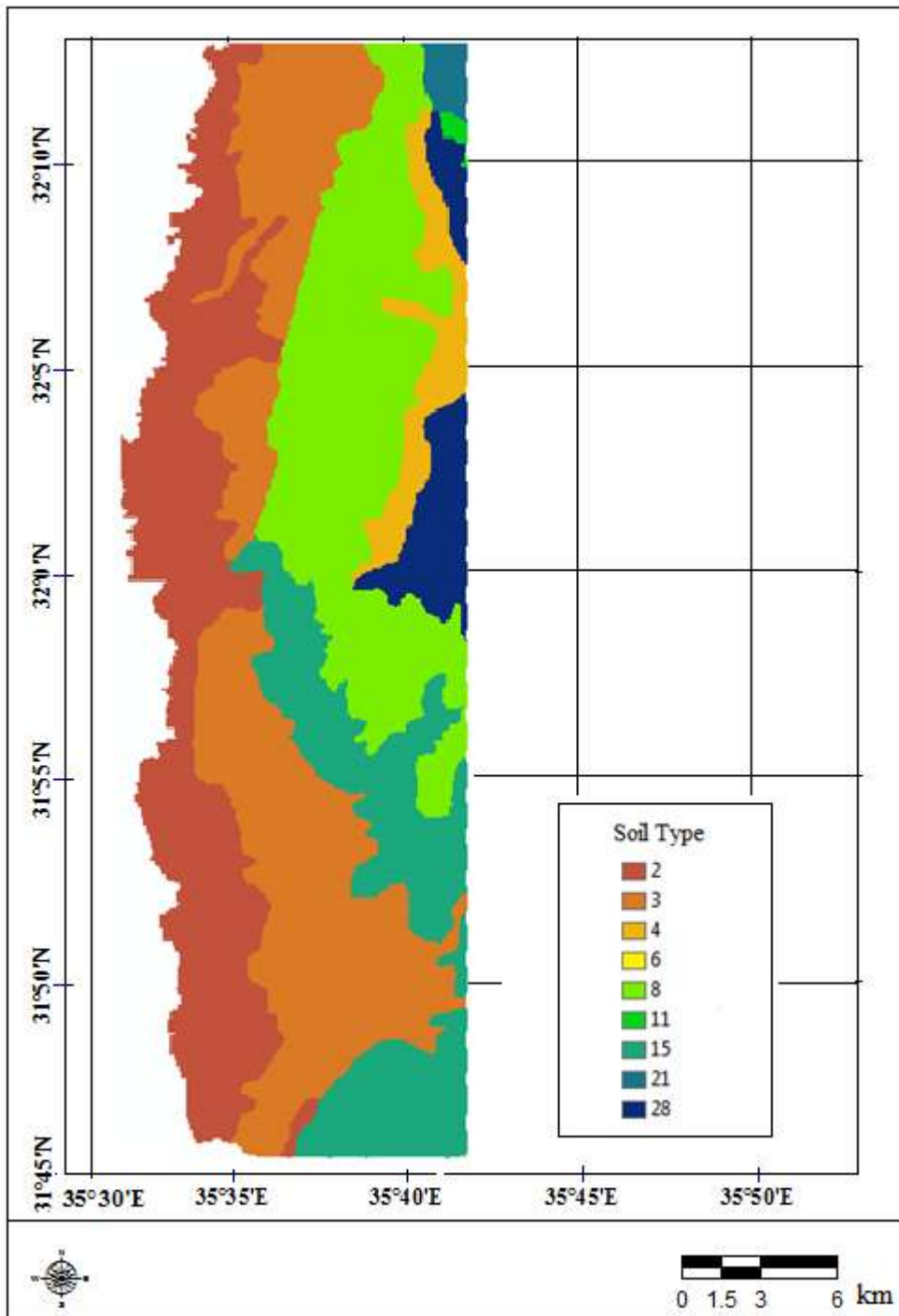
Figure 3.17: Weighted Soil map of the study area

3.6.1.6 Slope Steepness

Arc-Hydro10 tool was used to extract the slope map in addition to the other Geomorphological parameters in the study area which is divided accordingly into 5 steepness classes as shown in Table 3.19.

Table 3.19: Slope steepness classes of the study area

Class (degrees)	Assigned Weight
Flat (0-2.26)	100
Gentle (2.27-4.52)	80
Moderate (4.53-7.54)	60
Steep (7.55-11.8)	40
Very Steep (11.90-38.4)	20

Paired comparison matrix of the slope steepness was prepared as shown in Table 3.20 the highest weight was assigned to the steepest slope, while the lowest weight assigned to flat areas, cause this parameter adversely affect the groundwater recharge, as we know flat areas are capable of holding the rainfall and facilitate recharge to groundwater as compared to steep slope area where water moves as runoff quickly (Godebo, 2005), Figure 2.6 in Chapter 2 shows the different slope classes of the study area. Consistency ratio CR for this matrix was computed and found 0.053.

Table 3.20: Paired comparison matrix of the Slope Steepness

Class	Flat	Gentle	Moderate	Steep	Very Steep	Weight
Flat	1	3	5	7	9	52
Gentle	1/3	1	3	5	7	27
Moderate	1/5	1/3	1	3	5	13
Steep	1/7	1/5	1/3	1	3	6
Very Steep	1/9	1/7	1/5	1/3	1	1

3.6.1.7 Elevation

Water tends to be stored at lower topography than at higher topography, therefore high weight is assigned for lower elevation areas as compared to higher elevations (Godebo, 2005). The area was classified into 5 classes as shown in Table 3.21 and Figure 3.18, Paired comparison matrix of the elevation was prepared as shown in Table 3.22, Consistency ratio CR for this matrix was computed and found 0.044.

Table 3.21: Elevation classes of the study area

Class	Assigned Wight
Very Low((-390) – (-110))	100
Low((-110)- (170))	80
Moderate(170 - 450)	60
High(450- 730)	40
Very High(730 - 1010)	20

Table 3.22: Paired comparison matrix of the Elevation

Class	Very Low	Low	Moderate	High	Very High	Weight
Very Low	1	3	4	7	9	50
Low	1/3	1	3	4	7	26
Moderate	1/4	1/3	1	3	4	13
High	1/7	1/4	1/3	1	3	7
Very High	1/9	1/7	1/4	1/3	1	3
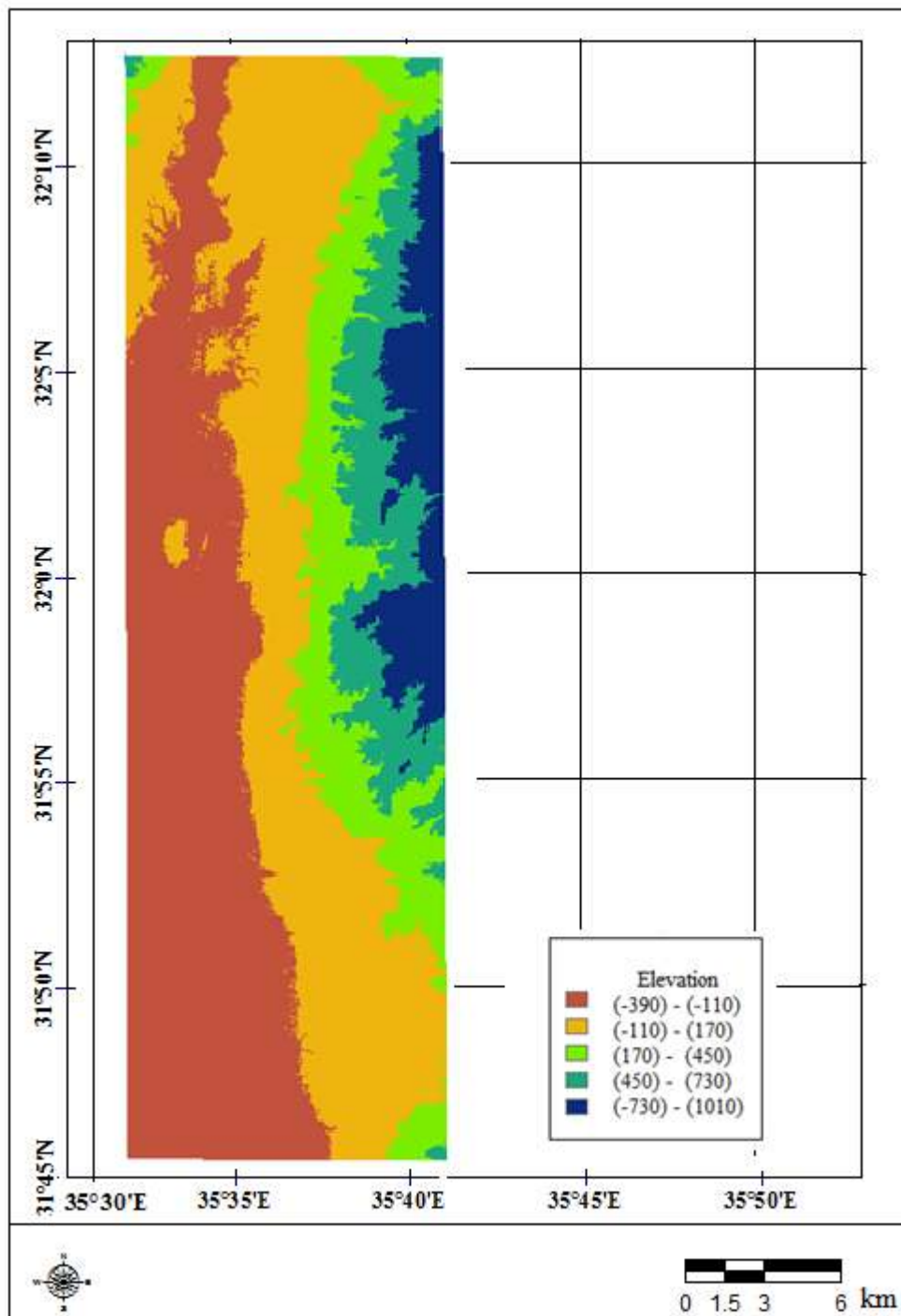
Figure 3.18: Weighted Elevation classes of the study area

3.6.1.8 Land Cover/Use

Depending on the importance of each class in the GWPZ mapping the land cover/ use classes are weighted as shown in Table 3.23. Paired comparison matrix of Land cover /use was prepared as shown in Table 3.24 Figure 2.8 in Chapter 2 shows the different Land cover/use classes of the study area. Consistency ratio CR for this matrix was computed and found 0.021.

Table 3.23, Land cover/use classes of the study area

Class	Assigned Weight
Surface Water	80
Soil	60
Trees	40
Irrigated Crops	30
Non Irrigated	30
Greenhouse	20
Settlement	10

Table 3.24: Paired comparison matrix of Land cover/use classes

Class	Surface Water	Soil	Trees	Irrigated Crops	Non Irrigated Crops	Greenhouse	Settlement	Weight
Surface Water	1	2	3	4	5	6	8	36
Soil	1/2	1	2	3	4	5	6	24
Trees	1/3	1/2	1	2	3	4	5	16
Irrigated Crops	1/4	1/3	1/2	1	2	3	4	10
Non Irrigated Crops	1/5	1/4	1/3	1/2	1	2	3	7
Greenhouse	1/6	1/5	1/4	1/3	1/2	1	2	4
Settlement	1/8	1/6	1/5	1/4	1/3	1	1	3

3.6.1.9 Rainfall

The area classified into 5 classes depending on the mean rainfall amount (mm/year) as shown in Table 3.25 and in Figure 2.9 in chapter 2.

Table 3.25: Rainfall classes in the study area mm/year

Class	Assigned Weight
0-200	20
200-300	40
300-400	60
400-500	80
>500	100

Paired comparison matrix of mean annual Rainfall (mm/year) was prepared as shown in Table 3.26. Consistency ratio CR for this matrix was computed and found 0.067.

Table 3.26: Paired comparison matrix of mean Rainfall (mm/year)

Class	>500	400-500	300-400	200-300	0-200	Weight
>500	1	3	6	7	9	54
400-500	1/3	1	3	6	7	28
300-400	1/6	1/3	1	3	6	13
200-300	1/7	1/6	1/3	1	3	6
0-200	1/9	1/7	1/6	1/3	1	3

3.6.1.10 Generation of Groundwater potential zone map by integrating all evaluated parameters

Generation of Groundwater potential zone map is done by integrating the parameters using weight index overlay method, to combine the thematic layers -the GWPZ were generated to present the relative probability of each pixel that there is a certain groundwater potential, more precisely to show that according the recharge conditions groundwater could occur on this place. Paired comparison matrix of the whole parameters was prepared as shown in Table 3.27; consistency ratio CR for this matrix was computed and found 0.035.

Table 3.27: Paired comparison matrix of all parameters

Class	Geology & Lithology	Geo-morphology	Lineament Density	Slope	Soil	Drainage Density	Land Use	Rainfall	Elevation	Weight
Geology& Lithology	1	2	3	4	5	6	7	8	9	31
Geomorphology	1/2	1	2	3	4	5	6	7	8	22
Lineament Density	1/3	1/2	1	2	3	4	5	6	7	16
Slope	1/4	1/3	1/2	1	2	3	4	5	6	11
Soil	1/5	1/4	1/3	1/2	1	2	3	4	5	7
Drainage Density	1/6	1/5	1/4	1/3	1/2	1	2	3	4	5
Land Use	1/7	1/6	1/5	1/4	1/3	1/2	1	2	3	4
Rainfall	1/8	1/7	1/6	1/5	1/4	1/3	1/2	1	2	2
Elevation	1/9	1/8	1/7	1/6	1/5	1/4	1/3	1/2	1	2

Index overlay method was used to generate the GWPZ depending on the assigned and calculated weights; the generated GWPZ map is shown in Figure 3.19.
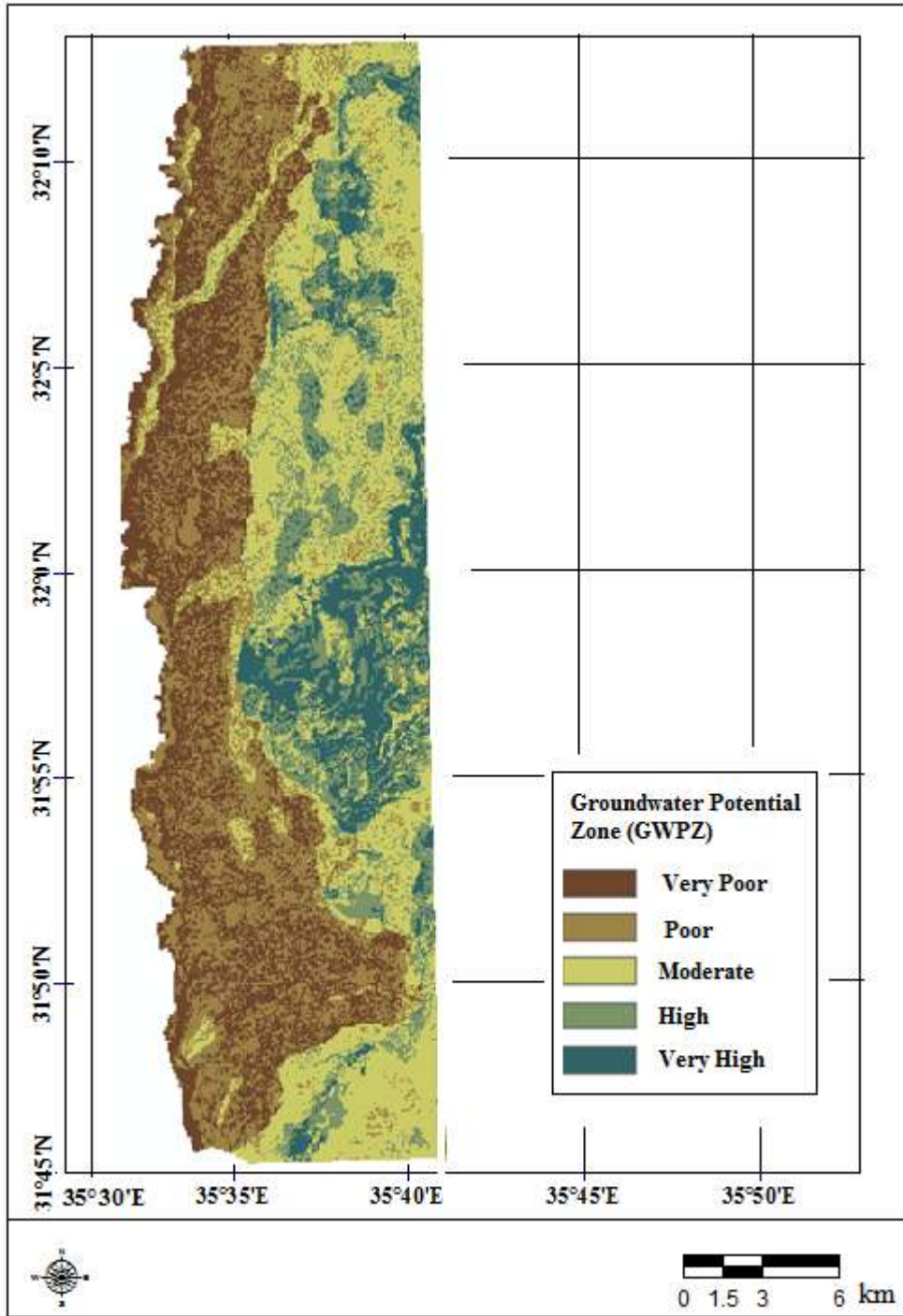
Figure 3.19: GWPZ map of the study area using AHP approach

on the base of 9 evaluated parameters.

According to the generated GWPZ map the study area can be classified into 5 potential zones: Very Poor, Poor, Moderate, High and Very High, as shown in Table 3.28.

Table 3.28: Distribution of GWPZ over the study area

GWPZ Class	Very High	High	Moderate	Poor	Very Poor
Area %	14.8	6.9	24.8	30.8	22.7

3.6.2 Classification, weighting, and analysis of the parameters using Fuzzy Logic

3.6.2.1 Fuzzy Logic Approach for Generating GWPZ

Fuzzy Logic (FL) was used in this study to generate GWPZ map by an alternative way. The study area was classified into five zones ranging from very poor to very high according to the contribution of different parameters in the formation of GWPZ, all maps and parameters are connected using Fuzzy Gamma operator. In this work Mamdani's Fuzzy Inference method (MFIS) is used as shown in Figure 3.20. This method is considered as the most commonly used fuzzy methodology. MFIS was developed using fuzzy set theory by (Mamdani *et al.*, 1975) based on (Zadeh, 1973), this method mainly consists of the four steps as follows:

1. Fuzzification of the entries.
2. Definition of the rules.
3. Processing of the rules (inference).
4. Defuzzification of the output fuzzied values.
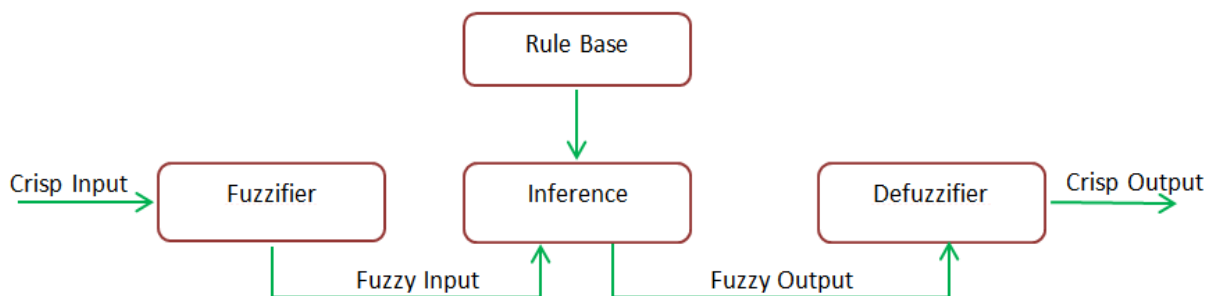
Figure 3.20: Scheme of the method performed for the application of fuzzy logic

3.6.2.2 Fuzzification of the entries

In this study several membership functions were used, for example Gaussian shape membership function is used for representing the lineaments density parameter as shown in Figure 3.21,where very high lineament density area have value of 1 (full membership) while very low lineament density areas have value of 0 (full non-membership), the other classes range between these two values according to their importance in the GWPZ, every value of x is associated with a value of μ(x), and the ordered pairs [x, μ(x)] are known as Fuzzy set.
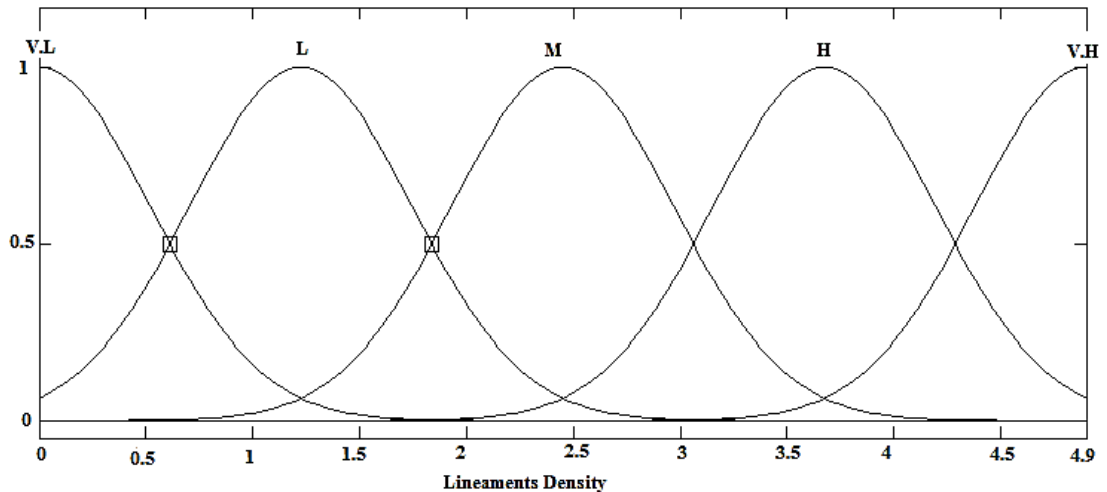
Figure 3.21: Membership function of Lineament density

All the classes of each parameter were weighted using Fuzzy Logic and ranked according to their Fuzzy number as shown in the Tables (3.29 – 3.37), the same criteria applied in the AHP method for weighting the parameters and the classes of each parameter is also applied here.

Table 3.29: Slope Classes and ranking of the study area

Class	Slope(Degree)	Fuzzy Number	Ranking
Flat	0-2.26	0.54	Excellent
Gentle	2.27-4.52	0.42	Good
Moderate	4.53-7.54	0.27	Moderate
Steep	7.55-11.8	0.18	Poor
Very Steep	11.90-38.4	0	Very Poor

Table 3.30: Geological & Lithological Classes and ranking of the study area

Group	Class	Assigned Weight	Ranking
Jordan River and wadi Deposits	Fluviatile and lacustrine gravels	0.1	Very Poor
	Alluvium and wadi sediments	0.62	Moderate
	Alluvial fan	0.65	Good
	Alluvium gravel	0.73	Excellent
	At Tayan siltstone / Soil over bedrock	0.56	Moderate
Jordan Valley	Lisan marl	0.09	Very Poor
	Lisan marl gravel/ Lisan beachrock	0.11	Very Poor
	Basalt/Thaur Gabbro	0.49	Moderate
	Damya Siltstone	0.1	Very Poor
	Travertine and calcrete	0.51	Moderate
	Ghuwayr - volcanic tuff -	0.69	Good
Balqa	Amman silicified limestone	0.74	Good
	Wadi Umm Ghudran – chalk, marl	0.33	Poor
Ajlun	Wadi As Sir - limestone	0.81	Excellent
	Fuhays/Hummar/Shueib – limestone, dolomite	0.78	Excellent
	Na'ur – marly limestone	0.11	Very Poor
Kurnub	Kurnub – sandstone, shale	0.11	Very Poor
Zarqa Azab	Ramla & Hamman - marlstone	0.53	Moderate

	Dhahab – limestone, marl	**0.28**	**Poor**
	Hayyala - volcanoclastic /	**0.24**	**Poor**
	Rachel Hornblende Quartz Diorite Numayri Dolomite/Hihi	**0.26**	**Poor**

Table 3.31: Soil Classes and ranking of the study area by Fuzzy Logic

Class/Soil	Fuzzy Number	Ranking
Ajlun (AJL)	0.76	Excellent
Zarqa (ZAR)	0.68	Good
Himara (HIM)	0.66	Good
Anjara (ANJ)	0.55	Moderate
Uzaymi (ZAY)	0.38	Moderate
Su'eidat (DAT)	0.39	Moderate
Tell Alluba (ALL)	0.34	Moderate
Ghor (GOR)	0.13	Poor
Katar (KAT)	0.11	Poor
Zor (ZOR)	0	Very Poor

Table 3.32: Slope Classes and ranking of the study area by Fuzzy Logic

Class/Geomorphology	Fuzzy Number	Ranking
Escarbment	0.62	Excellent
Terrace Plains in the JV	0.53	Good
JV and Wadi Flow	0.11	Poor

Table 3.33: Elevation Classes and ranking of the study area by Fuzzy Logic

Class/Elevation	Fuzzy Number	Ranking
50>	0.46	Excellent
50-250	0.32	Good
250-500	0.24	Moderate
500-700	0.16	Poor
>700	0	Very Poor

Table 3.34: Rainfall Classes and ranking of the study area by Fuzzy Logic

Class/Rainfall	Fuzzy Number	Ranking
>500	0.65	Excellent
400-500	0.44	Good
300-400	0.28	Moderate
200-300	0.17	Poor
0-200	0.05	Very Poor

Table 3.35: Land cover Classes and ranking of the study area by Fuzzy Logic

Class/Land-cover	Fuzzy Number	Ranking
Surface Water	0.75	Excellent
Soil	0.68	Excellent
Trees	0.45	Good
Irrigated Crops	0.38	Good
Non Irrigated Crops	0.19	Moderate
Greenhouse	0.10	Poor
Settlement	0.08	Very Poor

Table 3.36: Lineaments Density Classes and ranking of the study area by Fuzzy Logic

Class/Lineament Density	Density(km/km2)	Fuzzy Number	Ranking
Very Low	2.8-4.9	0.83	Excellent
Low	1.9-2.7	0.72	Good
Moderate	1.2-1.8	0.49	Moderate
High	0.49-1.1	0.22	Poor
Very High	0-0.48	0.10	Very Poor

Table 3.37: Drainage Density Classes and ranking of the study area by Fuzzy Logic

Class/Drainage Density	Fuzzy Number	Ranking
Very High	0.88	Excellent
High	0.76	Good
Moderate	0.54	Moderate
Low	0.34	Poor
Very Low	0.19	Very Poor

3.6.2.3 Definition of the rules

The weights are indirectly taken in account through the rules defined (Karakazi *et al.*, 2001), following is an example from this study on link rule of slope steepness:

    Rule 1.

    IF slope is flat or

    Slope is Moderate and

    Lineament density is Very High and

    Drainage Density is Very Low

    THEN GWPZ is Very High.

    Rule 2.

    IF slope is Very Steep or

    Slope is Steep and

    Geology is Lisan Marl and

    Drainage Density is Very High

    THEN GWPZ is Very Low.

3.6.2.4 Processing of the rules (inference)

For the used Fuzzy Gamma operator; Bonham-Carter (1994) discussed the effect of variations in (γ) for the case of combining two values $\mu A = 0.75$ and $\mu B = 0.5$ as shown in Figure 3.22.

In this study several trials were done to determine the value of gamma (γ) which yields the best reliable GWPZ map, $\gamma = 0.85$ is the most satisfactory value for that.
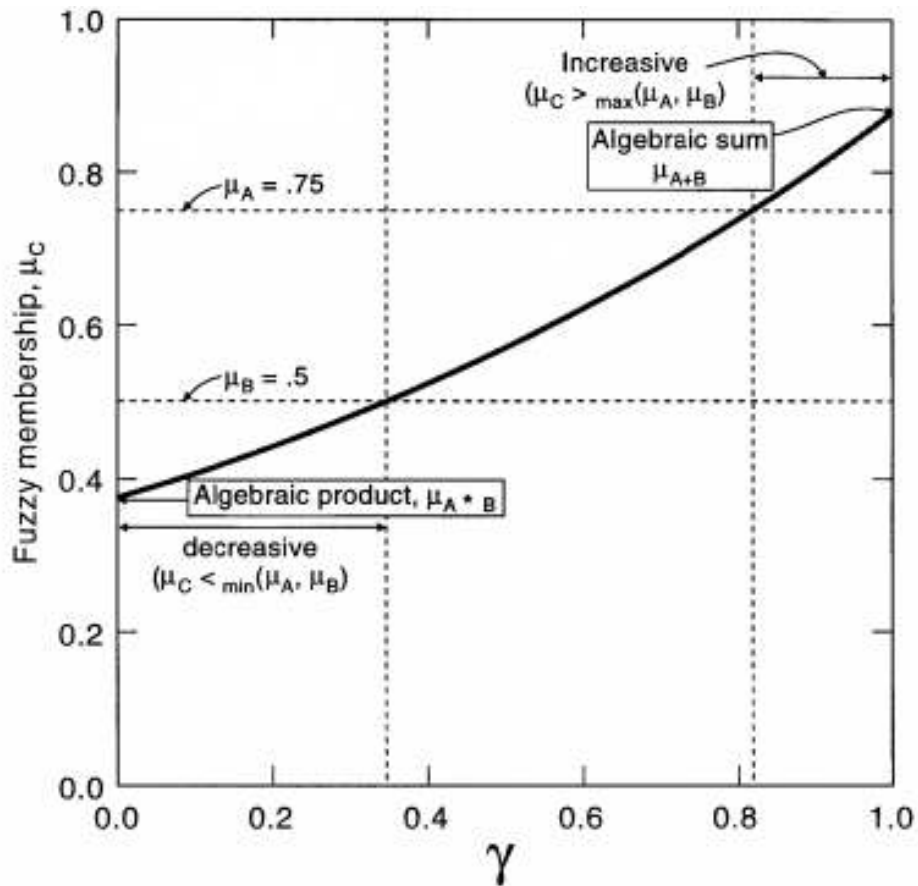
Figure 3.22: Graph of Fuzzy membership µc, obtained by combining two Fuzzy memberships

µA and µB versus γ.

3.6.2.5 Defuzzification of the output fuzzied values

The resultant map of the fuzzy approach is shown on Figure 3.23, in this map the study area classified into 5 potential zones: Very Poor, Poor, Moderate, High and Very High, the area that has very high groundwater potential zone covering about 7.7 % of the study area. The high potential area covers 12.6 % while the greatest portion of the area about 37.1% belongs to poor groundwater potential zone as shown in Table 3.38, the generated GWPZ map is also related to the geology and lithology, geomorphology, slope and lineament density.

Table 3.38: Distribution of GWPZ over the study area

GWPZ Class	Very High	High	Moderate	Poor	Very Poor
Area %	7.7	12.6	20.2	37.1	22.4
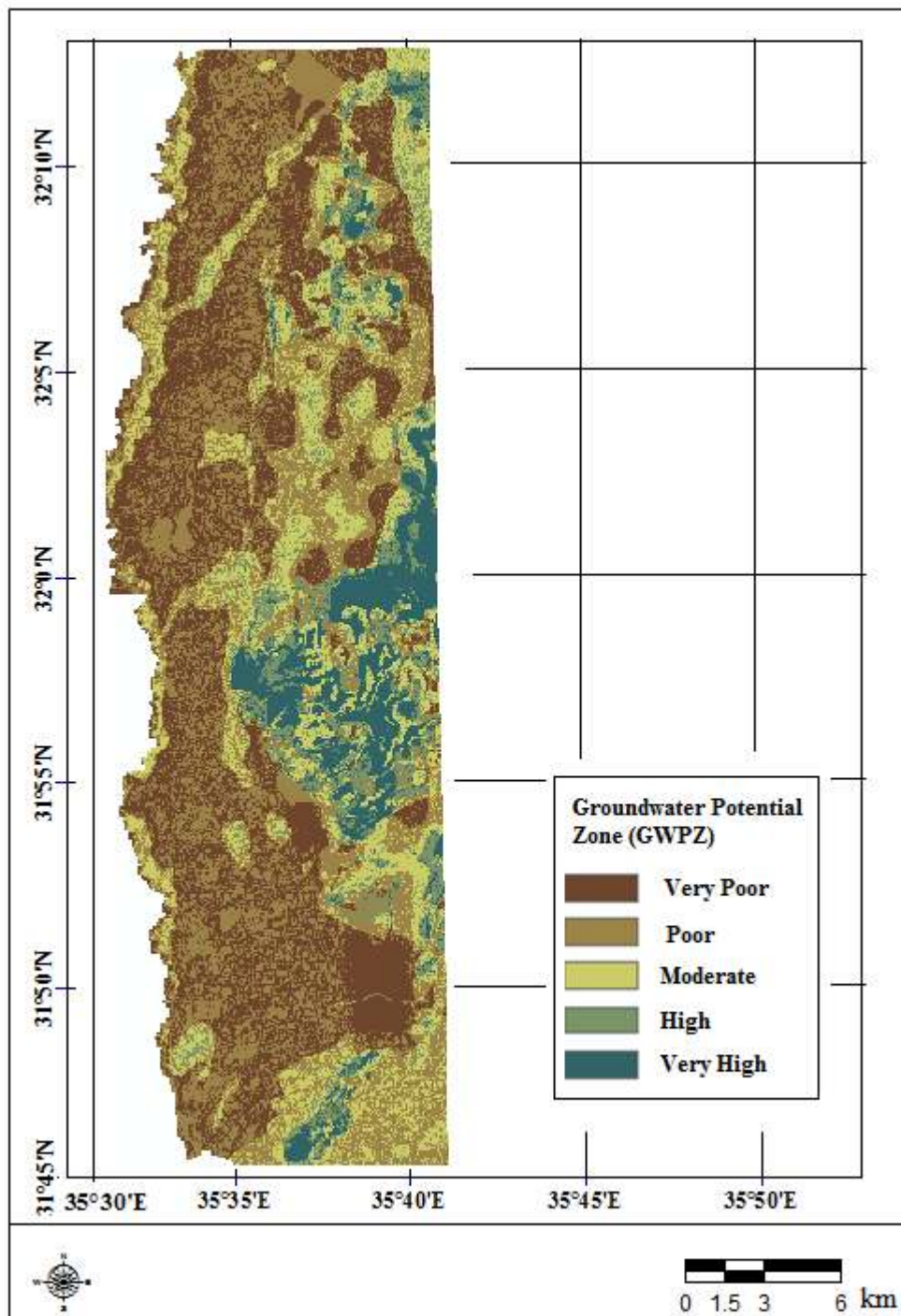
Figure 3.23: GWPZ map of the study area using Fuzzy logic

on the base of 9 evaluated parameters.

4. RESULTS, VERIFICATION OF THE RESULTS AND DISCUSSION

4.1 Results of image classification for land cover/land use thematic map

The result of image classification is land cover/use thematic map shown in Figure 4.1, this map shows different classes in the study area ,which includes 6 types of soils , urban areas, irrigated crops areas , non-irrigated crops areas, trees, surface water, sea water and green houses.
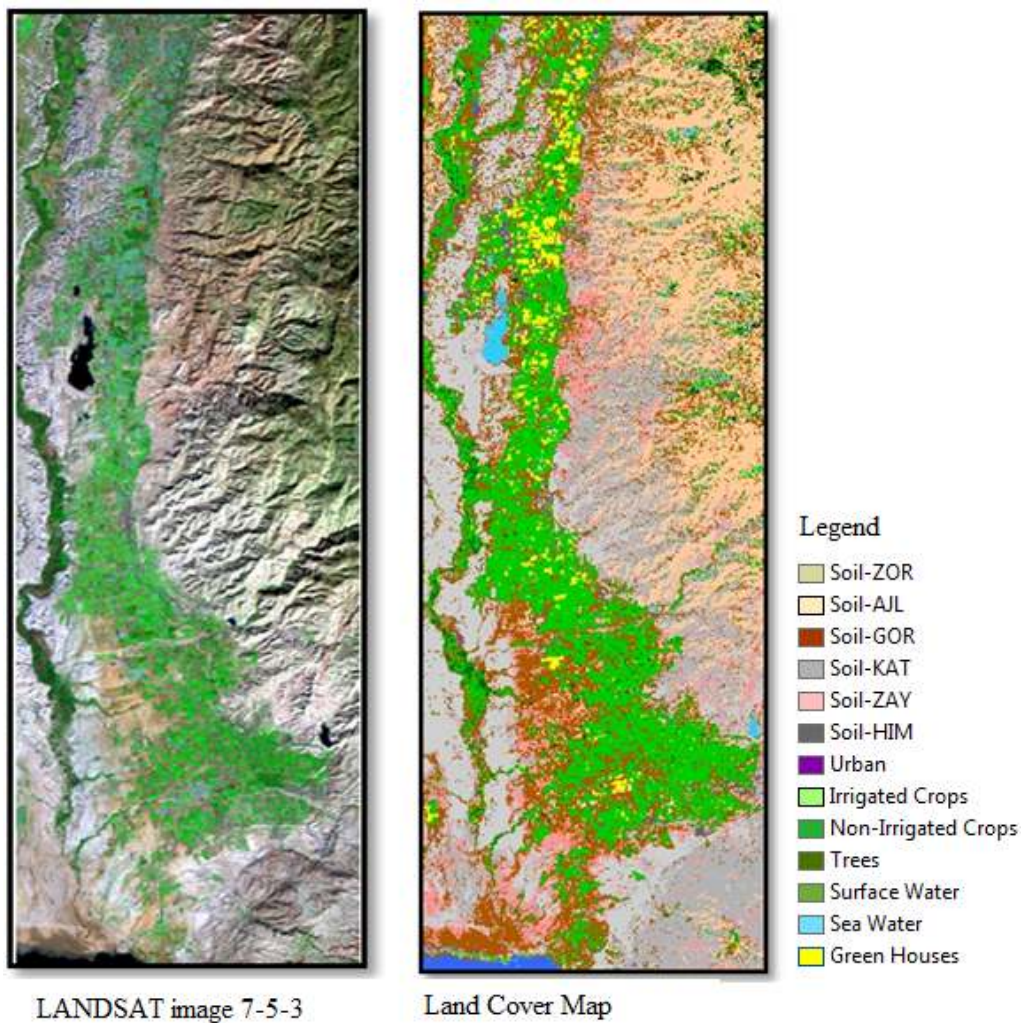
Figure 4.1: Land-cover thematic map with the results of the remote sensing evaluation

on the right side ,and the original LANDSAT image for comparison on the left side

4.1.1 Accuracy Assessment

Classification process is not complete until its accuracy is assessed. Accuracy assessment is performed by comparing two sources of information (Jensen, 1996):

1. Remote-sensing derived classification data
2. Reference test data

The relationship of these two sets is summarized in an error matrix where columns represent the reference data while rows represent the classified data. Error matrices compare on a category by category basis, the relationship between known reference data and the corresponding results of an automated classification. Such matrices are square, with the number of rows and columns equal to the number of categories whose classification accuracy is being assessed (Sivakumar *et al.*, 2003). Table 4.1 is an error matrix; entries are in (km^2) prepared to assess the quality of the classification, where Table 4.2 shows the pixel statistical report.

1Table 4.1: Error Matrix (km2) of the classification of LANDSAT images, classes from 1 to 13 are defined in Table 4.2

|	Class	Reference													Total	C.A (%)
		1	2	3	4	5	6	7	8	9	10	11	12	13		
Classification	1	4.61	0.00	0.00	0.00	0.00	0.00	0.00	0.00	0.00	0.00	0.00	0.00	0.00	4.61	100.00
	2	0.00	54.64	6.15	0.00	1.49	0.00	0.00	0.00	0.00	0.00	0.00	0.00	0.00	62.29	87.73
	3	0.41	29.21	134.29	0.00	8.53	2.03	5.27	0.41	0.00	0.00	0.00	0.00	0.00	180.14	74.55
	4	0.00	0.00	0.00	105.10	0.15	0.00	0.00	0.00	0.00	0.00	0.00	0.00	0.00	105.25	99.86
	5	0.00	0.51	3.09	0.00	77.28	1.55	0.00	0.00	0.00	0.00	0.00	0.00	0.00	82.43	93.75
	6	0.00	0.00	1.08	0.55	1.08	120.50	1.08	0.00	0.00	0.00	0.00	0.00	0.00	124.31	96.94
	7	0.00	0.00	0.34	0.00	0.00	0.00	14.85	0.00	0.00	0.00	0.00	0.00	0.00	15.18	97.78
	8	0.00	0.00	0.00	0.00	0.00	0.00	0.00	129.15	3.05	0.00	0.00	0.00	0.00	132.20	97.69
	9	0.00	0.00	0.00	0.00	0.00	0.00	0.00	0.10	9.98	0.00	0.00	0.00	0.00	10.09	98.97
	10	0.00	0.00	0.00	0.00	0.00	0.00	0.00	0.08	0.00	9.08	0.00	0.00	0.00	9.16	99.08
	11	0.00	0.00	0.00	0.00	0.00	0.00	0.00	0.00	0.00	0.00	2.26	0.02	0.00	2.28	99.13
	12	0.00	0.00	0.00	0.00	0.00	0.00	0.00	0.00	0.00	0.00	0.05	8.41	0.00	8.45	99.47
	13	0.00	0.00	0.00	0.00	0.00	0.00	0.00	0.19	0.19	0.00	0.00	0.00	21.40	21.78	98.26
	Total	5.02	84.37	144.95	105.65	88.53	124.08	21.20	129.93	13.22	9.08	2.30	8.43	21.40	758.16	
	P.A (%)	91.91	64.77	92.65	99.48	87.29	97.12	70.01	99.40	75.50	100.00	98.05	99.80	100.00		91.21

Table 4.2: Tabular summary of the thematic map- Pixel Classification Report

Class No.	Class Name	Legend	No pixels	Area(km^2)	Image%
1	Soil-ZOR		4151	4.61	0.59
2	Soil-AJL		56058	62.29	7.92
3	Soil-GOR		162130	180.14	22.90
4	Soil-KAT		94721	105.25	13.38
5	Soil-ZAY		74185	82.43	10.48
6	Soil-HIM		111875	124.31	15.80
7	Urban		13664	15.18	1.93
8	Irrigated Crops		118977	132.20	16.81
9	Non Irrigated		9078	10.09	1.28
10	Trees		8244	9.16	1.16
11	Surface Water		2050	2.28	0.29
12	Sea Water (Dead Sea)		7609	8.45	1.07
13	Green houses		19606	21.78	2.77
0	Unclassified		25524	28.36	3.61
	Total		712023	786.52	100

4.1.1.1 User's and Producer's Accuracy

The Error Matrix shows two measures of accuracy for individual classes. The accuracy values for each column indicate the percentage of cells in that ground truth class that were correctly classified. Values less than 100% indicate errors of omission (ground truth cells omitted from the output class). This value is sometimes called the producer's accuracy. Conversely, the accuracy values for each row show the percentage of sample cells in each output class that were correctly classified. Values less than 100% indicate errors of commission (cells incorrectly included in the output class). This value is sometimes termed the user's accuracy (Gercek, 2002).

4.1.1.2 Overall Accuracy

The overall accuracy is weighted by the number of samples (pixels) in each class, i.e. the sum of all samples on the diagonal divided by the total number of samples. However, as a single measure of accuracy, the overall accuracy (or percentage classified correctly) gives no insight into how well the classifier is performing for each of the different classes. In particular, a classifier might perform well for a class which accounts for a large proportion of the test data and this will bias the overall accuracy, despite low class accuracies for other classes. Therefore error matrix itself is not a sufficient way to predict the accuracy of the classified image (Bharti, 2004). In other words the average accuracy is the average of the accuracies for each class, and the overall accuracy is a similar average with the accuracy of each class weighted by the proportion of test samples for that class in the total training or testing set. Thus, the more accurate estimates of accuracy, (i.e., those from larger test samples), are weighted more heavily in the overall accuracy.

Average Accuracy and Overall accuracy are computed and found as follows:

Average Accuracy = 91.21 %

Overall accuracy = 90.33 %

4.1.1.3 Kappa coefficient

Kappa analysis is a discrete multivariate technique used in accuracy assessment for determining statistically if one error matrix is significantly different from another (Bishop *et al.*, 1975). Kappa coefficient is a measure of how true the correctly classified validation points really are, as compared to by pure chance (Milne and Trevor, 2007).

The Kappa statistic is given by the following equation (Foody and Atkinson, 2002):

$$K = \frac{N \sum_{i=1}^{k} nii - \sum_{i=1}^{k} ni + n + i}{N^2 - \sum_{i=1}^{k} ni + n + i}$$

Where (k) is the number of rows in the matrix, (n_{ii}) is the number of observation in row (i) and column (i), and n_i and (n_{+i}) are the marginal totals for row (i) and column (i), respectively, and (N) is the total number of observations. Kappa coefficient is calculated using this equation and found : **K = 0.948**

In order to maintain consistent nomenclature when describing the relative strength of agreement associated with kappa statistics, the following labels will be assigned to the corresponding ranges of kappa as shown in Table 4.3 (Landis and Koch, 1977):

Table 4.3: Kappa Statistics Ranges, (Landis and Koch, 1977):

Kappa Statistic	Strength of Agreement
< 0.00	Poor
0.00-0.20	Slight
0.21-0.40	Fair
0.41-0.60	Moderate
0.61-0.80	Substantial
0.81-1.00	Almost Perfect

According to this table the revealed K=0.948 shows that the strength of agreement is almost perfect and that supports the calculated average and overall accuracies of the error matrix.

4.1.1.4 Quality assessment and control positions
Testing areas are areas of representative, uniform land cover that are different from and considerably more extensive than training areas. They are often located during the training stage of supervised classification by intentionally designating more candidate training areas than are actually needed to develop the classification statistics. Normally, the training sites would always be verified in the field, using PCI Geomatica-10 software 100 points were randomly identified to be used as control positions, not all of the points are accessible such as points located in the border areas, only 43 points were verified in the field as shown in Table 4.3 and Figure 4.2, and all of these points were expected perfectly by the classification.

Table 4.3: Selected control positions

Class Name	Point NO.
Soil-ZOR	11,58,59
Soil-AJL	8,10, 12
Soil-GOR	29, 44,49
Soil-KAT	67, 86,89
Soil-ZAY	30,34,35,40
Soil-HIM	90,93,98
Urban	47, 54,74
Irrigated Crops	55,57,60,62,68, 71,76,78, 84
Non Irrigated	23,53,72
Trees	24,36, 25
Surface Water	32
Water	99
Green houses	2,6, 22, 28

Figure 4.2: Location of selected random points for control positions

4.2 Results of extracted Lineaments map

In this study two lineament maps were extracted by manual and semi- automatic methods, the extracted lineaments map by manual extraction is shown in Figure 2.3, resultant lineaments map from the semi-automatic method after removing the non-Geological lineaments is shown in Figure 4.5.

There are three directions dominating the pattern, these are SE-NW (148°), SSW-NNE (208°) and SW-NE (230°). This only partly interferes with the main tectonic directions, because the N-S direction-which follows the main transform shear zone-is also frequently present in the area with normal faults, and that is only weakly documented in the satellite images. Circular and angular variations of manually extracted lineaments map are given in Table 4.4 and Figure 4.4, circular descriptive statistical analysis and rose-diagram of the semi-automatic extracted lineaments maps are shown in Table 4.5 and Figure 4.6

Table 4.4: Circular Descriptive Statistical analysis of the manually extracted Lineaments Map

Parameter	Manual extracted lineaments
Number of analyzed Features	93
Mean Direction (Degrees)	221.8
Resultant Length (km)	173.4
Circular Variance	0.912
Angular Variance	1.335
Circular Standard Deviation (Degrees)	126.593
Angular Deviation (Degrees)	77.419
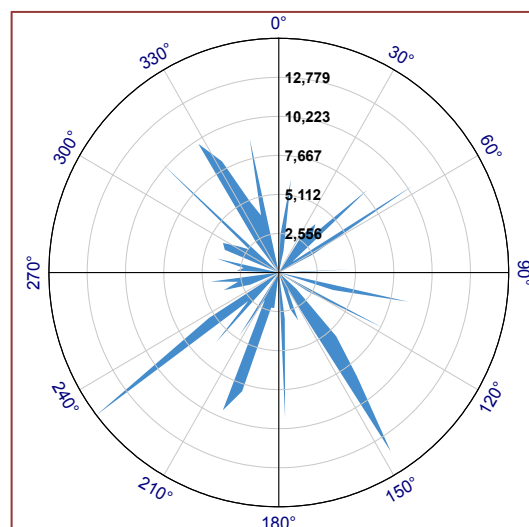
Figure 4.4: Rose Diagram of the manually extracted map
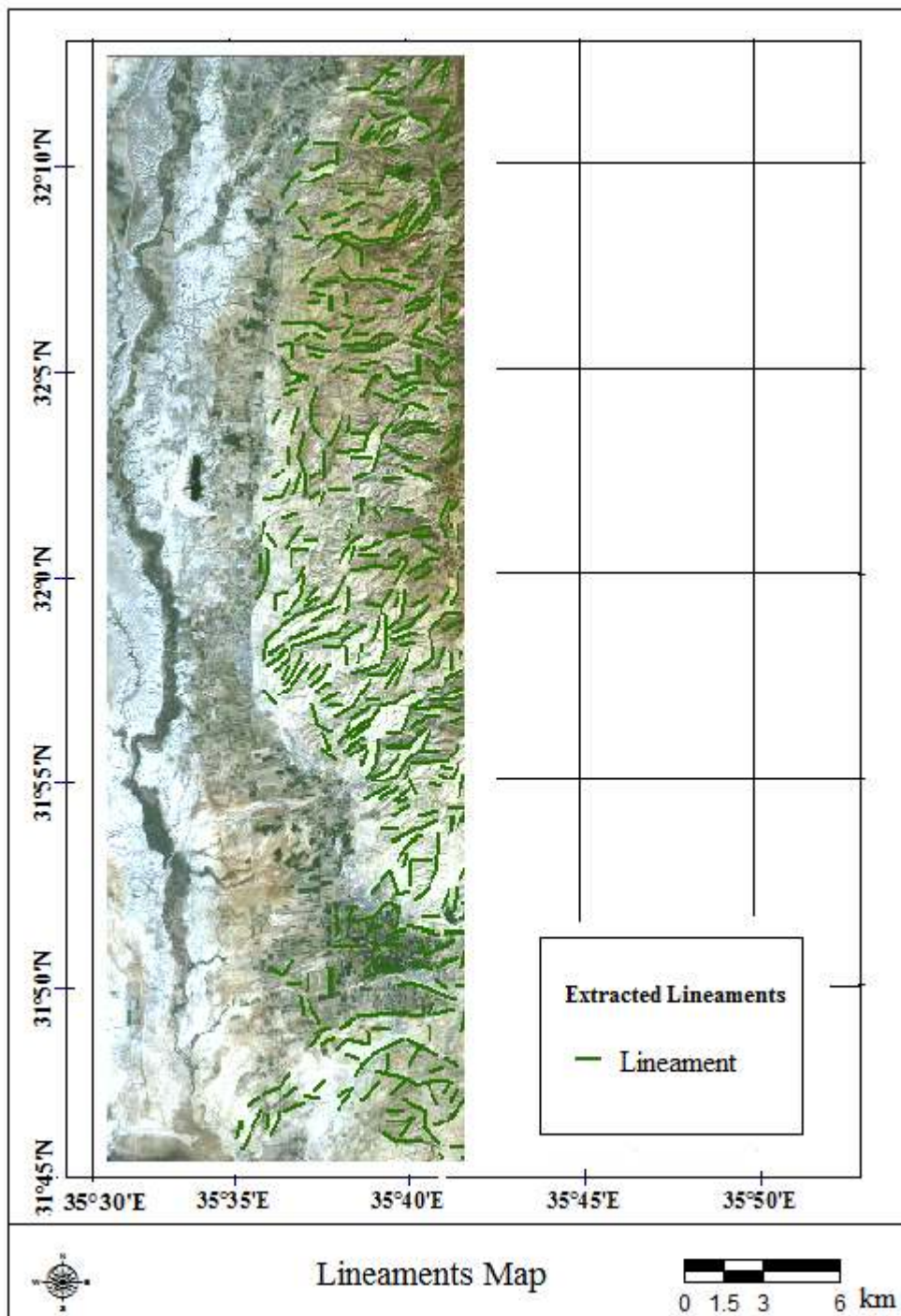
Figure 4.5: Semi- Automatic-Extracted lineaments map

after removing the non-Geological lineaments

Table 4.5: Circular Descriptive Statistical analysis of Semi-Automatic extracted Lineaments Maps

Parameter	Semi-Automatic
Number of analyzed Features	203
Mean Direction (Degrees)	209.683
Resultant Length (km)	145
Circular Variance	0.470
Angular Variance	0.941
Circular Standard Deviation (Degrees)	64.623
Angular Deviation (Degrees)	55.587
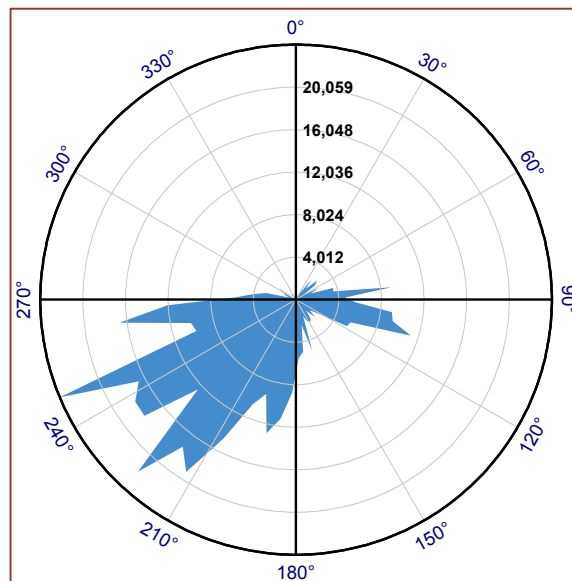
Figure 4.6: Rose Diagram of the Semi-Automatic extracted maps

Overlay method was used in this study to assess the results. In Figure 4.7.a the two generated maps by Manual and semi-Automatic methods were overlaid, it is clear that the number of lineaments extracted by manual method forms 23% of the total number of lineaments extracted by semi-automatic method, this doesn't mean higher accuracy of semi-automatic method as most of the extracted lineaments by this method are short lineaments and couldn't be connected together by the LINE algorithm, it is clear that the maximum length of the extracted lineaments by semi-automatic method equals 4.8 km , where the maximum length extracted by Manual method is 5.9 km which is more reasonable according to the structural Geological map of the study area.
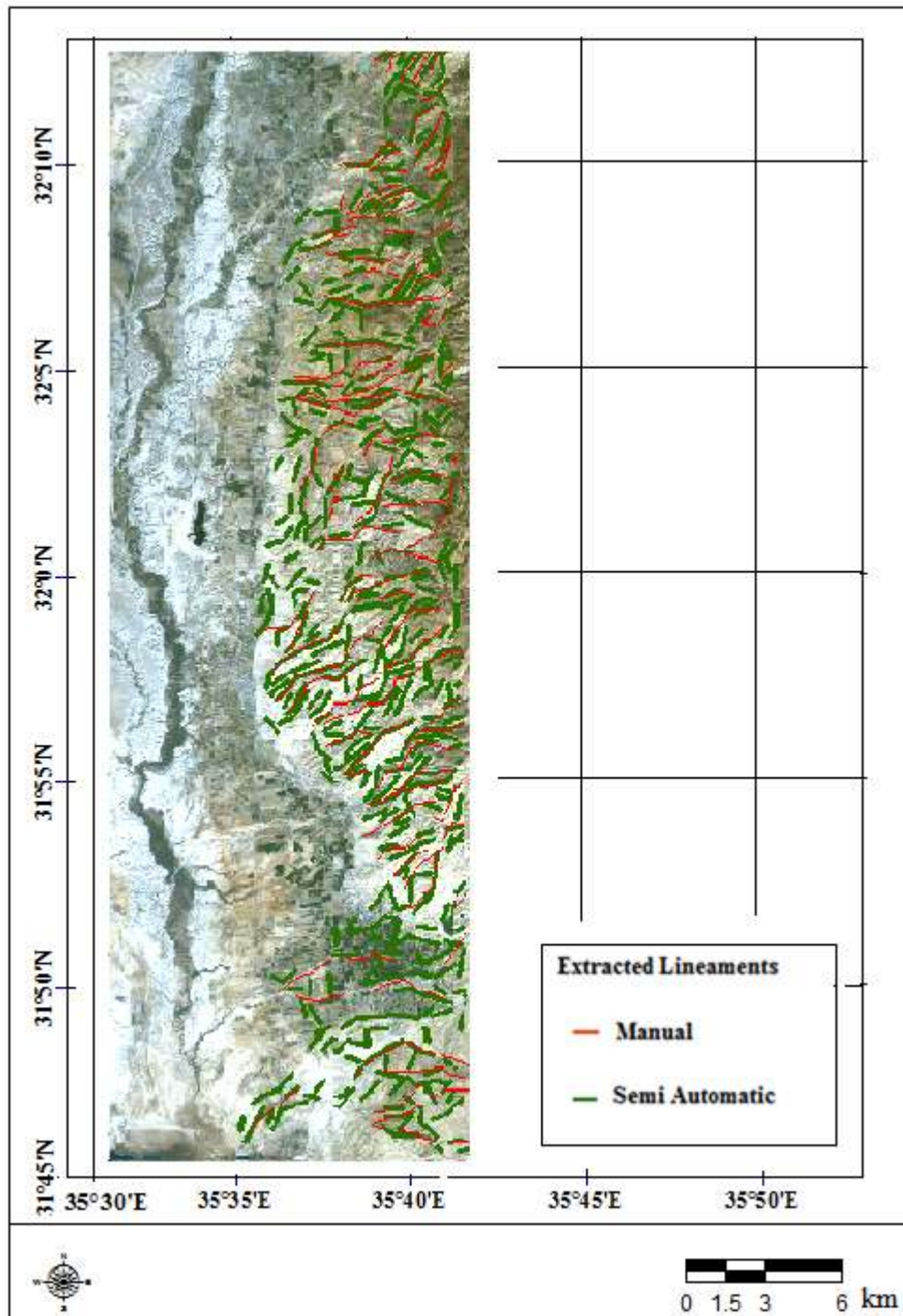
Figure 4.7.a: overlaying of the two extracted lineaments maps

Total length of manually extracted lineaments is 173.4 km, where it is 145 km in case of Semi-Automatically extracted lineaments, and that more reasonable according to the structural lineament map. Orientation of the lineaments for both lineament maps are also compared using rose diagrams as shown in Figure 4.4 and Figure 4.6, the mean direction of manual method results is 221.8 degrees and for the Semi-automatic is 209.68 degrees which

are quite similar and reasonable specially with reference to the high correlation between the angular variance of the two methods which equals 0.912 and 1.335.

Structural map is presented in Figure 4.7.b ,there are three directions dominating the pattern, these are, SE (155°), SW (190°) and NE (12°), this map shows that most of the lineaments extracted from these satellite images are partially matching with the drainage patterns not the tectonic features, especially in the hard rock area.
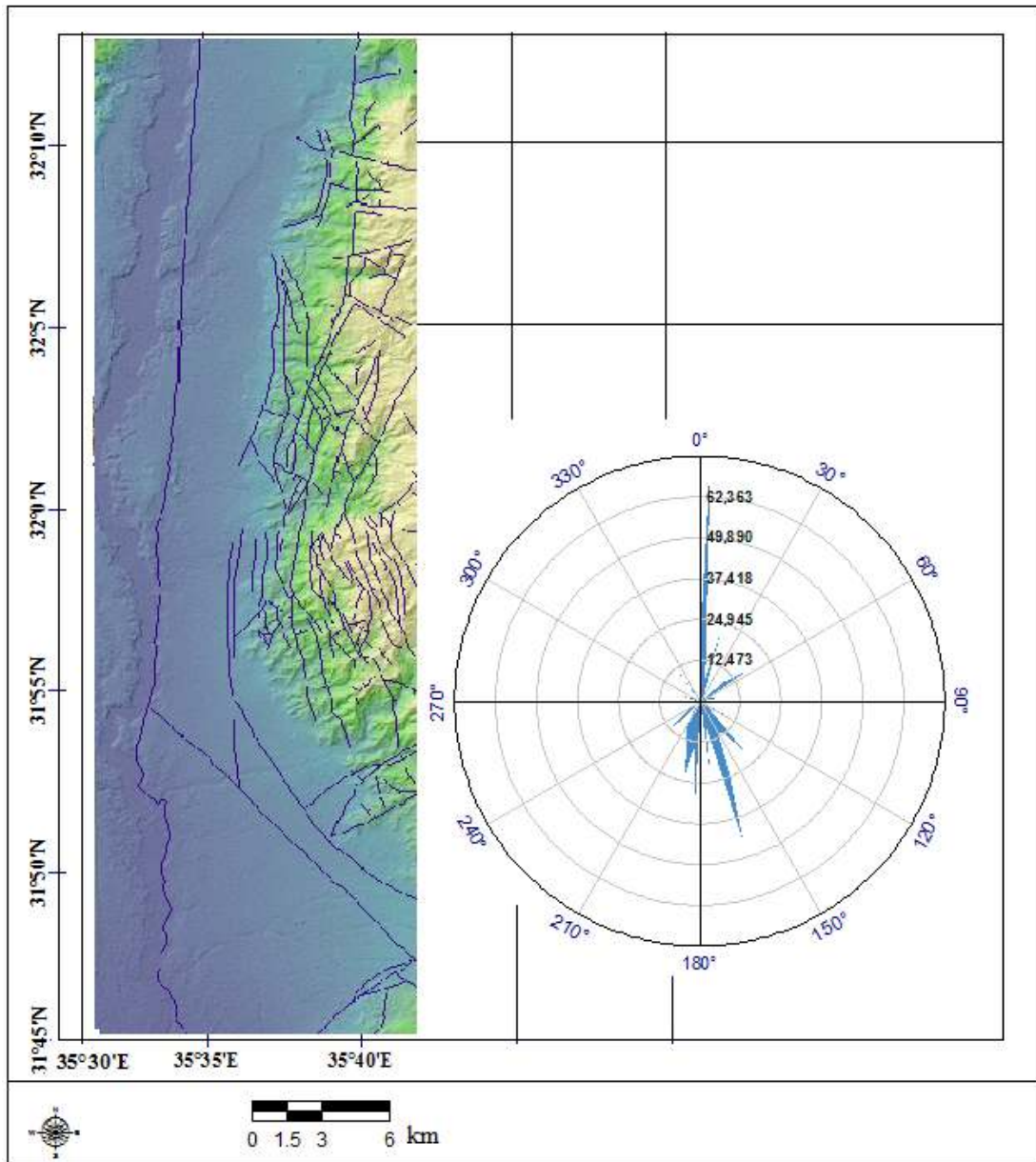
Figure 4.7.b: lineaments map showing major tectonic features.

(Reference: Natural Resources Authority, 1989)

At the end we conclude that the manually extracted lineaments map is more reasonable and representative, that might because it depended on an existing geological structural map and on the experience and interference of the analyst.

4.3 Results of extracting DTM

Two models were used to assess the accuracy of the generated DTM depending on the number of used GCP's:

Model A: using 18 GCPs, and 10 check points (CP's) collected from the field.

Model B: using 17 points chosen from the overlap area between the two DTM's,

Using model A for assessing the generated CARTOSAT-1 DTM : the mean difference in elevation was 3.27 m with 4.68 standard deviation as shown in Table 4.6, the Root Mean Square Error (RMSE) is 4.73m; around (1.89) pixels.

Table 4.6: Accuracy Assessment of Generated CARTOSAT DTM using Model A

point	GCP	CARTOSAT_DEM	Error
GCP1	-324.865	-323	1.865
GCP2	-303.275	-305	-1.725
GCP3	-178.065	-179	-0.935
GCP4	-176.987	-178	-1.013
GCP5	-191.081	-190	1.081
GCP6	-243.578	-246	-2.422
GCP7	-211.923	-213	-1.077
GCP8	-247.389	-249	-1.611
GCP9	321.457	323	1.543
GCP10	256.826	257	0.174
GCP11	-282.232	-281	1.232
GCP12	-255.819	-257	-1.181
GCP13	-283.765	-284	-0.235
GCP14	-237.126	-237	0.126
GCP15	330.858	329	-1.858
GCP16	-241.343	-239	2.343
GCP17	-211.783	-210	1.783
GCP18	-177.632	-178	-0.368

CP1	-361.7645	-359	-2.7645
CP2	-296.2213	-292	-4.2213
CP3	-251.1563	-257	5.8437
CP4	-223.8764	-232	8.1236
CP5	-279.3342	-268	-11.3342
CP6	-256.0875	-245	-11.0875
CP7	-101.2385	-99	-2.2385
CP8	15.1692	10	5.1692
CP9	1077.205	1068	9.205
CP10	926.8659	936	-9.1341

Using model B for assessing the generated CARTOSAT-1 DTM : the mean difference in elevation was 2.23 m with 2.4 standard deviation as shown in Table 4.7 the Root Mean Square Error (RMSE) is 2.37m ; around (0.94) pixels

Table 4.7: Accuracy Assessment of the Generated CARTOSAT DTM, using Model B

Point	DEM1	DEM2	Error
1	-313	-315	-2
2	-320	-317	3
3	-311	-309	2
4	-334	-335	-1
5	-342	-339	3
6	-341	-339	2
7	-313	-312	1
8	-274	-277	-3
9	-314	-311	3
10	-264	-267	-3
11	-227	-224	3
12	-180	-181	-1
13	-136	-137	-1
14	66	64	-2
15	130	133	3
16	169	167	-2
17	462	465	3

Profiles at different locations of CARTOSAT and ASTER DTM's also compared as shown in Figures 4.8, 4.9, 4.10 and 4.11; the results of this comparison at different distances (10, 20, 30 and 40 km) from the north edge of the study area are shown in Table 4.8.
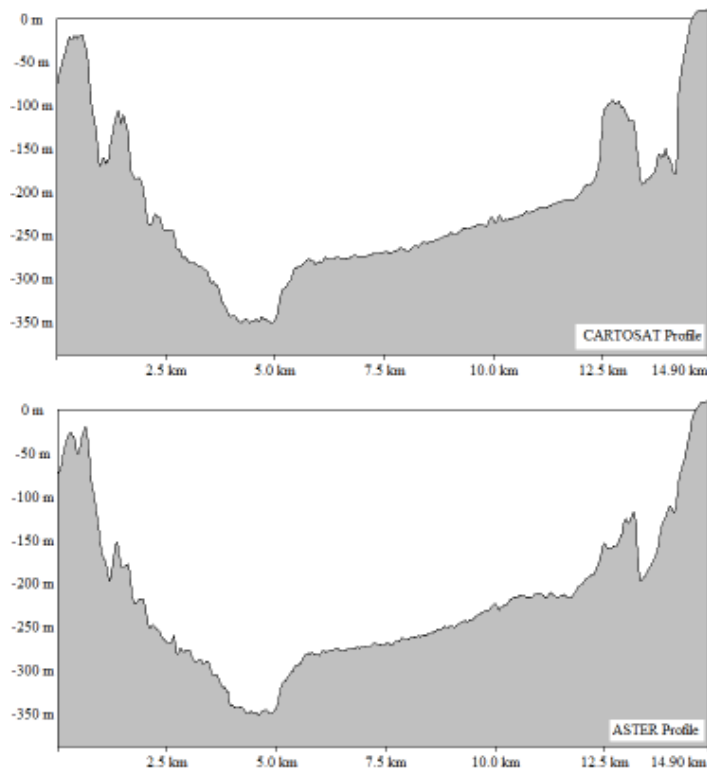
Figure 4.8: Comparison of a Profile 10km from the North edge of the study area produced by CARTOSAT and ASTER satellite images
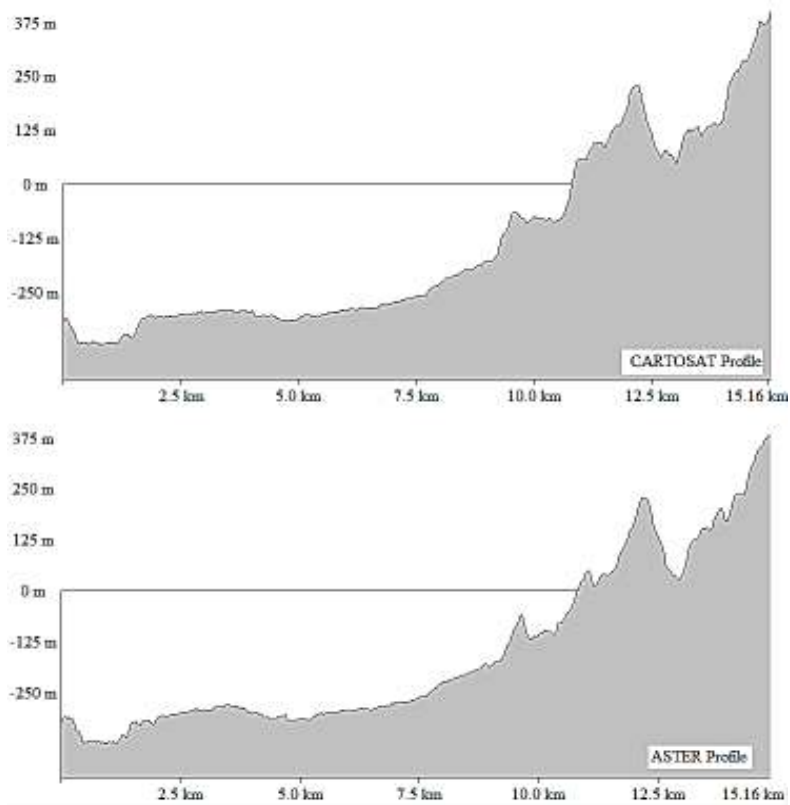
Figure 4.9: Comparison of a Profile 20km from the North edge of the study area

produced by CARTOSAT and ASTER satellite images
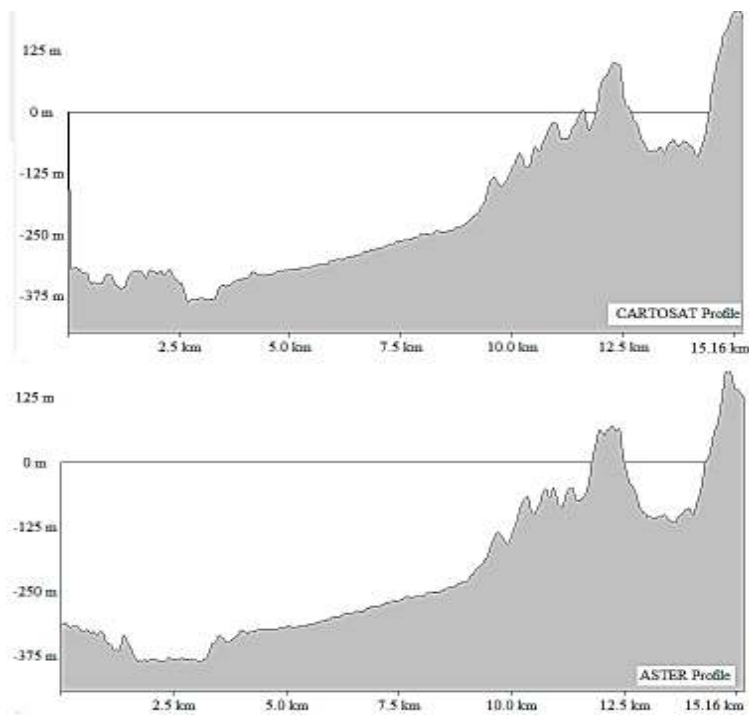
Figure 4.10: Comparison of a Profile 30km from the North edge of the study area

produced by CARTOSAT and ASTER satellite images
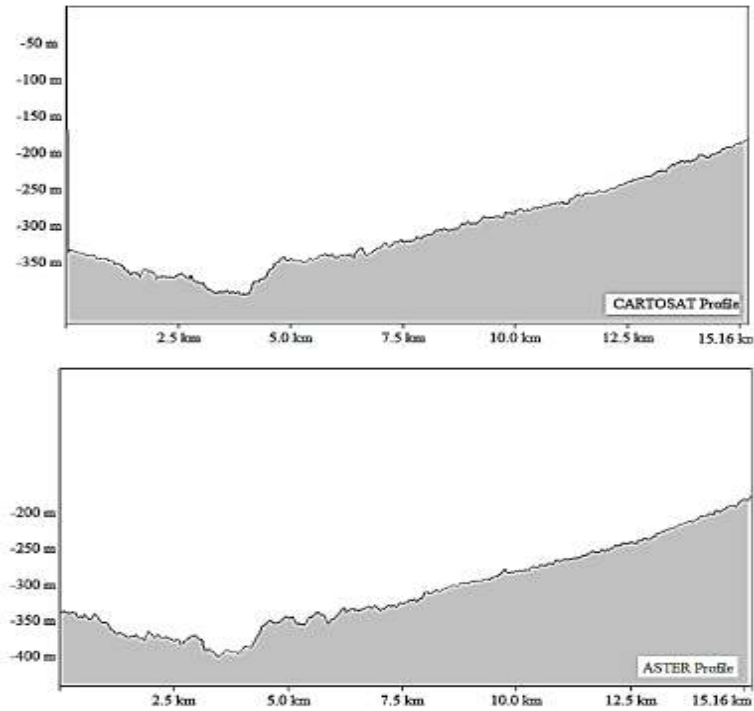
Figure 4.11: Comparison of a Profile 40km from the North edge of the study area

produced by CARTOSAT and ASTER satellite images

Table 4.8, Comparison between CARTOSAT and ASTER DTMs profiles at different locations by
Root Mean Square Error (RMSE)

CARTOSAT-ASTER	RMSE			
	at 10 km	at 20 km	at 30 km	at 40 km
	24.136	27.374	37.210	14.560

According to Table 4.8 it is clear that the minimum difference between the two DTM's is at 10 and 40 km from the north edge of the study area, which are almost flat areas with no steep mountains or narrow canyons, this reflects the ability of CARTOSAT data to generate DTM's in mountainous regions, and steep areas.

Topologic assessment for the extracted Drainage network from CARTOSAT and ASTER data also done in this study as shown in Table 4.9 & 4.10 , the two sub basins located in the study area were used to assess ,the results of this assessment shows a significant differences between the two extracted networks .

Table 4.9: Test of significance in drainage density, Data from CARTOSAT 2011

Basin	Stream Order	No. of Streams	Mean Drainage Density (km/km^2)
Shuna (Jericho)	First order	297	0.0574
	Higher order	78	0.0324
Damia	First order	341	0.0478
	High order	82	0.0271

Table 4.10: Test of significance in drainage density, Data from ASTER 2011

Basin	Stream Order	No. of Streams	Mean Drainage Density (km/km^2)
Shuna (Jericho)	First order	92	0.0495
	Higher order	23	0.04102
Damia	First order	104	0.0352
	High order	25	0.0294

4.4 Verification of the results of AHP and Fuzzy Logic methods

Verification of the results was carried out using two methods: using collected data from wells and boreholes, and by Geophysical studies as shown below:

4.4.1 Verification of the results using collected data from wells and boreholes

In order to compare the results from the two methods the RMSE was calculated and found 3.64, and the coefficient of determination $R^2 = 0.88$ as shown in Figure 4.12.Tentatively this shows good indication about the reliability of the results; however more verification methods were applied in order to get he he significance and reliability of the results.
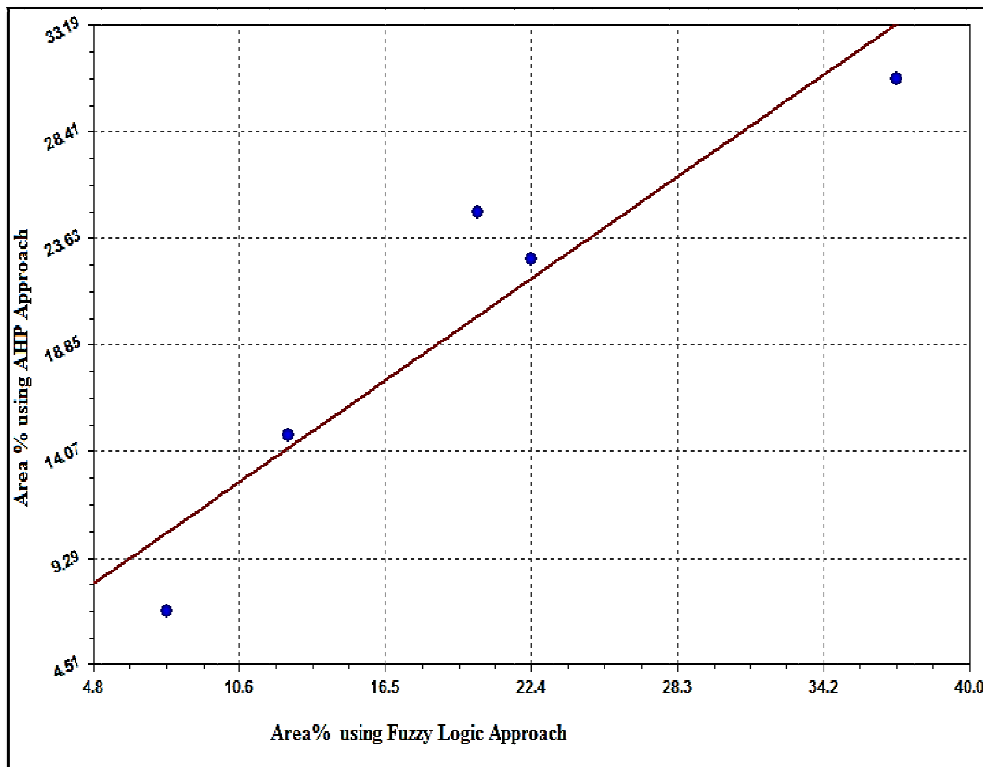
Figure 4.12: Comparison between GWPZ Categories using Fuzzy Logic and AHP approaches

Several studies used collected yield data from boreholes to verify the generated GWPZ maps such as (Krishnamurthyl *et al.*, 2000; TALABI and Tijani, 2011; Srivastava and Bhattacharya, 2006; Singh and Prakash, 2003), in these studies the collected data were used to categories the area into several zones according to the yield of each well and/or according to the depth of the well, these zones were then compared with the generated GWPZ maps. Well yield of an area depends upon the permeability of the aquifer, in addition to the amount of groundwater available in the aquifer system. Higher well yields indicate relatively greater groundwater availability than areas with low well yields. (Krishnamurthyl *et al.*, 2000)

 In this study data of existing wells were collected from the records of Ministry of Water and Irrigation (WAI), and Water Authority in Jordan (WAJ), in order to be used for the verification of the results. Some of the data could not be used for the verification due to the following reasons (WAJ, 2006):

- In the Jordan valley area many wells were illegally drilled and operated and there are no data available.
- In the highlands, privately managed individual farms are irrigated by groundwater from different private wells.

- Industries and others are located outside of cities limits and therefore secure their own water supplies either by using surface water like the Arab Potash company or drill their own private wells as the case of the phosphate company; these well data are also not available.

- The loss of well capacity is stronger in the private sector than in the public sector, as public-sector wells are developed over the whole depth of the aquifer.

Table 4.11 shows the characteristics of the used wells in the verification over the groundwater potential zones in the study area.

Table 4.11: Characteristics of wells over GWPZ's

GWPZ	Min Yield (m^3/h)	Max Yield (m^3/h)	Mean Yield (m^3/h)	Min Depth (m)	Mean Depth (m)	Max Depth (m)
Very Poor	20	75	46	45	71	92
Poor	23	110	78	61	98	126
Moderate	50	70	57	140	227	400
High	60	150	101	45	59	69
Very High	75	178	135	247	379	412

The assessment of the GWPZ by remote sensing techniques refers mainly on the recharge conditions for the uppermost aquifer in each region. For these aquifers the appropriate well yield can be an excellent parameter to verify the assessment of the GWPZs. Less relevant is the depth of the wells. One would expect that remote sensing techniques are rather adaptable for shallow aquifers with depths down to 30 to 50 m. In case of the Jordan Valley Escarpment there occur thick limestone sequences of several hundred meters, which form the uppermost unconfined aquifer. Beside good infiltration condition they offer also a high storage volume, which can be responsible for the high yield. In the Jordan Valley floor the shallow aquifers are rather thin and underlain by the impervious Lisan marls, so that wells with depths of more than 40 m usually belongs to the deeper confined aquifers, whose recharge are not influenced by direct vertical infiltration and percolation, which is the process selected in this study for the assessment of the GWPZ, but by lateral recharge. Therefore it was tried to avoid to include wells of the confined aquifers. Under these conditions well yield and well depth was

checked for the quality of the GWPZ delineation. Although there is no certain trend controlling the relation between wells yield and GWPZ, we can notice that the highest yield wells located in high and very high groundwater potential zones. Thus the generated groundwater potential map could be used as a reference for future exploration.

4.4.2 Verification of the results using Geophysical studies

Results are verified by subsurface data obtained from geophysical studies (ground truth) in order to increase the accuracy of the resultant maps. Shallow geophysical study carried out in the Jordan Valley by (Al-Zoubi *et al.*, 2012) to estimate the depth of shallow aquifer, to estimate the aquifer properties (water content and permeability), to monitor the variation of water contents with the time, to delineate buried wadis and ancient channels and to delineate water boundary between fresh and saline water.

In this Geophysical study several methods were used, as summarized below:

1. **Ground Penetrating Radar (GPR)**

   Twenty five GPR profiles were conducted in the Jordan valley area in order to delineate water saturated zones, buried wadis channels and the wadis fan. Only 3 profiles located in the study area, these profiles are GRP-4, GPR-9, and GPR-14 (Figure 4.16).

   GPR-14 shows different sub surface anomalies the shallow one represent shallow fault and the deeper two anomalies may present buried old channels which run from the east to the west.

   GPR-4 profile: as shown in Figure 4.13 , the radar cross sections shows water saturated zones represented by high reflection of the electromagnetic waves between 14 to 23m deep. This profile located in moderate groundwater potential zone as per the AHP and Fuzzy logic approaches.

Figure 4.13: Ground Penetrating Radar Profile (GPR- 4) from the lower Jordan Valley measured with 40 MHz Antenna showing the unsaturated top sedimentary sequence as well as the water saturated lower sequence with the groundwater table. (Al-Zoubi *et al.*, 2012)

Contrary GPR-9 profile as shown in Figure 4.14 shows shallow water saturated zones between 1 and 12m depth. This profile located in low groundwater potential zone according to the results revealed from AHP approach, while it is located in moderate groundwater potential zone as per Fuzzy logic approach results.

Figure 4.14: Ground Penetrating Radar Profile (GPR- 9) from the lower Jordan Valley measured with 100MHz Antenna showing the water saturated top sequence. (Al-Zoubi *et al.*, 2012)

The GPR-14 profile shows different sub surface anomalies, the shallow one represent shallow fault and the deeper two anomalies may present buried old channels which run from the east to the west. No saturated zone appears in the top of this profile with more impervious sediments. As per the results of AHP approach this section was classified in poor GWPZ, and in very poor zone according to Fuzzy logic results, though it could be possible that the two gravel channels might be confined aquifers (as shown in Figure 4.15), but receiving the groundwater recharge not from the top, but by lateral groundwater flow.
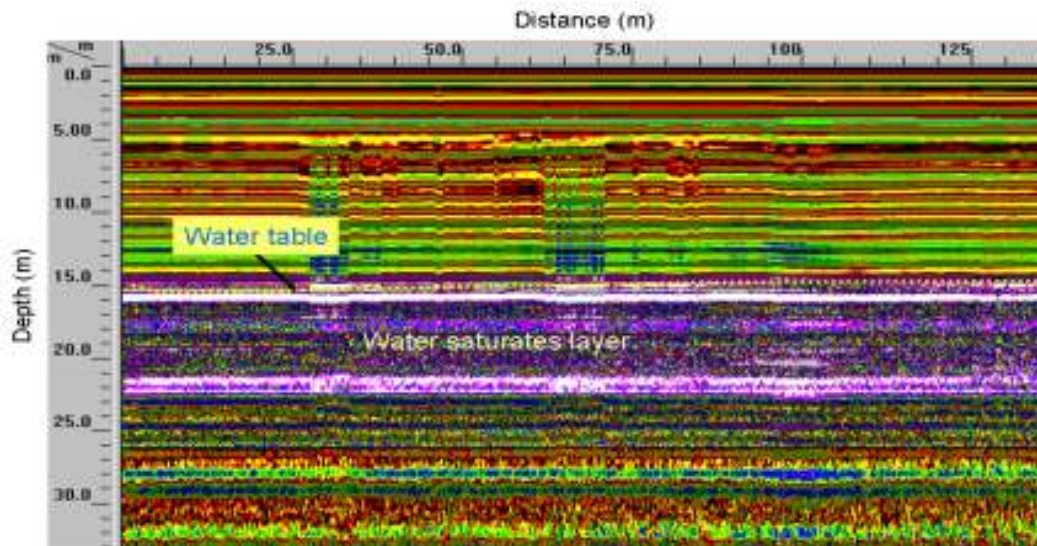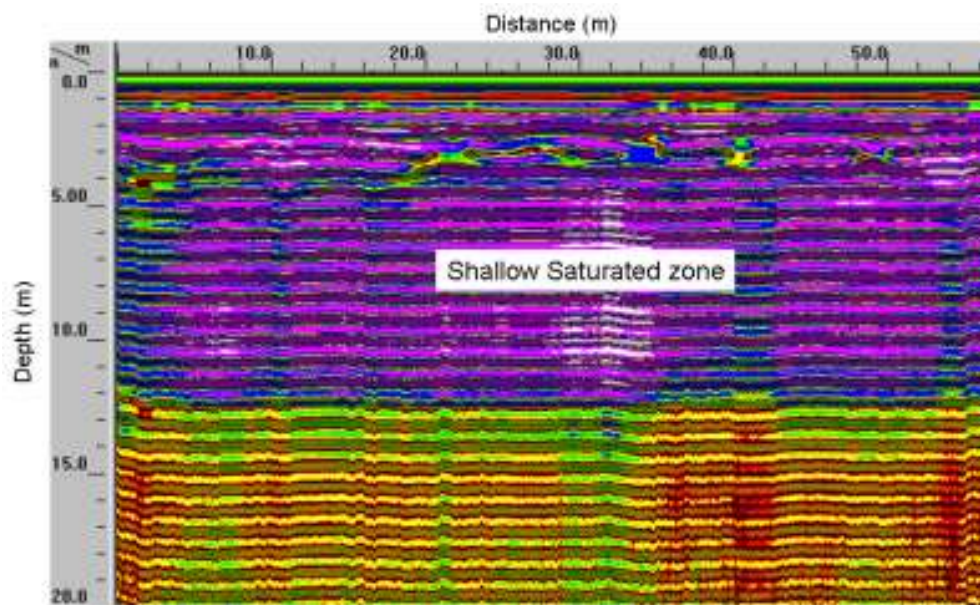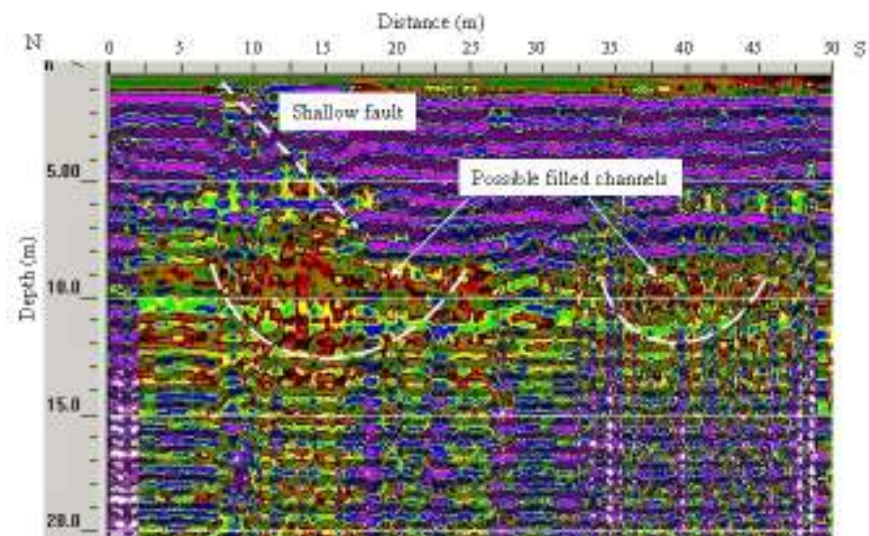

Figure 4.15: Ground Penetrating Radar Profile (GPR- 14) from the lower Jordan Valley measured with 100MHz Antenna; the section showing unsaturated top layer with a normal fault and two old buried gravel channels . (Al-Zoubi *et al.*, 2012)
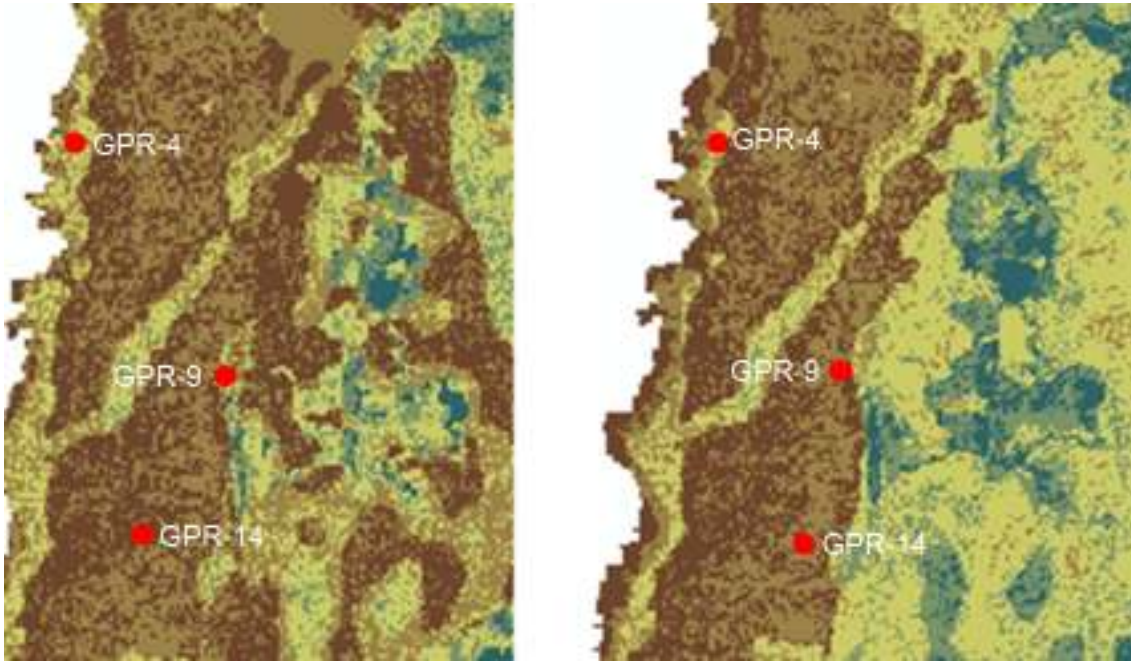
Figure 4.16: locations of used GPR-profiles: GPR-4, GPR-9 and GPR-14

left: Fuzzy logic generated GWPZ-map, Right: AHP generated GWPZ-map

2. Nuclear Magnetic Resonance (NMR)

Nuclear magnetic resonance NMR or proton magnetic resonance PMR is a new geophysical technique which is used to indirectly estimate the water content of saturated and unsaturated zones of the subsurface; it is mainly used for estimating porosity, permeability and transmissivity of groundwater aquifers (AL-Zoubi et al., 2012).

As an example one short profile is shown after AL-Zoubi et al. (2012) with the PMR-stations 1,2,3,5,7,9. Permeability changes with depth along the study area are shown in Figure 4.17 , where water content distribution with depth along this short profile is shown in Figure 4.18

In the surface near 0-10 meters to which the applied remote sensing techniques refers it shows rather low permeability's, with possible small buried channels with higher permeability between 10-20 m depth. This area is considered as poor to very poor GWPZ as per the Fuzzy logic approach classification, where it is considered as poor to moderate GWPZ as per the classification of the AHP model, this shows the significant of Fuzzy logic approach results compared with the AHP approach. In the depth of 40-60 m are higher permeable zone of sandy or gravelly material which

forms the deeper confined aquifer, but this depth can't be assessed by the applied remote sensing technique.

The area located between stations 1 and7 has poor to moderate water content down to a depth of 30 m, only between PRM to PRM 1 seems that there occurs on the surface a thin wet soil layer. As mentioned GWPZ in both maps (AHP and Fuzzy Logic) show rather poor, partly in the AHP approach moderate conditions.

Figure 17.4: Permeability changes with depth along the short measuring section

(Reference: Al-Zoubi *et al.*, 2012)

Figure 4.18: Water content distribution with depth along the short measuring section
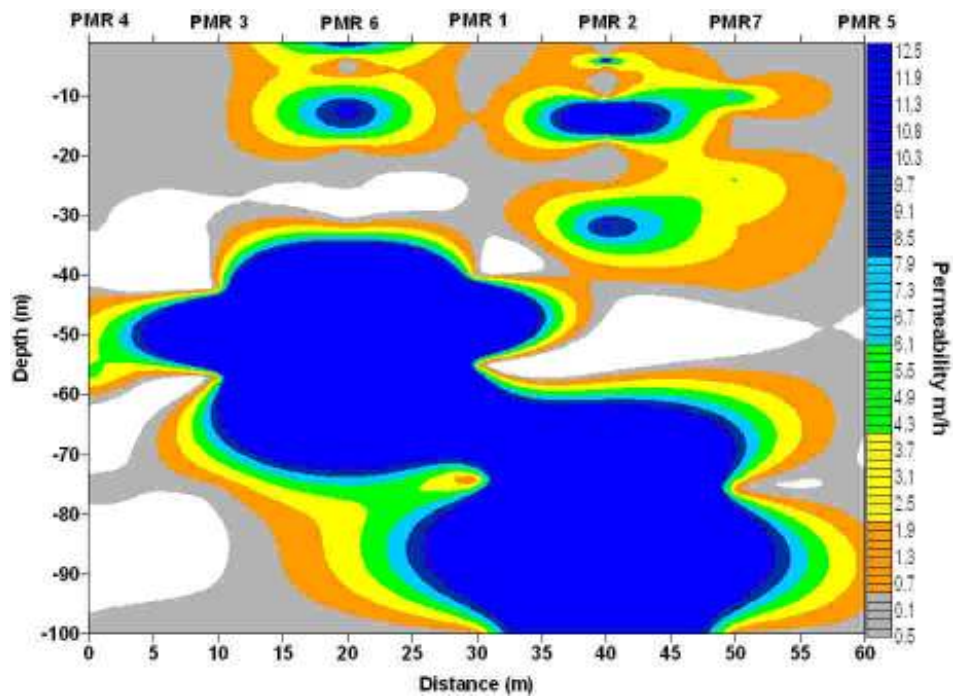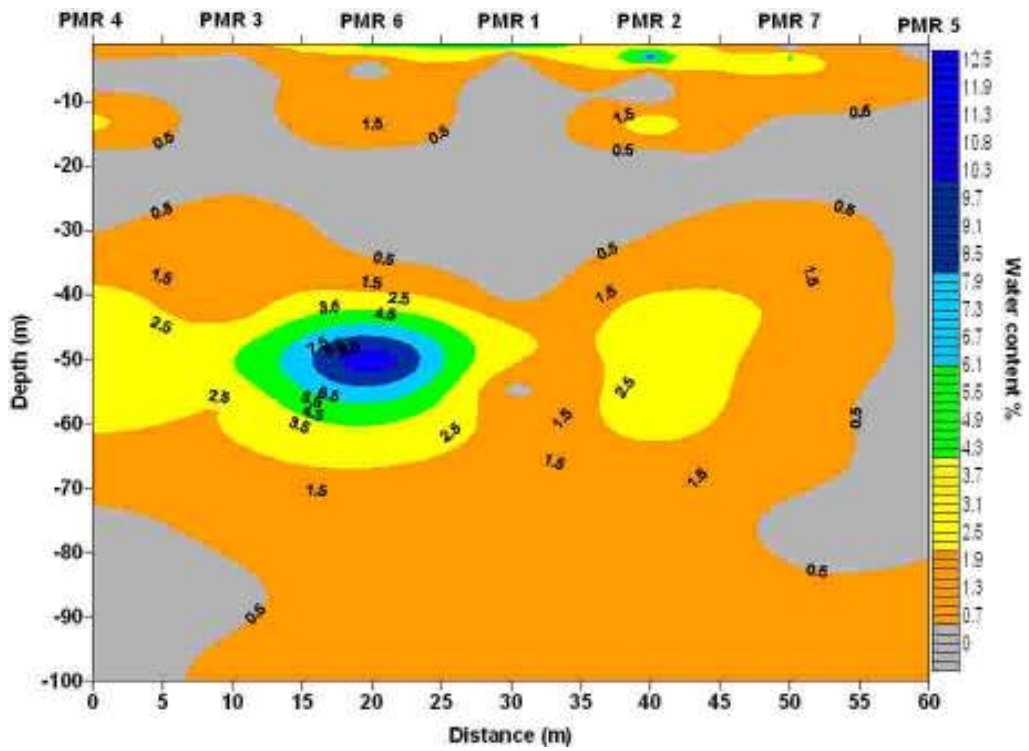
(Reference: Al-Zoubi *et al.*, 2012)
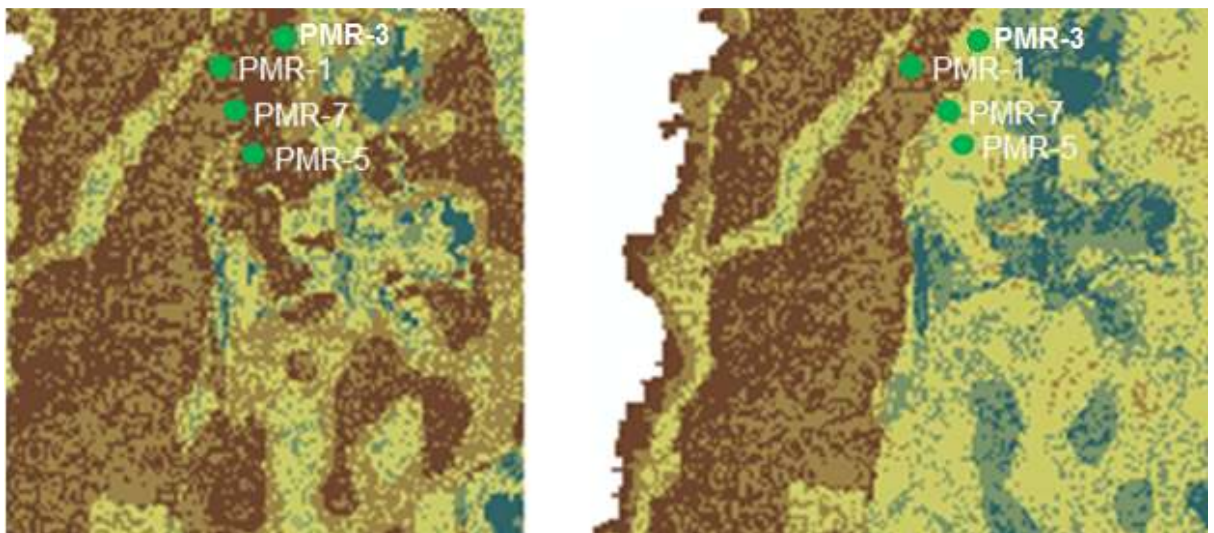
Figure 4: locations of the short NMR profile with the PMR stations 1, 3,5and 7

left: Fuzzy logic generated GWPZ-map, Right: AHP generated GWPZ-map

3. Vertical Electrical Sounding (VES)

This method is used to investigate the subsurface structure and to evaluate the geo-hydrological conditions of the study area. Fortytwo VES measurements in the Lower Jordan Valley (Shuna/ Jericho) basin were carried out (Al-Zoubi et al. 2012), 3 of these profiles located in the study area were used for verifying the GWPZ-results (profile-9, profile-6, profile-3).

The resistivity of coarse-grained, well-consolidated sandstone saturated with fresh water is higher than that of unconsolidated silt of the same porosity, saturated with the same water (Sabet ,1975).

Figure 4 shows VES profile-.9, this profile which is formed mainly by varying marly Lisan Formation in the upper 20 meters, shows low to moderate water content with partly high saline content according to the values of the resistivity which vary from (1.82 to 48.6 ohm). This profile is located in poor GWPZ area in both maps.

In Figure 4 with the VES profile -6, which is formed by coarse sand and gravel layers of the wadi channel, the high content of fresh waters appears clearly at shallow depth from (1.00 to 8 m).This profile section is located in a very high GWPZ area as per the generated map from Fuzzy logic, while it is located in high GWPZ area as per the generated map from AHP as shown in figure.4 and.4 below.

Figure 20.4: Electric Resistivity cross section along profile 9 in southern Jordan Valley

(Reference: Al-Zoubi *et al.*, 2012)

In Figure.4 the VES profile 3 shows once again at the top impervious varying marly Lisan formation at two places disturbed by faults with some higher permeability. The water content is low to moderate water, partly once again with higher salt content. A certain Zonation appears at distances of 1 to 60 m and from 60 to 200 m) from E to W, this profile located in low GWPZ area as per the results from AHP approach, while it is located in low to moderate

GWPZ areas as per the Fuzzy logic results, as shown in Figure 4.23 and Figure 4.24 which gives good indication about the significance of this method.

Figure 4.21: Electric Resistivity cross section along profile 6 in southern Jordan Valley
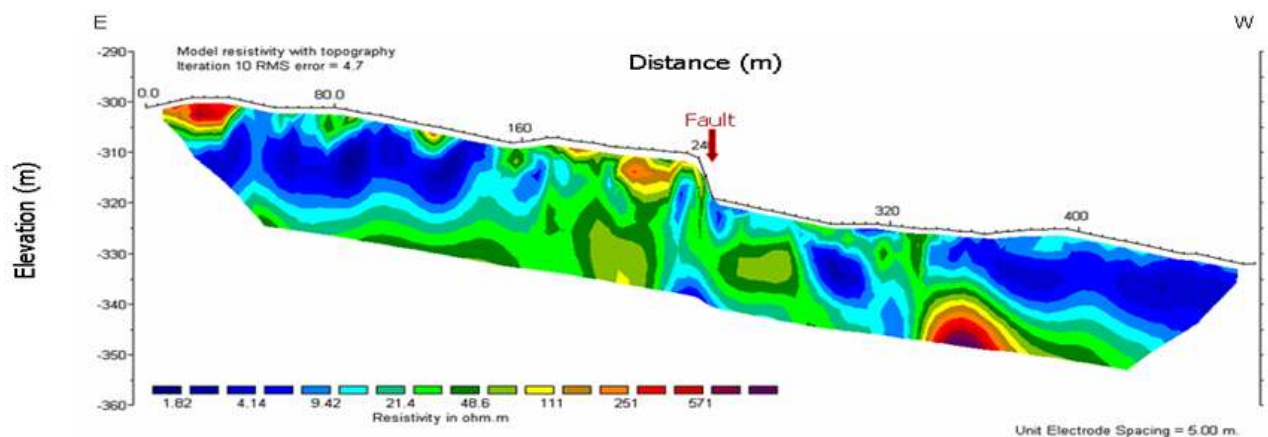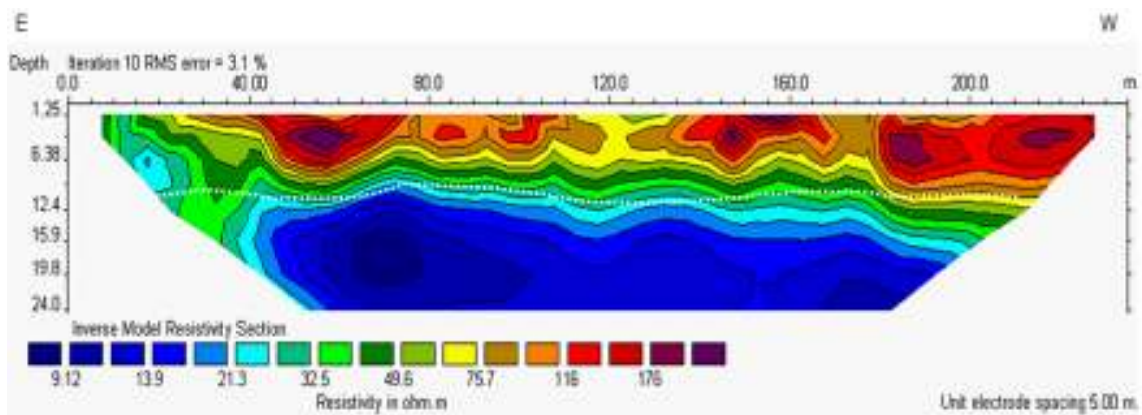
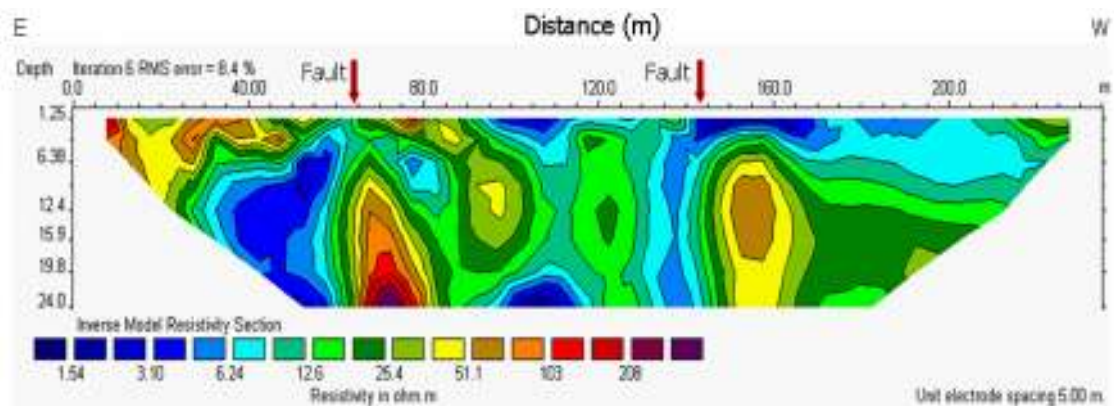(Reference: Al-Zoubi *et al.*, 2012)

Figure 4.22: Electric Resistivity cross section along profile 3 in southern Jordan Valley
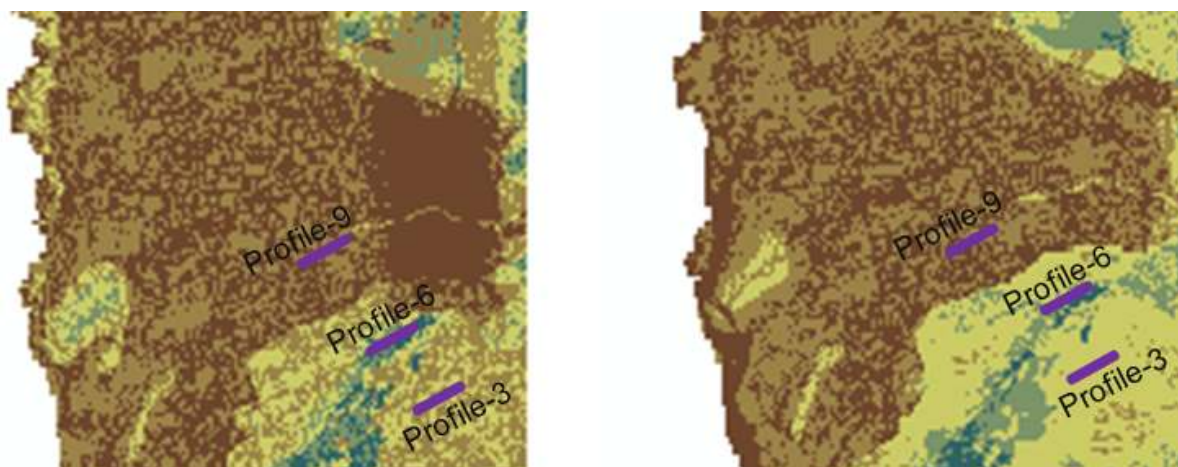
(Al-Zoubi *et al.*, 2012)

Figure 4.23: Locations of used VES profiles
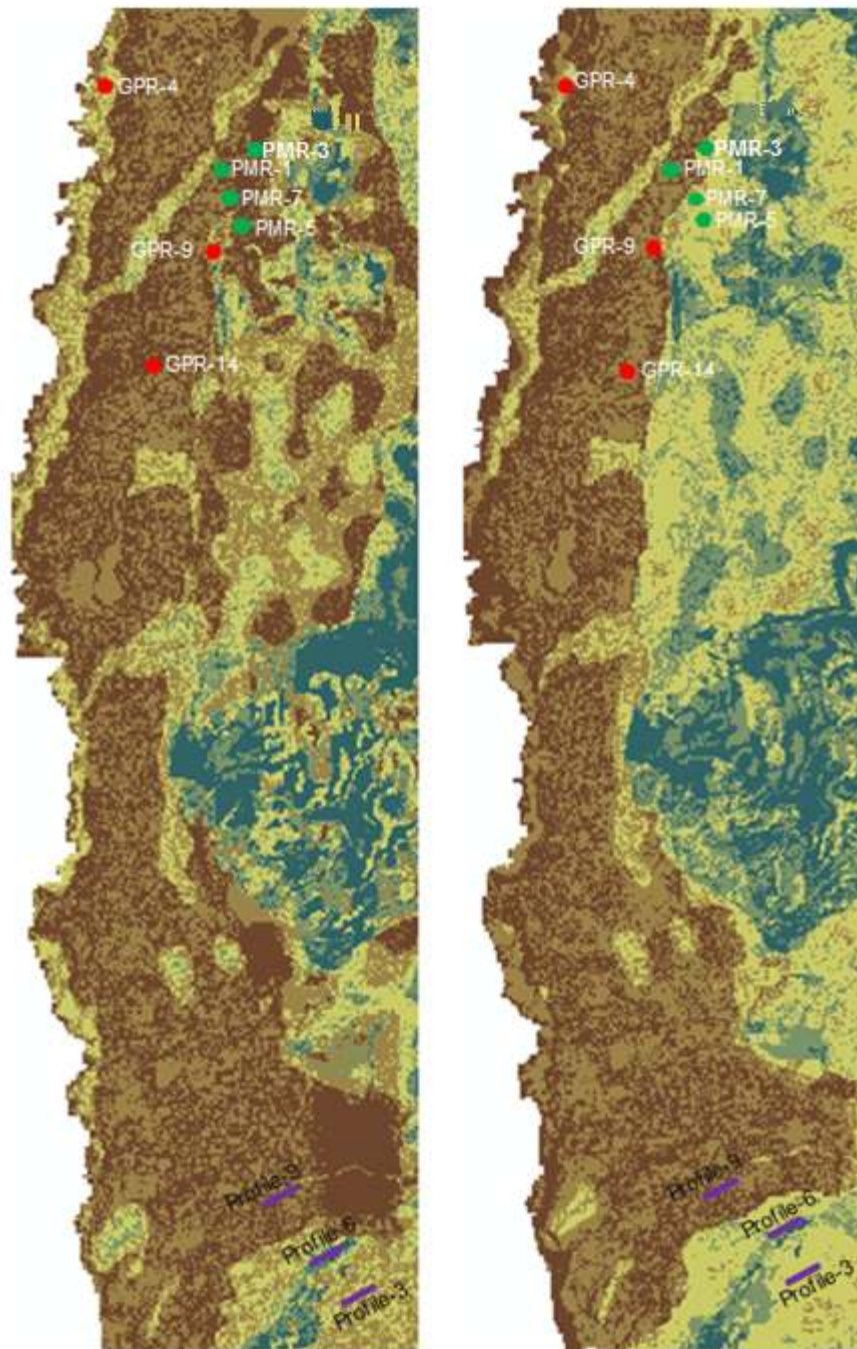
Figure 4.24: Locations of all used Geophysical Data

4.3 Discussion of the Results

In this study several assumptions could positively or negatively influence the accuracy of the GWPZ map such as:

1. Selection of parameters: It is obvious that some parameters have an effect in certain areas, for example; lineaments density has clear effect in the escarpment area (hard-rocks) and has no effect at all in the Jordan Valley where the young sedimentation covers the polder tectonic lines. Rainfall as another example has significant importance only in the highlands as well as slope steepness which has low importance in the Jordan valley area. On the other hand; Land cover/ land use plays an important role in the determination of the GWPZ in the Jordan valley (low lands) which is mainly an agricultural area compared with bared mountains in high lands.

2. The weighting and ranking of the parameters: the way we weight the parameters has an important effect on the final result of GWPZ map, especially when the parameter has high importance and possess high weight, therefore we should give high accuracy in assigning the relationship between the parameters and the relationship between the classes of each parameter. Literature review should not be the only way for weighting, weights might be different due to the nature and characteristics of the study area, therefore expert's interference should appear when assigning weights according to their experience in specific area.

3. The overlaying map procedure to receive the GWPZ: Fuzzy logic and AHP methods were used to provide weights for the parameters by means of overlay procedure using various thematic maps for the delineation of groundwater potential zones. The overlaying procedure for demarcation the final groundwater potential zone map differs from one method to another according to the used function of overlaying, and that accordingly affect the final results.

4. Aspect of resolution: Medium and high spatial resolution satellite images were used in this study, using high resolution images makes different features such as buildings, and other infrastructure are easily visible, and increases the accuracy of the resultant map.

The GWPZ map generated by the Fuzzy logic approach shows higher significance than the map generated by AHP model, therefore it is used for analysis and discussion. The area that has very high groundwater potential zone is located in the Middle Eastern part covering about 7.7 % of the study area, another small areas that have very high Groundwater potential scattered along the Middle strip of the study area, this area located on high lineament density

zone and (Fuhays-Hummar-Shua'ab) Geological formation in the Jordan Valley Escarpment .The high potential area covers 12.6 % while the greatest portion of the area about 37.1 % belongs to poor groundwater potential zone; which is located over lisan-marl Geological formation in low lineament density area in wadi flow. Moderate GWPZ forms 20.2% of the area, located between escarpment and Alluvial fans Geomorphological features. Wadi flow with low lineament density, very steep slope and very high drainage density area lie in very poor potential zones which forms about 22.4 % of the study area.

4.3.1 Sensitivity analysis

Sensitivity analysis was carried out in order to have valuable information on the influence of rating values and weights assigned to each parameter (Gogu and Dassargues, 2000); map removal sensitivity analysis is used in this study to determine the sensitivity of GWPZ map by removing one parameter at each generation of the GWPZ map.

(Napolitano and Fabbri, 1996; Lodwik *et al.*, 1990; Samake *et al.*, 2003) applied different techniques to define and assess map removal sensitivity analysis and they used the following expression:

$$\text{Six} = \frac{\text{Pi}}{N} - \frac{Pxi}{n}$$

Where S_{ix} is sensitivity associated with the removal of one map of parameter X, P_i is the computed potential value of the cell or the area, P_{xi} is the potential value of the cell or the area after excluding parameter X. N is the total number of used parameters for computing potential value of the cell or the area, n is the number of used parameters for computing potential value of the cell or the area after excluding one parameter.

In order to assess the magnitude of the variation created by removal of one parameter, the variation index is computed as:

$$Vi = \left[\frac{Pi - Pxi}{Pi}\right] * 100\%$$

Where V_i is the variation index, P_i is the computed potential value of the cell or the area, P_{xi} is the potential value of the cell or the area after excluding one parameter.

Applying this analysis will give clear idea about the contribution of each parameter in the potential value of each cell or area; the results of the analysis are shown in Table 4.12

Table 4.12: Statistics of variation index produced by map-removal sensitivity analysis

Parameter of Sensitivity	Min	Max	Mean	Std. Deviation
Geology& Lithology	0	53.46	41.22	3.41
Geomorphology	0	51.17	41.09	3.19
Lineament Density	1	50.22	40.67	3.23
Slope	0	52.73	40.12	2.95
Soil	0	48.23	38.56	2.67
Drainage Density	0	47.93	36.98	3.01
Land Use	1	49.86	35.67	2.78
Rainfall	0	42.04	35.41	1.98
Elevation	0	40.93	34.75	2.31

It is clear that the generated GWPZ map is mainly related to the three parameters; geology and lithology, geomorphology and lineament density. This could mainly be attributed to the high assigned weight to these parameters. The lowest effective parameters are land cover/use, Rainfall and Elevation, However this doesn't mean the model is not sensitive to the lowest effective parameters or to the other parameters, as the mean values of the potential areas are relatively in the same range.

5. CONCLUSIONS, RECOMMENDATIONS AND OUTLOOK

5.1 Conclusions

Mainly, it is concluded that GIS and remote sensing techniques are very efficient and useful for the identification of groundwater potential zones (GWPZ). The acquisition by remote sensing techniques of relevant parameters which influences and control the infiltration capacity of a certain area for rain water into the underground and therewith the recharge rate of groundwater has proofed as a fast tool to determine groundwater-potential zones, which can be applied in an economical way especially for investigation of larger areas.

Because of the restriction of remote techniques for phenomena, which are mainly noticeable on the land surface or close to it, the integration of geophysical studies can usefully extend the information towards the underground, where the groundwater is stored.

Land-cover/land-use thematic map was generated by supervised classification using different LANDSAT data with an average accuracy of 91.21 % ,Lineaments map also generated by manual and semi-automatic extraction procedure, the results of the two maps were compared and tested, the result showed that manually extracted lineaments map is more reliable and representative.

To have an idea about the heights of the study area and to integrate that in the GWPZ map ; DTM was generated from high spatial resolution images (CARTOSAT) which is used also for extracting morphometric parameters and drainage network of the study area which are essential in hydrological modeling and water resources management, it also used for many other studies like modeling water flow or mass movement (landslides), terrain analyses in geomorphology and physical geography, rectification of aerial photography or satellite imagery.

The validation of the produced GWPZ-maps by AHP and Fuzzy logic revealed that using Fuzzy logic for generating such maps gives more accurate results compared with AHP approach, these results were verified with the yield data of existing wells, and also by geophysical data collected from the field using (GPR, CVES and NMR) technique and found to be in good agreement.

The recent study has proved the proficiencies of integrating remote sensing, Geographical Information System (GIS) and geophysical surveys for the delineation of ground water potential zones in arid to semi-arid areas, which can be used for groundwater development and management projects and serves as a base line for future exploration.

It has been noticed that all of the used parameters are relatively important in this work, as the sensitivity analysis showed that the model is sensitive to all parameters, this analysis indicates that all parameters are significant, but the most effective parameters are: lineaments density, geomorphology, drainage density, geology and lithology.

The Middle Eastern area is a promising area for the applied techniques which can help to explore additional groundwater resources and that could be achieved using high-quality remotely sensed data, and assigning proper weights to enhance the generated groundwater potential zones by Fuzzy logic method.

5.2 Recommendations and Outlook

This study showed nonconventional method for assessment and mapping of groundwater potential zones (GWPZ), which was applied and verified in the lower Jordan valley. As an outcome of this study many important maps were generated and extracted from different sources and integrated together to produce GWPZ map of the study area, such as landcover/landuse thematic map which was extracted from LANDSAT satellite images, the results of using such satellite images were quite acceptable, but definitely could be improved using high resolution time series satellite images covering dry and wet seasons.

It has been noticed that the generated thematic map couldn't highly distinguish between different types of the crops in the study area, for that reason using high accurate data from multispectral sensors with higher resolutions is recommended for more reliable results.

Additionally, during the generation of the GWPZ map a DTM was needed to present the importance of the topography on the formation of groundwater, therefore CARTOSAT-1 data was used for extracting DTM's and gave great results compared with the conventional surveying methods, in addition to that this kind of images covers large areas compared with air-borne images, and saves time and money, for these reasons, the use of CARTOSAT-1 data or similar data in extracting elevation models is highly recommended in developing countries such as Jordan.

Lineaments map was also integrated in this work, two lineaments maps were extracted by two procedures; manual and semi-automatic procedure, the use of manual extraction procedure is recommended because it showed more reliable results compared to an existing recently structural geological map of the Jordan valley.

Another important result was choosing fuzzy logic to represent the importance of each individual map in the generation of the final GWPZ map; it showed higher significance than the map generated by AHP method. Therefore, the developed methodologies by this research are highly recommended to be applied in similar environmental settings in the whole Jordan Valley and all promising areas such as Amman-Zarqa basin to identify areas of potential groundwater.

Moreover, for future investigations, more geophysical studies should be done to assess the quality of the generated GWPZ map, in addition to that, integrating many other types of data such as water table map is also recommended to have broad idea about the situation of groundwater in the area; integrating water table map also gives clearer idea about the movement and allocation of groundwater in the studied basins ,which also gives an indication about the future of the groundwater in that location.

Finally, the study was covering the issue of forming groundwater by direct infiltration of rainfall due to many different parameters as discussed before, and that's not the only possible way to form groundwater naturally, it's also possible to accumulate groundwater in basins from lateral paths and conduits, therefore it's recommended to extend the use of this method for further investigations covering all the related issues, and integrating the quality of water as well.

6. REFERENCES

1. Abdullah, A., Akhir, J. & Abdullah, I. (2009) A Comparison of Landsat TM and SPOT Data for Lineament Mapping in Hulu Lepar Area, Pahang, Malaysia. European Journal of Scientific Research, 34 (3):406-415.

2. Aguilar, M. , Aguera, F., Aguilar, F. & Carvajal, F.(2008) Geometric accuracy assessment of the orthorectification process from very high resolution satellite imagery for common agricultural policy purposes . International Journal of Remote Sensing, 29(24):7181–7197.

3. Al- Mahamid, J. (2005) Integration of water resources of the upper aquifer in Amman-Zarqa basin based on mathematical modeling and GIS, Jordan. Freiberg online Geology, Vol 12:186-193.

4. Al-Mohammad, M. (2009) Integrated GIS and remote sensing for mapping Groundwater potential zones in Tulul al Ashqif Highlands, NE Jordan. Master of Science thesis in Environmental Sciences, unpublished thesis .Yarmouk University, Jordan.

5. Al-Saud, M. (2010) Mapping potential areas for groundwater storage in Wadi Aurnah Basin, western Arabian Peninsula, using remote sensing and geographic information system techniques. Hydrogeology Journal 18:1481–1495.

6. Al-Zoubi A., Akawwi E. & Abueladas A. (2012) Geophysical Investigation for Groundwater Aquifer in the Joran Valley, SMART project, unpublished report.

7. Al-Zoubi, A. & Ben-Avraham Z. (2002) Structure of the earth's crust in Jordan from potential field data. Tectonophysics, 346:45-59.

8. Al-Zoubi, A. & ten-Brink U. (2001) Salt diapers in the Dead Sea Basin and their relationships to Quaternary extensional tectonic. *Marine and Petroleum Geology, 18:* 779-797.

9. Al-Zoubi, A. & ten-Brink U. (2002) Lower crustal flow in small continental Basins: An example from the Dead Sea basins. International Journal of Earth and Planetary Sciences Letters. *199:*67-79.

10. Al-Zoubi, A., Heinrich T., Qabani I. & ten-Brink U. (2007) The Northern end of the Dead Sea Basin: Geometry from the Seismic Evidence. Tectonophysics, 434: 55-69.

11. Al-Zoubi, A., Heinrichs T., Sauter M. & Qabani I. (2005) Geological structure of the eastern side of the lower Jordan Valley-Dead Sea rift: Reflection seismic evidence. Marine and Petroleum Geology. 23: 473-484.

12. Al-Zoubi, A., Shulman H. & Ben-Avraham Z. (2002). Seismic reflection Profiles across the southern Dead Sea basin. Tectonophysics, 346: 61-69.

13. AUSGEO (2005) Geoscience Australia new, IMPROVED Landsat composite products, issue 7. Available Online at: http://www.ga.gov.au/webtemp/image_cache/GA7182.pdf ,Accessed in October 2013.

14. Ayten, C. (2005) Remote sensing study SÜRGÜ Fault zone-Maltaya, Turkey. Master of Science thesis in Geodetic and Geographical information technology. Middle East technical university.

15. Baltsavias, E., Zhang, L. & Eisenbeiss, H. (2006) DSM Generation and interior orientation for determination of IKONOS images using a testfield in Switzerland. Photogrammetrie, Fernerkundung, Geoinformation, Vol.1:41-54, 2006

16. Bayer, H.-J. , Hoetzel, H. , Jado, A. R. , Roscher, B; Vogenreiter, W. (1988) Sedimentary and structural evolution of the northwest Arabian Red Sea margin. - Tectonophysics, 153: 137-151.

17. Beek, M. (2000) Fuzzy logic analysis for modeling of natural resource processes. International Archives of Photogrammetry and Remote Sensing. Vol. 33, Part B4. Amsterdam.

18. Belitzky S. (2002) The morphotectonic structure of the lower Jordan Valley, an active segment of the Dead Sea Rift. EGU Stephan Mueller Special Publication Series, 2(2): 95–103.

19. Belitzky, S. (2002) The morphotectonic structure of the lower Jordan Valley – an active segment of the Dead Sea Rift. EGU Stephan Mueller Special Publication Series, Vol.2: 95-103.

20. Bezdek, C. J. (1981) Pattern Recognition with Fuzzy Objective Function Algorithms. New York: Plenum Press.

21. Biediger, J. (2012) The use of digital image processing to facilitate digitizing land cove zones from gray level aerial photos. A Master of Science thesis in Geology and Geographic. Northwest Missouri State University Maryvilled, Missouri.

22. Bhardwaj, A. (2013) Evaluation of DEM, and orthoimage generated from Cartosat-1 with its potential for feature extraction and Visualization. American Journal of Remote Sensing, Vol.1:1-6.

23. Bharti, A. (2004) A Decision Tree Approach to Extract Knowledge for Improving Satellite Image Classification. Master Thesis in Geo-informatics, Indian Institute of Remote Sensing, Indian Space Research Organization, India.

24. Bishop, V., Fienberg, S. & Holland, P. (1975) Discrete multivariate analysis: Theory and practice. MIT Press.

25. Bonham-Carter, G.F. (1996) Geographic Information Systems for Geosciences, Modeling With GIS. Pergamon-Love Printing Service Ltd., Ontario, Canada. 398 pp.

26. Bonham-Carter, Graeme F., (1994) Geographic Information Systems for Geoscientists, Modelling with GIS, Oxford; Pergamon Press.

27. Brnder, F. (1974) Geology of Jordan. Gebrueder Borntraeger. Berlin. 196.

28. Büyüksalih, G., Jacobsen, K. (2008) Digital Height Models in Mountainous Regions based on Space Information. EARSel Workshop Remote Sensing - New Challenges of High Resolution, Bochum.

29. Chopra, R. & Sharma, P.K. (1993) Landform analysis and ground water potential in the Bist Doab area Punjab, India. International Journal of Remote Sensing ,14 :17.

30. Chuma, C., Orimoogunje, O., Hlatywayo, D. & Akinyede, J. (2013) Application of Remote Sensing and Geographical Information Systems in Determining the Groundwater Potential in the Crystalline Basement of Bulawayo Metropolitan Area, Zimbabwe. Advances in Remote Sensing, Vol.2: 149-161

31. Coyle, G. (2004) Analytic Hierarchy Process (AHP), Practical Strategy. Open Access Material. Pearson Education Limited.

32. Daniel E. J. (1963) International Lexicon of stratigraphy for Jordan. Lexique stratigraphique international, vol. III A sie, Dubertret dir, fasc 10-c1, Liban, Syria, Jordanie. CNRS Paris, 295-396 pp.

33. De Jong, S.M., Hornstra T. & Maas, H. (2001) An integrated spatial and spectral approach to the classification of Mediterranean land cover types: the SSC method. International Journal of Applied Earth Observation and Geoinformation, 3(2):176-183.

34. Dubey, A., Singh, P.K., Choudhary, A. (1999) Morpho-geological analysis for groundwater resources evaluation and management. P.G. Diploma Report. Indian Institute of Remote sensing, Dehradun, India.

35. Edet, A.E., Okereke, C.S., Teme, S.C. & Esu, E.O. (1998) Application of remote sensing data groundwater exploration: A case study of the Cross River State, Southeastern Nigeria. Hydrogeology Journal, 6:394-404.

36. El-Naqa, A., Hammouri, N., Ibrahim, K. & El-Taj, M. (2009) Integrated Approach for Groundwater Exploration in Wadi-Araba Using Remote Sensing and GIS. Jordan Journal of Civil Engineering. 3 (3).

37. El-Sammany, M. , Abou El-Magd, I. & Hermas, E.(2011) Creating a Digital Elevation Model (DEM) from SPOT 4 Satellite Stereo-Pair Images for Wadi Watier - Sinai Peninsula, Egypt Nile Basin. Water Science & Engineering Journal, Vol.4 (1).

38. Engman, ET. & Gurney, RJ. (1991) Remote sensing in hydrology. Chapman and Hall, London, 225 pp.

39. ENVI DEM Extraction Module User's Guide (2009), DEM Extraction Module Version 4.7.

40. Ettazarini, S. (2007) Groundwater potentiality index: a strategically conceived tool for water research in fractured aquifers. Environmental Geology. 52:477–487.

41. Feng, L. , Wang, C. & Zhang, Q.w. (2005) Comparison of SRTM Data with other DEM sources in Hydrological Researches. Proceedings of International symposium on remote sensing of environment; global monitoring for sustainability and security : 961-963.

42. Foody, G. & Atkinson, P. (2002) Uncertainty in Remote Sensing and GIS, John Wiley & Sons Inc.

43. Ford-Robertson, F.C. (1971) Terminology of forest science, technology, practice, and products: English-language version / Edited by F. C. Ford-Robertson and authorized by the Joint FAO/IUFRO Committee on Forestry Bibliography and Terminology. Washington: Society of American Foresters.

44. Freund, R., Z. Garfunkel, I. Zak, M. Goldberg, T. Weissbord, and B. Derin (1970). The shear along the Dead Sea rift. Phlilos. Trans. R. Soc. London, Ser. A., 267: 107- 130 pp.

45. Gaber, A., Koch, M., and F. El-Baz (2010) Textural and compositional characteristics of Wadi Feiran deposits, Sinai Peninsula, using Radarsat-1, PAlSAR, SRTM and ETM+ data. Remote Sensing, (2): 52-75.

46. Garfunkel, Z. (1981) Internal structure of the Dead Sea leaky transform (rift) in relation to plate kinematics. Tectonophysics, Vol. 80: 81-108.

47. Garibi, H., Mavi, A., Nabizadeh, R., Arabalibeik, H., Yunesian, M. & Sowlat,M. (2012) A novel approach in water quality assessment based on fuzzy logic . Journal of Environmental Management, 112: 87-95.

48. Geomatica OrthoEngine User Guide (2003) PCI Geomatics Enterprises Inc, Version 9.0.

49. Gercek, D. (2002) Improvement of land cover classification with the integration with topographical data in uneven terrain. A Master of Science thesis in Geodetic and Geographic information technologies, the Middle East technical university.

50. Ghayoumian, J., Mohseni Saravib, M., Feiznia, S., Nourib, B. & Malekian, A. (2007) Application of GIS techniques to determine areas most suitable for artificial groundwater recharge in a coastal aquifer in southern Iran. Journal of Asian Earth Science 30, 364–374.

51. Godebo, T. (2005) Application of remote sensing and GIS Geological investigation and Groundwater potential zone identification , southeastern Ethiopian plateau, bale mountains and the surrounding areas. Master of Science thesis in GIS and remote sensing, Addis Ababa University.

52. Gogu, RC. & Dassargues, A. (2000) Sensitivity analysis for the EPIK method of vulnerability assessment in a small karstic aquifer, Southern Belgium. Hydrogeology Journal 8(3):337–345.

53. Hancock, G., Martinez, C., Evans, K. & Moliere, D. (2006) A comparison of SRTM and high-resolution digital elevation models and their use in catchment geomorphology and hydrology: Australian examples. Earth Surface Processes and Landforms 31: 1394–1412.

54. Hoja, D. & d'Angelo, P. (2009) Analysis of DEM combination methods using high resolution optical stereo imagery and interferometric SAR data. ISPRS Hannover Workshop: High-Resolution Earth Imaging for Geospatial Information.

55. Horton, R. E. (1932) Drainage basin characteristics. Eos Trans, 13: 350– 361.

56. Horton, R. E. (1945) Erosional development of streams and their drainage basins: hydro-physical approach to quantitative morphology. Geol. Soc. Am. Bull. 56: 275–370.

57. Hung, L.Q. (2001) Remote sensing based hydrogeological analysis of Suoimuoi catchment Vietnam. Master of Science thesis .Vrije Universiteit Brussel, 87p.

58. Hung, L.Q., Batelaan, O. & De Smedt, F. (2005) Lineament extraction and analysis, comparison of LANDSAT ETM and ASTER imagery. Case study:

Suoimuoi tropical karst catchment, Vietnam , Remote Sensing for Environmental Monitoring, GIS Applications, and Geology , edited by Manfred Ehlers, Ulrich Michel, Proc. of SPIE Vol. 5983, 59830T.

59. Jacobsen, K. (2004) DEM generation from satellite data. In: Goossens, R. (Ed.): Remote Sensing in Transition, Proceeding of the 23rd EARSeL Symposium 2003, Ghent, Belgium, pp.513–525.

60. James, P., Dorothy, S. & Robert, G. (2011) Physical Geography, Tenth Edition, Cengage Learning.

61. Jensen, J.R. (1996) Introductory digital image processing: a remote sensing perspective. Prentice-Hall, New Jersey.

62. Kamal, J., Mandla, R., Javed, S. & Suredra, S. (2009) Using Rational Polynomial Coefficients (RPC) to generate digital elevation models - a comparative study. Applied GIS, 5(2): 1.

63. Karanth, K. (2008) Ground Water Assessment Development and Management. Tata McGraw-Hill, 12th edition, 381.

64. Karkazi, A. ,Hatzichristos, T. ,Mavropoulos, A. , Emmanouilidou, B. & Elseoud, A. (2001) Landfill siting using GIS and Fuzzy logic. 8th International waste management and landfill symposium; Sardinia: 67-76.

65. Kayastha, P., Bijukchhen, S., Dhital, M. & Smedt, F. (2013) GIS Based Landslide Susceptibility Mapping using a Fuzzy Logic Approach: A Case Study from Ghurmi-Dhad Khola Area, Eastern Nepal. Journal Geological society of India, Vol.82:249-261.

66. Kesten, D. (2004) Structural observations at the southern Dead Sea from seismic reflection data and ASTER satellite images. PhD thesis in Geography, Potsdam University.

67. King, D. ,Jollineau, M. & Fraser, B. (1999). Evaluation of MK-4 multispectral satellite photography in land cover classification of eastern Ontario. International Journal of Remote Sensing, 20(17): 3311-3331.

68. Kocal, A. (2004) A Methodology for detection and elevation of lineaments from satellite imagery. Master of Science thesis in mining engineering, Middle East technical university.

69. Kocal, A., Duzgun, H.S. & Karpuz, C. (2007) An accuracy assessment methodology for the remotely sensed discontinuities: a case study in Andesite Quarry area, Turkey. International Journal of Remote Sensing, Vol. 28(17).

70. Krishna, B., Amitabh, Srinivasan, T. & Srivastava, P. (2008) DEM Generation from high resolution multi-view data product . The International Archives of the Photogrammetry, Remote Sensing and Spatial Information Sciences. Vol. 39. Part B1. Beijing.

71. Krishnamurthy, J. & Srinivas, G. (1995) Role of geological and geomorphological factors in groundwater exploration: a study using IRS LISS data. International Journal of Remote Sensing 16 (14), 2595–2618.

72. Krishnamurthyl J., Arul M. , Jayaramanl V. & Manivel M. (2000) Groundwater resources development in hard rock terrain- an approach using remote sensing and GIS techniques . International Journal of Applied Earth Observation and Geoinformation, Vol. 2.

73. Landis, JR. , Koch, GG. (1977) The measurement of observer agreement for categorical data. Biometrics 33:159-174.

74. Libasse, S. (2007) Application of Remote Sensing and GIS for Groundwater Potential Zone Mapping in Northern Ada'a Plain (Modjo Catchment). Master of Science thesis in GIS and remote sensing, Addis Ababa University.

75. Lillesand, T. M., Kiefer, R. W., & Chipman, J. W. (2004) Remote Sensing and Image Interpretation ,Fifth Edition ed. Hoboken, NJ: Wiley.

76. Lillesand, T., Kiefer, R. & Chipman, J. (2004) Remote Sensing and Image Interpretation. Fifth edition, John Wiley & sons Inc, 550 pp.

77. Lodwik, WA. ,Manson, W. and Svoboda, L. (1990) Attribute error and sensitivity analysis of map operations in geographical informations systems: suitability analysis. International journal of Geographic information systems, vol.4:413:428.

78. Machiwal, D., Jha, M. & Mal, B. (2011) Assessment of Groundwater Potential in a Semi-Arid Region of India Using Remote Sensing GIS and MCDM Techniques. Water Resources Management, 25:1359–1386.

79. Mamdani, E.H. & S. Assilian (1975) An experiment in linguistic synthesis with a fuzzy logic controller. International Journal of Man-Machine Studies, 7(1):1-13.

80. Mandelas, E., Hatzichristos. T. , Prastacos, P. (2007) A Fuzzy Cellular Automata Based Shell for Modeling Urban Growth − A Pilot Application in Mesogia Area .10th AGILE International Conference on Geographic Information Science , Aalborg University, Denmark.

81. Marghany, M. (2012) Fuzzy B-spline algorithm for 3-D lineament reconstruction. International Journal of Physical Sciences, 7(15): 2294 – 2301.

82. Meijerink, A., Bannert, D., Batelaan, O., Lubczynski, M. & Pointet, T.(2007) Remote sensing applications to Groundwater . Printed by UNESCO.

83. Milne, T. (2007) Fundamentals of remote sensing, Lecture 13: Accuracy assessment. COGS.

84. Muneizel, S. & Khalil, I. (1993) Geological map of As Salt-3154 III, scale 1: 50000. Internal Report of Jordan, Natural Resources Authority, Amman, Jordan.

85. Naaz, S., Alam, A. & Biswas, R. (2011) Effect of different defuzzification methods in a fuzzy based load balancing application. International Journal of Computer Science Issues, 8(5).

86. Nagle, G. (2000) Advance Geography .Oxford university press, 1st edition, 84.

87. Napolitano, P. and Fabbri, A.G. (1996) Single-parameter sensitivity analysis for aquifer vulnerability assessment using DRASTIC and SINTACS. HydroGIS 96: Application of Geographic Information Systems in Hydrology and Water Resouces Management (Proceedings of the Vienna Conference, April 1996). IAHS Publ. No.235, 1996, 559-566.

88. Neev, D., and J.K. Hall (1979) Geophysical investigations in the Dead Sea. Sedimentary Geology, Vol.23: 209-238 pp.

89. Niocaill, C., Rayan,P. (1999) Continental Tectonics. Geological Society special edition ,No. 164. The geological society publishing house, UK.

90. Nour, S. (1996) Groundwater potential for irrigation in the East Oweinat area, Western Desert, Egypt. Environmental Geology, 27(3):143–154.

91. OLeary, D. W., Friedman, J. D. & Pohn, H. A. (1976) Lineament, linear, lineation: some proposed new standards of old terms: Geological Society of America Bulletin, Vol.87:1463-1469.

92. Passini, R., Betzner, D. & Jacobsen, K. (2002) Filtering of Digital Elevation Models, ASPRS annual convention, Washington.

93. PCI Geomatica Online User's Manual (2001) Available online at: http://www.pcigeomatics.com/services/support_center/tutorials/tutorials.php

94. Picard, L. (1931) Geological Research in the Judean Desert. 108 pp.

95. Quennell, A.M. (1958) The structure and geomorphic evolution of the Dead Sea rift. Q. J. Geol. Soc. London, Vol.64: 1-24 pp.

96. Rajeswari, S. & Theiva Jeyaselvi, K. (2012) Support vector machine classification for MRI images. International Journal of Electronics and Computer Science Engineering, Vol.1 (3). Suezen M and Torprak V, Filtering of satellite images in

geological lineament analyses: an application to a fault zone in Central Turkey, international journal of remote sensing, 1998, vol. 19, no. 6, 1101-1114.

97. Rao, N.S. (2006) Groundwater potential index in a crystalline terrain using remote sensing data. Environmental Geology. 50 (7):1067–1076.

98. Rao, YS. & Jugran, DK. (2003) Delineation of groundwater potential zones and zones of groundwater quality suitable for domestic purposes using remote sensing and GIS. Hydrology Science Journal, 48(5):821–833.

99. Rather J., Raouf Z. (2012) Fuzzy Logic Based GIS Modeling for Identification of Groundwater Potential Zones in the Jhagrabaria Watershed of Allahabad District, Uttar Pradesh, India. International Journal of Advances in Remote Sensing and GIS, Vol.1 (2).

100. Rather, A. & Andrabi, Z. (2012) Fuzzy Logic Based GIS Modeling for Identification of Ground Water Potential Zones in the Jhagrabaria Watershed of Allahabad District, Uttar Pradesh, India. International Journal of Advances in Remote Sensing and GIS, Vol. 1(2).

101. Riad, P. , Billib, M. , Hassan, A. , Omar, M. (2011) Overlay Weighted Model and Fuzzy Logic to Determine the Best Locations for Artificial Recharge of Groundwater in a Semi-Arid Area in Egypt , Nile Basin .Water Science & Engineering Journal, Vol. 4(1).

102. Richards, J. (1999) Remote Sensing Digital Image Analysis. Springer-Verlag, Berlin.

103. Roark, DM., Healy, DF. (1998) Quantification of deep percolation from two flood-irrigated alfalfa fields, Roswell Basin, New Mexico. USGS Water Resources Investigation Report, 98-4096, 32pp.

104. Rodecki, J. & Dial, G. (2003) Block Adjustment of High-Resolution Satellite Images Described by Rational Polynomials. Photogrammetric Engineering & Remote Sensing, Vol. 69(1): 59– 68.

105. Saaty, TL. (1980) The analytic hierarchy process: planning, priority setting, resource allocation. McGraw-Hill, New York, 287.

106. Saaty, TL. (2008) Decision making with the analytic hierarchy process. International Journal of Services Sciences, Vol.1 (1).

107. Sabet, M. (1975) Vertical Electrical Resistivity Soundings to locate Groundwater Resources: A Feasibility Study. Virginia Polytechnic Institute and State University, research division, lacksburg, Virginia.

108. Sahawneh, J. (2011) Structural Control of Hydrology, Hydrogeology and Hydrochemistry along the Eastern Escarpment of the Jordan Rift Valley, Jordan. PhD thesis in Geosciences and Environmental Sciences, Karlsruhe institute of technology.

109. Samake M., Ta Z., Hlaing W, M'Bue I., Kasereka K. (2003) Assessment of Groundwater Pollution Potential of the Datong Basin, Northern China. Journal of Sustainable Development, 2003, 140-152.

110. Sankar, K. (2002) Evaluation of groundwater potential zones using remote sensing data in Upper Vaigai river basin, Tamil Nadu, India. Journal of Indian Society of Remote Sensing 30(30):119– 29.

111. Saraf, A. K. & Jain, S. K. (1994) Integrated use of remote sensing and geographical information system methods for groundwater exploration in parts of Lalitpur district, UP. India. International Conference on Hydrology and Water Resources (New Delhi, 20–22 December 1993) Kluwer Academic Publishers, Dordrecht, Netherlands.

112. Sarp, G. (2005) Lineament analysis from satellite images, North- West of Ankara. Master of science thesis in Geodetic and geographic information technologies. Middle east technical university, Turkey.

113. Scaramuzza, P., Micijevic, E. & Chander, G. (2004) SLC gap-filled products: phase one methodology. Available Online at: http://landsat.usgs.gov/documents/SLC_Gap_Fill_Methodology.pdf, Accessed in October 2013.

114. Schnetzer, P. (2007) Supervised Classification: A Landsat 7 ETM+ Scene Covering Portions of New Brunswick, Prince Edward Island and Nova Scotia. Pg. 16.

115. Schulze, F. Levy, Z., Kuss, J. and Gharaibeh, A. (2003) Cenomanian – Turonian carbonate platform deposits in west central Jordan. Int. J. Earth Sciences (Geol Rundsch), Vol.92: 641-660.

116. Sener, E., Davraz, A. & Ozcelik (2005) An integration of GIS and remote sensing in groundwater investigations: a case study in Burdur, Turkey. Hydrogeology Journal, 13:826–834.

117. Sener, E., Davraz, A., Ozcelik, M. (2005). An integration of GIS and remote sensing in groundwater investigations: A case study in Burdur, Turkey. Hydrogeology Journal ,14:826–834

118. Shahid, S. , Nath, S. K. & ROY, J. (2000) Groundwater potential modeling in a soft rock area using a GIS. International journal of remote sensing, 21(9):1919–1924.

119. Shahid, S., Nath, S.K. & Roy, J. (2000) Groundwater potential modelling in a soft rock area using a GIS. International Journal of Remote Sensing, 21 (9):1919–1924.

120. Shahid, Sh. , Nath, S. & Kamal A. (2002) GIS Integration of Remote Sensing and Topographic Data Using Fuzzy Logic for Ground Water Assessment in Midnapur District, India. Geocarto International, Vol. 17(3).

121. Shamir, G., Eyal, Y., Bruner. I. (2005) Localized versus distributed shear in the transform plate boundary: the case of the Dead Sea Transform in the Jericho Valley. 6 (5):1-21.

122. Sharma, R., Ghosh, A. & Joshi, P. (2013) Decision tree approach for classification of remotely sensed satellite data using open source support. Journal of Earth System Science. 122(5):1237–1247.

123. Shawabkeh, K. F. (2001) Geological map of Al Karama - 3153-IV, 1:50.000, Internal Report of Natural Resources Authority, Amman, Jordan.

124. Shawabkeh, K. F. (2001) Geological map of Al Karama. Internal Report of Natural Resources Authority, Amman, Jordan.

125. Singh, A. & Prakash, S. (2003) An integrated approach of Remote Sensing, Geophysics and GIS to evaluation of Groundwater potentiality of Ojhala subwatershed, Mirzapur district, U.P., India. Map India Conference.

126. Sivakumar, M. , Roy, P. , Harmsen, K. & Saha K (2003) Satellite remote sensing and GIS applications in agricultural meteorology. Proceedings of the Training Workshop7-11 July, 2003, Dehra Dun, India, Available on : http://www.scribd.com/doc/49983279/18116936-WMOTD1182-Satellite-Remote-Sensing-and-GIS-Applications-in-Agricultural-Meteorology

127. Sreedevi, P.D., Subrahmanyam, K. & Ahmed, Sh. (2005) Integrating approach for delineating potential zones to explore for groundwater in the Pageru river basin, Cuddapah district, Andhra Pradesh, India. Hydrogeology Journal, 13:534–543.

128. Srivastava, A. & Bhattacharya, A. (2006) Groundwater assessment through an integrated approach using remote sensing, GIS and resistivity techniques: a case

study from a hard rock terrain. International Journal of Remote Sensing, 27(20):4599–4620.

129. Stirling, M.W., S.G. Wesnousky, and K. Shimazaki, (1996) Fault trace complexity, cumulative slip, and the shape of the magnitude-frequency distribution for strike-slip faults; a global survey, Geophysical Journal International, vol.124: 833-86.

130. Suzen, M., Toprak, V. (1998) Filtering of satellite images in geological lineament analyses: An application to a fault zone in Central Turkey. International Journal of Remote Sensing, 19(6):1101-1114.

131. Swain, P. H. & Davis, S. M. (1978) Remote Sensing: The Quantitative Approach. New York:McGraw-Hill.

132. Talabi, A., & Tijani M. (2011) Integrated remote sensing and GIS approach to groundwater potential assessment in the basement terrain of Ekiti area southwestern Nigeria. RMZ – Materials and Geoenvironment, 58(3) : 303–328.

133. Tarboton, D., G., R. L. Bras & Rodriguez-Iturbe I. (1991) On the Extraction of Channel Networks from Digital Elevation Data, Hydrologic Processes, 5(1): 81-100.

134. Ten-Brink, U., Z., Ben-Avraham, R., Bell, M., Hassounah, D., Coleman, G., Andreason, G., Tibor, B. & Coakley (1993) Structure of the Dead Sea pull- apart basin from gravity analysis. Journal of Geophysical Research, 98, 21,887-21,894.

135. Thapa, R., Kumar, R. and Sood, R.K , Study of morphotectonics and hydrogeology for groundwater prospecting using remote sensing and GIS in the north west Himalaya, district sirmour, himachal pradesh, India , The International Archives of the Photogrammetry, Remote Sensing and Spatial Information Sciences. Vol. 38. Part B4. Beijing 2008

136. Thirukumaran, V. (2011) Geoinformatic Modelling for certain Geo-resources and Geohazards of Attur Vallry,Tamil Nadu, India. PhD thesis in Geological remote sensing, India. Bharathidasan University.

137. Toll, M. (2007) An integrated approach for the investigation of unconsolidated aquifers in a brackish environment – A case study on the Jordanian side of the lower Jordan Valley. PhD Dissertation, Gottingen University.

138. Ufimtsev, G. F., (2008) The geomorphological features of Jordan .Geography and Natural Resources ,29: 88–92.

139. WAJ (2007) Water Authority of Jordan. Annual report of 2006, Amman, Jordan.

140. Waters, P., Greenbaum, P., Smart, L. & Osmaston, H. (1990) Applications of remote sensing to groundwater hydrology. Remote Sensing Reviews, 4:223–264.

141. Wesnousky, S.G., (1998) Seismological and structural evolution of strike-slip faults, Nature, Vol.335: 340-343.

142. Willneff, J., Weser, T., Rottensteiner, F. & Fraser, C. (2008) Precise Georeferencing of CARTOSAT imagery via different orientation models. The International Archives of the Photogrammetry, Remote Sensing and Spatial Information Sciences. Vol. 37. Part B1. Beijing.

143. YCEO (2011) Filling Gaps in Landsat ETM Images, unpublished report, the Yale center for earth observation.

144. Zadeh, L.A. (1973) Outline of a new approach to the analysis of complex systems and decision processes. IEEE Transactions on Systems, Man, and Cybernetics, 3(1): 28-44.

145. Zak, I. and Freund R. (1981). Asymmetry and basin migration in the Dead Sea rift. Tectonophysics, Vol.80: 27-38 pp.

146. Zadeh, L. A. (1965) Fuzzy set. Information control, 8(3): 338–353.

147. Zadeh, L. A. (1975) The concept of a linguistic variable and its application to approximate reasoning. Information Science, 8:199–249.

148. Zimmerman, H.J. (1996) Fuzzy set theory and it applications. Kluwer Academic Publishers, Norwell MA, USA. 435p.